KU LEUVEN

DOCTORAL SCHOOL
BIOMEDICAL SCIENCES

Single-Cell Omics to Reveal Mechanisms of Response to Immunotherapy

in Head and Neck Cancer

Amelie Franken

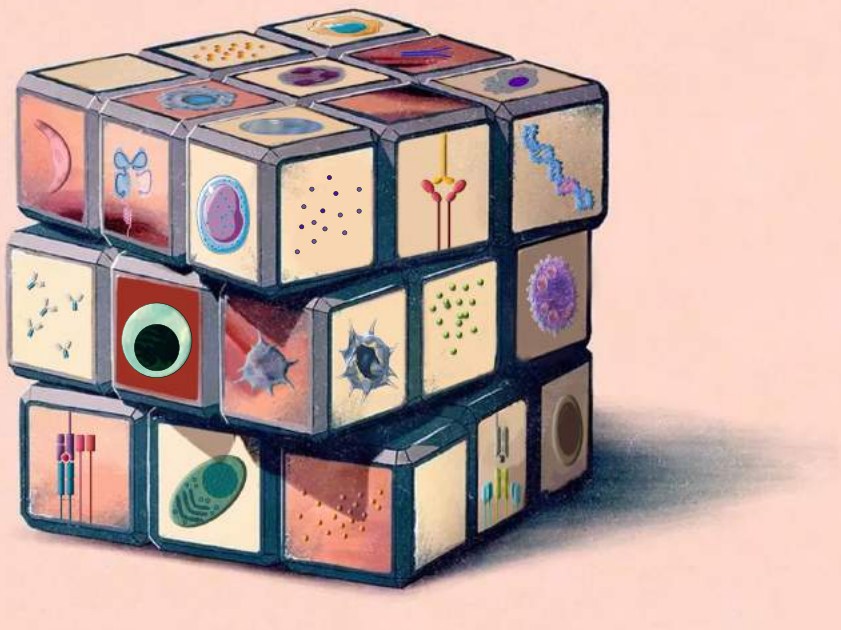

Supervisors:
Prof. dr. Diether Lambrechts
Prof. dr. Paul Clement

April 2024

KU Leuven
Biomedical Sciences Group
Faculty of Medicine
Department of Human Genetics

KU LEUVEN

DOCTORAL SCHOOL
BIOMEDICAL SCIENCES

Single-Cell Omics to Reveal Mechanisms of Response to Immunotherapy

in Head and Neck Cancer

Amelie FRANKEN

Jury:

Supervisor KU Leuven: *Prof. dr. Diether Lambrechts*
Co-supervisor: *Prof. dr. Paul Clement*
Chair examining committee: *Prof. dr. Marc Fransen*
Chair public defense: *Prof. dr. Patrick Callaerts*
Jury members: *Prof. dr. Abhishek Garg*
Prof. dr. Alejandro Sifrim
Prof. dr. Damya Laoui
Dr. Henoch Hong

Dissertation presented in partial fulfillment of the requirements for the degree of Doctor in Biomedical Sciences
15th of April 2024

Abstract

The body's natural defense system is designed to recognize and eliminate altered or foreign cells, including cancerous ones. Nonetheless, cancer cells can occasionally evade this system, allowing them to develop and progress. Immunotherapy, particularly immune checkpoint blockade (ICB) therapy enhances the immune system's ability to detect and attack cancer cells by releasing the brakes on the immune response, including PD-(L)1 and CTLA4. While ICB therapy has significantly improved cancer treatment, the majority of patients still does not respond or experiences relapse. To address this challenge, combining different agents, such as anti-PD-(L)1 and anti-CTLA4, is considered crucial. However, these combinations are often used without a complete understanding of their mechanisms or which patients would benefit the most.

To investigate the contribution of anti-CTLA4 to anti-PD-L1 therapy, we conducted a neoadjuvant window-of-opportunity study in head and neck squamous cell carcinoma (HNSCC). Analysis of tumor biopsies before and after treatment using single-cell technologies revealed that T-cell expansion serves as an early response biomarker. Whereas anti-PD-L1 primarily expanded CD8+ T-cells, combination therapy expanded both CD4+ and CD8+ T-cells, with CD4+ T-cells exhibiting an activated T-helper 1 phenotype. Spatial profiling of CD4+ and CD8+ T-cells revealed that they were surrounded by dendritic cells expressing T-cell attracting factors or antibody-producing plasma cells. We found that this environment existed already before treatment in patients who responded to anti-PD-L1 therapy, which was further augmented by the therapy. Conversely, combining anti-CTLA4 with anti-PD-L1 seems to trigger a *de novo* immune response by activating CD4+ T-cells in tumor-draining lymph nodes, which subsequently migrate to the tumor. This highlights the potential efficacy of combined anti-PD-L1/anti-CTLA4 therapy, especially for patients who initially failed to mount an anti-tumor immune response.

In conclusion, this research sheds light on the complexities of ICB therapies,

offering valuable insights into their mechanisms and paving the way for informed advancements in the treatment of HNSCC and potentially other cancer types as well.

Graphical abstract

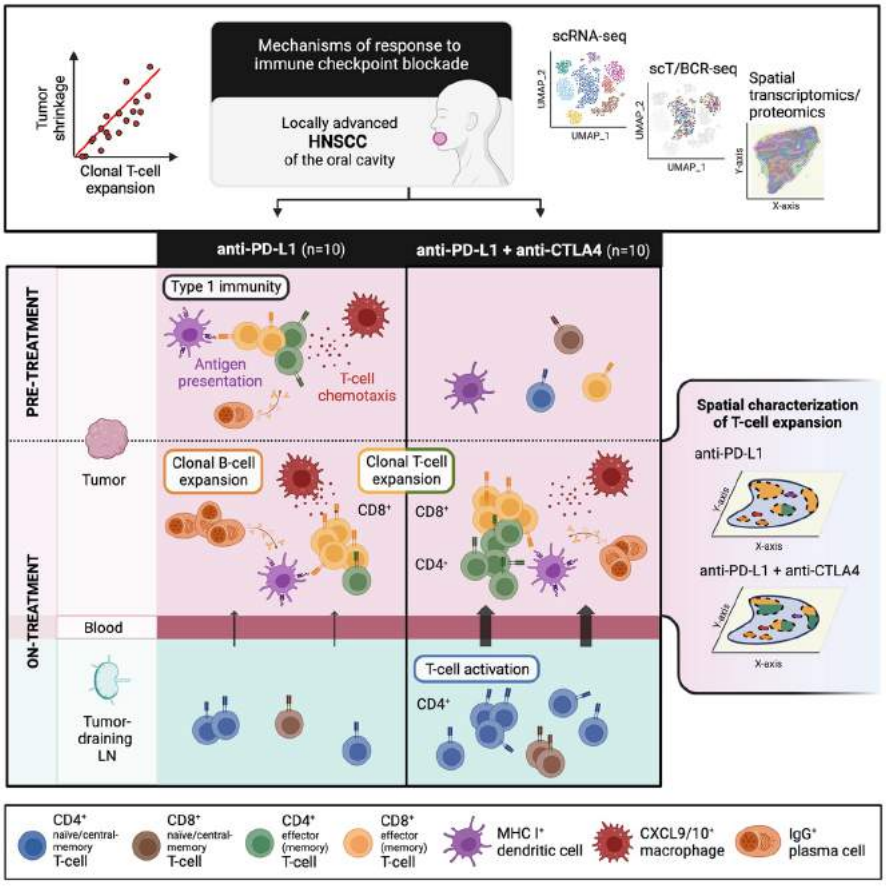

Graphical abstract: Single-cell RNA-sequencing (scRNA-seq), T- and B-cell receptor sequencing (scT/BCR-seq), and spatial transcriptomics and proteomics were performed to profile the tumor biopsies, tumor-draining lymph nodes (tdLN) and peripheral blood of head and neck squamous cell carcinoma (HNSCC) patients treated with anti-PD-L1 alone or combined with anti-CTLA4. Complementary mechanisms were identified underlying response to anti-PD-

L1 versus anti-PD-L1/anti-CTLA4 combination therapy. Highlights: **(1)** The addition of anti-CTLA4 to anti-PD-L1 amplifies CD4+ T-cell expansion; **(2)** Expanding CD4+ and CD8+ T-cells co-localize with dendritic cells and plasma cells; **(3)** Pre-existing type 1 immunity predicts expansion upon anti-PD-L1 but not anti-PD-L1/anti-CTLA4; **(4)** anti-PD-L1/ anti-CTLA4 activates CD4+ T-cells in the tdLN, which traffic to the tumor. MHC: major histocompatibility complex.

Beknopte samenvatting

Ons immuunsysteem is geëvolueerd om abnormale en lichaamsvreemde cellen te identificeren en te elimineren, maar onder bepaalde omstandigheden faalt het, waardoor kanker zich ongehinderd kan ontwikkelen. Immunotherapie, met name immuun-checkpoint inhibitie (ICI) die zich richt op eiwitten zoals PD-(L)1 en CTLA4, versterkt ons immuunsysteem door deze remmen op te heffen. Hierdoor kan het immuunsysteem kankercellen beter herkennen en aanvallen. Ondanks grote vooruitgang in kankerbehandeling met ICI therapie, blijft een aanzienlijk aantal patiënten ongevoelig voor deze therapie of wordt ze geconfronteerd met een terugval. Om dit te overwinnen, lijkt het essentieel om verschillende therapieën te combineren, zoals anti-PD-(L)1 plus anti-CTLA4. Echter, deze combinaties worden vaak gebruikt zonder volledig begrip van de onderliggende responsmechanismen of welke patiënten er het meeste baat bij hebben.

Dit proefschrift pakt deze uitdagingen aan door het effect van anti-CTLA4 bovenop anti-PD-L1 therapie te onderzoeken in patiënten met hoofd- en halsplaveiselcelcarcinoom (HHPCC). Door de individuele cellen van tumorbiopten voor en na de therapie uitgebreid in kaart te brengen, ontdekten we dat T-cel uitbreiding een vroege biomarker was voor therapie respons. Anti-PD-L1 zorgde voornamelijk voor een toename van CD8+ T-cellen, terwijl combinatietherapie zowel een uitbreiding van CD4+ als CD8+ T-cellen teweegbracht, waarbij de CD4+ T-cellen een geactiveerd T-helper 1 fenotype vertoonden. Ruimtelijke karakterisatie van CD4+ en CD8+ T-cellen toonde aan dat ze omringd werden door dendritische cellen met T-cel-rekruterende kenmerken, evenals antilichaam-producerende plasmacellen. Hoewel deze tumoromgeving al vóór de anti-PD-L1 therapie bestond, leek het niet noodzakelijk te zijn voor het opwekken van T-cel uitbreiding bij gecombineerde anti-PD-L1/anti-CTLA4 behandeling. Het traceren van T-cel receptoren doet vermoeden dat anti-CTLA4, maar niet anti-PD-L1, voor de migratie zorgt van meer naïeve CD4+ T-cellen van lymfeklieren, via het bloed, naar de tumor waar T-cellen een T-helper 1 fenotype verwerven. Dit benadrukt de cruciale rol van CD4+ T-cel activatie

en migratie vanuit de lymfeklier in de vroege respons op anti-PD-L1/anti-CTLA4 bij HHPCC. Bovendien kan dit mogelijk verklaren waarom een reeds bestaande immuunrespons geen voorspellende factor was voor de respons op gecombineerde therapie.

Kortom, dit onderzoek werpt een nieuw licht op de complexiteit van immunotherapie met ICI, biedt waardevolle inzichten in hun werking en opent perspectieven voor geïnformeerde vooruitgang in de behandeling van HHPCC.

Contents

Preface

In this dissertation, the single-cell spatial landscape of immunotherapy response is metaphorically represented by the familiar complexity of a Rubik's Cube. Each facet of the cube symbolizes a key player of the immune system, offering a lens through which we explore the dynamic interactions and challenges inherent in immunotherapeutic approaches.

The precision required to solve the Rubik's Cube mirrors the specificity sought in targeting cancer cells, and the adaptability needed to conquer the puzzle reflects the ever-learning nature of the immune response. Each turn of the metaphorical Rubik's cube represents a different approach or intervention in the search for effective immunotherapy, echoing the diverse strategies employed by researchers in their quest to unlock the secrets of immune system modulation.

Much like each Rubik's cube configuration is unique, tailored immunotherapy approaches must be developed for individual patients, emphasizing the importance of personalized treatment strategies in navigating the complexities of cancer care. Let this metaphor guide you through the pages ahead, where we introduce the complexities of immunotherapy and its responses, seeking not only understanding but also solutions in the face of this medical puzzle.

List of abbreviations

APC ..... Antigen-presenting cell

aCTLA4 ..... Anti-cytotoxic T-lymphocyte-associated protein 4

aPD-(L)1 ..... Anti-programmed cell death protein (ligand) 1

BCR ..... B-cell receptor

CAR ..... Chimeric antigen receptor

CCA ..... Canonical correlation analysis

CITE-seq ..... Cellular indexing of transcriptomes and epitopes by sequencing

cDNA ..... Copy DNA

cDC(1/2) ..... Conventional (type 1/2) dendritic cell

CDR1/2/3 ..... Complementarity-determining region 1/2/3

cMo ..... Classical monocyte

CTL ..... Cytotoxic T-lymphocyte

CTLA4 ..... Cytotoxic T-lymphocyte-associated protein 4

DAMP ..... Damage-associated molecular pattern

DC ..... Dendritic cell

DMEM ..... Dulbecco's Modified Eagle Medium

DMSO ..... Dimethylsulfoxide

dNTP ..... Deoxynucleotide triphosphate

DUTRELASCO DUrvalumab with or without Tremelimumab in REsectable Locally Advanced Squamous cell Carcinoma of the Oral cavity

EC ..... Endothelial cell

EGFR ..... Epidermal growth factor receptor

Exp ..... Expanded

FBS ..... Fetal bovine serum

FC ..... Fold change

FFPE ..... Formalin-fixed paraffin-embedded

GC ..... Germinal center

H&E ..... Hematoxylin and eosin

HLA ..... Human leukocyte antigen

HNSCC ..... Head and neck squamous cell carcinoma

HPV ..... Human papilloma virus

ICB ..... Immune checkpoint blockade

IFN ..... Interferon

Ig ..... Immunoglobulin

KNN ..... K-nearest neighbor

KS ..... Kolmogorov-Smirnov

MAST ..... Model-based Analysis of Single-cell Transcriptomics

MHC ..... Major histocompatibility complex

migDC ..... Migratory dendritic cell

Mm ..... Millimeter

MRI ..... Magnetic resonance imaging

mRNA ..... Messenger RNA

NK ..... Natural killer

NK_{cyto}-cell ..... Cytotoxic natural killer cell

NK_{infla}-cell ..... Inflammatory natural killer cell

NMF ..... Non-negative matrix factorization

NSCLC ..... Non-small cell lung cancer

PBMC ..... Peripheral blood mononuclear cell

PC(A) ..... Principal component (analysis)

PCR ..... Polymerase chain reaction

pDC ..... Plasmacytoid DC

PD-(L)1 ..... Programmed cell death protein (ligand) 1

PTM ..... Post-translational modification

RECIST ..... Response Evaluation Criteria In Solid Tumors

rRNA ..... Ribosomal RNA

scBCR-seq ..... Single-cell B-cell receptor sequencing

scRNA-seq ..... Single-cell RNA-sequencing

scTCR-seq ..... Single-cell T-cell receptor sequencing

T_{CM}-cell ..... Central memory T-cell

TCR ..... T-cell receptor

tdLN ..... Tumor-draining lymph node

T_{EM}-cell ..... Effector memory T-cell

T_{EMRA}-cell ..... Effector memory re-expressing CD45RA T-cell

T_{EX}-cell ..... Exhausted T-cell

T_{FH}-cell ..... Follicular helper T-cell

T_{H1}-cell ..... T-helper 1 cell

T_{H17}-cell ..... T-helper 17 cell

TIL ..... Tumor-infiltrating lymphocyte

TLS ..... Tertiary lymphoid structure

TME ..... Tumor microenvironment

T_N-cell ..... Naïve T-cell

T_{REG}-cell ..... Regulatory T-cell

T_{RM}-cell ..... Resident memory T-cell

UMAP ..... Uniform manifold approximation and projection

UMI ..... Unique molecular identifier

V(D)J ..... Variable-(diversity)-joining

Chapter 1

General introduction

The growing incidence of cancer cannot be overlooked as it affects daily lives, manifesting in the emotional, physical, and socioeconomic burdens associated with the disease and its management [1]. Fortunately, advancements in cancer therapies offer a promising outlook for treatment outcomes. One notable advancement involves immunotherapy, which entails the activation of the patient's own immune system to recognize and eliminate cancer cells. Considering the complexity of the tumor microenvironment (TME) and its interactions with the immune system, single-cell and spatial omics technologies capable of profiling *e.g.* the transcriptome and proteome of individual cells, are increasingly used, thereby delivering comprehensive insights into this field. In this dissertation, we profiled the microenvironment of head and neck cancer before and after immunotherapy through single-cell and spatial omics technologies. Thereby, we strive to understand the mechanisms underlying response to immunotherapy, specifically immune checkpoint blockade (ICB) therapy, and to ultimately find predictive biomarkers of response.

In the remainder of this chapter, we set the stage for the core of this dissertation. Our journey begins by introducing the role of the immune system in cancer evasion in Section 1.1. Based on this knowledge, ICB therapies have been introduced which will be addressed in Section 1.2. In Section 1.3, we consider head and neck cancer as a specific area of interest and highlight the challenges and opportunities associated with ICB therapies as compared to the standard of care. Moving forward, we discuss the single-cell omics technologies and analyses which we used to study the cell types residing in the TME in Section 1.4. Finally, in Section 1.5, we underline the value of these technologies in studying immunotherapy response and highlight the gaps in the existing literature that

were addressed by this work.

1.1 Oncology meets immunology

In 2000, Hanahan and Weinberg published "The Hallmarks of Cancer", a conceptual framework aimed at understanding the complex biology of cancer. This framework outlined six key capabilities, known as the hallmarks of cancer, that render cancer cells malignant. These include self-sufficiency in growth signals, resistance to anti-growth signals, evasion of cell death, infinite replicative potential, sustained blood supply, and the ability to invade tissue and metastasize [2]. However, alongside advancements in our comprehension, their 2011 update acknowledged that tumors encompass more than cancer cells alone. Instead, they recognized the coexistence of other cell types, including stromal cells (such as fibroblasts and endothelial cells (ECs)), and immune cells, collectively shaping the TME [3]. This holistic perspective of tumor biology necessitates the study of all cell types residing within the TME, surpassing the cell-autonomous properties of cancer cells. Over recent decades, research at the intersection of immunology and oncology has thrived, unveiling compelling evidence of immune cells' functionally effects on cancer progression. Historically, immune cells were already widely believed to efficiently eliminate cancer cells, a belief now gaining more support across diverse tumor types [4]. However, this concept has evolved, revealing its incompleteness and greater complexity than initially thought. In the context of the cancer-immunity cycle, the immune system plays a dual role, both antagonizing and promoting tumor development and progression [5]. Subsequently, recognizing the crucial role of the immune system, a new hallmark was proposed - the ability of cancer cells to evade immune destruction [3]. This nuanced understanding further emphasizes the interplay between the immune system and cancer biology.

1.1.1 The cancer-immunity cycle

The cancer-immunity cycle, illustrated in **Figure 1.1**, orchestrates a sequence of interactions vital for the effective elimination of cancer cells by the immune system. This dynamic process is carefully regulated to balance the recognition of abnormal cells and the prevention of autoimmune responses [5].

Triggered by cancer cells releasing damage-associated molecular patterns (DAMPs) or cancer neoantigens, marking them as "non-self" (*Step 1*), the innate immune response engages in rapid and nonspecific reactions orchestrated by myeloid cells and natural killer (NK) cells. This initiates downstream

maturation, activation, and subsequent cytotoxicity or phagocytosis of cancer cells, leading to an influx of immune cells and inflammation at the initial response site. Subsequently, as the immune response progresses, an adaptive immune response unfolds. This involves the capture of neoantigens by antigen-presenting cells (APCs) such as dendritic cells (DCs) and subsequent migration to tumor-draining lymph nodes (tdLN; *Step 2*). In the tdLN, APCs play a crucial role in priming and activating naïve T-cells (T_N-cells) to recognize the presented antigens through essential signals (*Step 3*), including antigen presentation on major histocompatibility complex (MHC; MHC class I presents to CD8+ T-cells, and MHC class II to CD4+ T-cells), co-stimulation, and favorable cytokine signaling (*e.g.*, activated conventional DCs produce IL-12 and type I interferon (IFN) during T-cell priming) [6]. Following priming and activation, central memory T-cells (T_{CM}-cells) undergo clonal expansion before transforming further into effector memory T-cells (T_{EM}-cells). Finally, T_{EM}-cells migrate via the blood (*Step 4*) to infiltrate the tumor (*Step 5*), where they recognize and target cancer cells for which they were primed (*Step 6*). Upon recognition, activated T-cells release cytolytic granules, inducing cancer cell death (*Step 7*) and initiating a new cycle with the release of cancer antigens. Recent insights reveal that, in addition to tdLNs, tertiary lymphoid structures (TLS) emerge as critical contributors to the cancer-immunity cycle, forming organized immune cell aggregates within the TME [5]. TLS serve as local hubs that facilitate the priming and activation of immune responses against cancer. These structures act as decentralized centers, fostering interactions between APCs, T-cells, as well as other immune cells, ensuring an efficient and localized immune response against cancer within the tumor itself. Thus, the original assumption that T-cell activation occurred only in tdLNs no longer seems correct.

Considering that the cancer-immunity cycle relies on a sequence of carefully regulated events to trigger an anti-tumor immune response, cancer cells may evade immune surveillance at different times, locations, and through various mechanisms. Cancer antigens might go unnoticed or DCs and T-cells could perceive these antigens as "self" rather than foreign. As a result, DCs can promote tolerance and trigger regulatory T-cell (T_{REG}-cell) responses instead of effector responses, opposing an antitumor response. Furthermore, T-cells may confront challenges in properly homing to tumors, encountering inhibitory factors in infiltrating the tumor, or facing crucial factors in the TME that suppress the generated effector cells. Immunotherapy serves as a strategic intervention, rebalancing the immune response and enhancing its ability to target and destroy cancer cells that might otherwise escape detection and elimination.

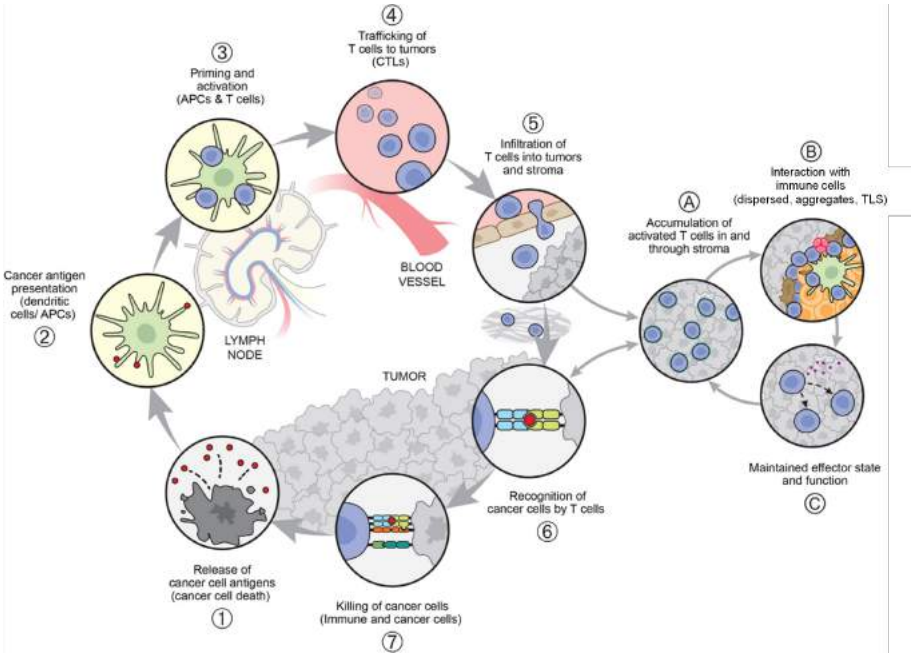

Figure 1.1: The cancer immunity cycle: an interplay between innate and adaptive immunity. Adapted from Demaria *et al.* [7]. APC: antigen-presenting cell, CTL: cytotoxic T-lymphocyte, TLS: tertiary lymphoid structures.

1.2 And then there were five

While surgery remains the cornerstone of curative cancer treatment, the development of alternative ways of eradicating cancer has contributed to a steady increase in survival rates of most cancer types. Chemo-, radio-, as well as targeted therapy are part of a multidisciplinary treatment approach. Individually and when utilized in combination, these four treatment modalities have collectively played a crucial role in the consistent rise of survival rates across various cancer types [8]. What these therapies have in common, is their direct targeting of cancer cells - whether through resection, radiation, chemical agents, or small-molecule drugs and monoclonal antibodies targeting specific cancer cell proteins. This direct approach can initiate selective evolutionary pressure, favoring subpopulations of cancer cells resistant to the therapy. Unfortunately, this often leads to the rapid onset of therapy resistance and subsequent tumor progression [9]. Currently, a fifth approach has joined this array of treatments - immunotherapy. The central goal of immunotherapy is to initiate or reinitiate a

self-sustaining cycle of cancer immunity, thereby engaging the immune system to evade cancer. Through this approach, the pressure on the tumor is indirect, and the anti-cancer immune response evolves in an inherently adaptive manner. Whereas the earliest case of cancer immunotherapy can be traced back to 1891, when William Coley treated cancer patients with mixtures of inactivated *Streptococcus pyogenes* and *Serratia marcescens* to provoke an anti-tumor immune response, these concepts did not see substantial progress for some time [10]. It wasn't until the groundbreaking work of researchers in ICB, including the 2018 Nobel Prize laureates James P. Allison and Tasuku Honjo who discovered cytotoxic T-lymphocyte-associated protein 4 (CTLA4) and programmed cell death protein 1 (PD-1) respectively, that immunotherapy gained renewed attention [11]. Today, there is a noticeable increase in interest among oncologists and oncology researchers to study immunotherapies and their combinations, highlighting the potential for groundbreaking advancements in cancer treatment. Clinicians currently have access to various immunotherapy modalities, and there are ongoing tests for several additional options [12]. These include antibody-based (*e.g.*, ICB therapy) and cell-based therapies (*e.g.*, chimeric antigen receptor (CAR) T-cell therapy), as well as anticancer vaccines. This dissertation focusses on the former, more specifically ICB targeting the PD-1/programmed cell death-ligand 1 (PD-L1) or CTLA4/CD80/CD86 pathways, depicted in **Figure 1.2**. The PD-1/PD-L1 axis stands as the most extensively targeted immunotherapy cascade across various cancer types, often combined with CTLA4 blockade or conventional anticancer therapies like chemotherapy and radiotherapy [13]. Some of these combinations have established themselves as the standard of care for several cancer types, with melanoma and non-small cell lung cancer (NSCLC) leading the way [14].

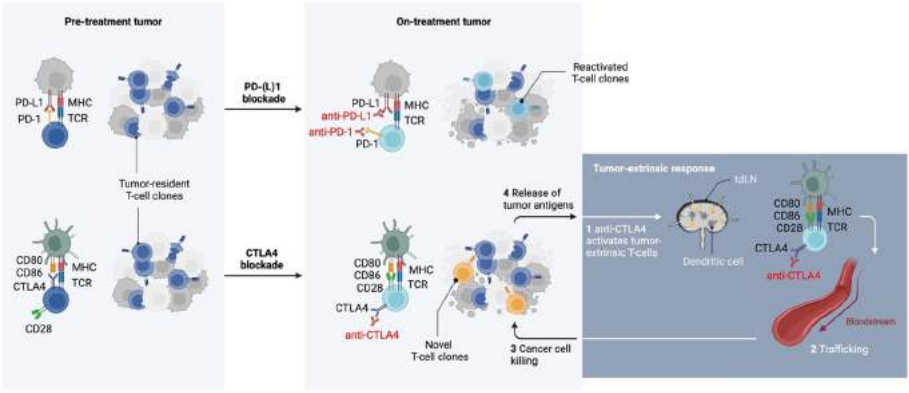

Figure 1.2: Anti-PD-(L)1 and anti-CTLA4 boost anti-tumor immunity by different mechanisms. Adapted from Yost *et al.* [15].

1.2.1 Programmed cell death (ligand) 1 (PD-(L)1)

During chronic infection or cancer progression, characterized by persistent exposure to inflammatory factors or antigens, the body introduces negative feedback loops to prevent an autoimmune response, where the immune system targets normal or healthy cells. Amongst other mechanisms, the upregulation of co-inhibitory checkpoints on T-cells gradually results in the loss of their effector functions, ultimately leading to dysfunction - a process known as 'exhaustion' [16]. One key inhibitory pathway involves the interaction between PD-1 on activated T-cells and PD-L1 on APCs, but also other cell types such as cancer cells. Thereby, the latter can exploit this pathway as a means of evading immune detection. Binding of PD-1 to PD-L1 results in inhibition of T-cell proliferation and activity, and thus provides a negative feedback loop to regulate the immune response (**Figure 1.2**) [17]. Studies have shown the ability of anti-PD-(L)1 (aPD-(L)1) monoclonal antibodies to promote T-cell responses, consequently boosting anti-tumor immunity and therapeutic efficacy [18].

1.2.2 Cytotoxic T lymphocyte-associated protein 4 (CTLA4)

While CTLA4 also functions as a co-inhibitory receptor and is upregulated upon T-cell activation, its impact can manifest at an earlier stage in immune responses. CTLA4 counteracts the activity of CD28, a costimulatory receptor which shares the same ligands - CD80 and CD86 - expressed on APCs [19]. CD28, constitutively expressed on T-cells, initiates T-cell activation through interaction with CD80/86, amplifying T-cell receptor (TCR) signals (**Figure 1.2**) [20]. Contrastingly, CTLA4 exhibits higher affinity for CD80/86, drastically diminishing T-cell activation [21]. This establishes a negative feedback loop regulating the immune response by impeding T-cell activation, proliferation, and cytokine production. Subsequently, anti-CTLA4 (aCTLA4) monoclonal antibodies enhance T-cell activation and immunological response to cancer [22].

As outlined above, the presence of tumor neoantigens and their presentation to immune cells within lymph nodes play an important role in initiating or enhancing an immune response. This raises the question whether neoadjuvant delivery, administered before tumor and/or lymph node resection, is more effective than adjuvant ICB in a curative setting. Moreover, investigating the efficacy of ICB in earlier disease stages might hold promise for optimizing surgical downstaging and even organ preservation. Notably, in several cancer types, a benefit has been reported from neoadjuvant ICB [23]–[27]. Additionally, targeting different checkpoints in the cancer-immunity cycle through combination therapy is an established strategy [28]. However, in

the neoadjuvant setting, evidence of a benefit from aCTLA4 combined with aPD-(L)1 is limited as many studies do not have a sufficiently large sample size to address this question. At this moment, it is not clear when to give combination therapy or which patients will benefit the most [13]. Shifting our focus to the specific context of head and neck squamous cell carcinoma (HNSCC), similar challenges are observed. Ongoing trials for neoadjuvant therapy in HNSCC predominantly adopt immunotherapy as the foundation, building on its success in recurrent and metastatic settings [29]. This underscores the importance of continuous research efforts to gain a deeper understanding of the most effective use of immunotherapeutic combinations.

1.3 Introduction to head and neck cancer

1.3.1 Historical perspective

Head and neck cancers rank as the seventh most common type of cancer globally [30], which accounts for approximately 900,000 cases and 400,000 deaths [31]. They comprise of a diverse group of tumors that develop in the upper aerodigestive tract. Among them, HNSCC are the most prevalent, accounting for 90% [32]. These carcinomas specifically arise from the mucosal linings of four major anatomical sites: the oral cavity, sinonasal cavity, pharynx, and larynx (**Figure 1.3**) [33]. The primary risk factors for HNSCC are tobacco use, alcohol abuse, and exposure to oncogenic viruses such as human papillomavirus (HPV) and Epstein-Barr virus [34].

1.3.2 Treatment and prognosis

The management of HNSCC is depending on both, the site and stage of the disease [33]. Over the past decades, notable advancements have been made in surgical techniques, radiotherapy strategies, and targeted therapies (mostly epidermal growth factor receptor (EGFR) inhibition). Despite these advances, the prognosis of HNSCC remains poor. More than 60% of patients still present with locally advanced stage III or IV disease, characterized by local invasion and/or involvement of regional lymph nodes [33]. Even with multimodal tumor-directed standard treatments (including surgery, chemotherapy, radiotherapy, and/or targeted therapy) for locally advanced disease with curative intent, half of the patients experience relapse within two years [33]. Furthermore, the 5-year overall survival rate for patients with recurrent or metastatic HNSCC is less than 50% [33]. Adding to the difficulty, these treatment modalities often have a

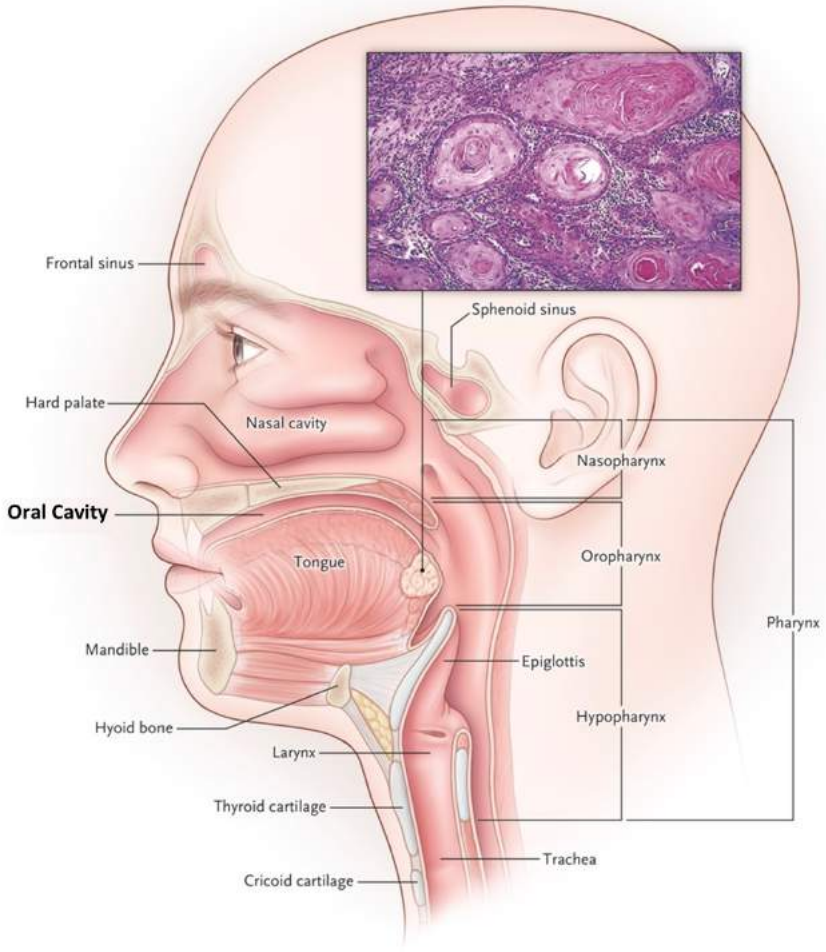

Figure 1.3: Major anatomical sites of Head and neck squamous cell carcinomas (HNSCC), as presented by Chow *et al.* [33].

profound negative impact on patients' quality of life [33]. Given the complex anatomy and physiological role of the aerodigestive tract, treatment incentives are not only focused on improving survival outcomes but also encompass the preservation of organ function.

In the last decade, immunotherapy has revolutionized the oncological treatment paradigm, including for HNSCC. Notably, FDA-approved drugs such as

nivolumab and pembrolizumab (both aPD-1) showed a clear survival advantage in patients with recurrent or metastatic HNSCC. This advantage was observed in both second and first-line settings when compared to the standard of care, offering more durable responses and fewer adverse events [35]–[39]. The combination of aPD-L1 with aCTLA4 was also tested, both in first- and second-line treatment, but failed to demonstrate benefit compared to aPD-L1 alone [40]–[42]. In the locally advanced setting, however, promising rates of improved response after combined aPD-1 plus aCTLA4 versus aPD-1 monotherapy have been observed [43], [44]. Although there was clear evidence of response in both arms, the combination performed slightly better: Schoenfeld *et al.* reported pathologic downstaging in 69% (n=15) versus 53% (n=14); Response Evaluation Criteria In Solid Tumors (RECIST) response in 38% versus 13%; and pathologic response in 73% versus 54% of patients, respectively [43]. Similarly, Vos *et al.* reported a major pathological response in 35% of patients (n=6) after aPD-1 plus aCTLA4 versus 17% (n=26) after aPD-1 monotherapy [44]. This raises the questions whether the addition of aCTLA4 to aPD-(L)1 would be more effective when administered during the earlier stages of cancer development. This could stem from the less immunosuppressive nature of the TME in these tumors compared to metastatic or recurrent tumors [45], and/or from the neoadjuvant administration before tumor and lymph node resection. A deeper evaluation of the TME before and after ICB is needed to study mechanisms of response.

1.4 Multi-omics: towards a comprehensive tumor profile

Multi-omics, as an explorational approach encompassing various levels of biology, such as the genome, transcriptome, and proteome, emerges as a pivotal step in gaining a comprehensive understanding of ICB therapy responses [46]. By integrating data from different levels of biological regulation, it is possible to gain a more holistic understanding of how genes are transcribed into RNA and translated into proteins. Every level individually offers distinct advantages in unraveling the complexities of biological systems such as the TME. Human cells, originating from the same genome, undergo modifications such as mutations due to random chance or exposure to carcinogens [47]. Genomics enables the comprehensive exploration of an organism's genetic makeup, revealing critical variations in DNA sequences. Transcriptomics, on the other hand, unveils the active genes and RNA expression patterns, providing a better understanding of cellular phenotypes and processes [48]. While ribosomal RNA (rRNA) or transfer RNA (tRNA) play essential roles in cellular functions, messenger RNA

(mRNA) is usually the primary focus. It represents the transcribed genetic information that codes for proteins and allows researchers to gain insights into the actively transcribed genes and understand the diversity of gene expression patterns across individual cells. Additionally, the proteome, encompassing a cell's translated proteins, has gained value as a diagnostic and prognostic tool across various tumor types [49]. Unlike genome and transcriptome sequencing, which may not conclusively unveil a cell's functional or activation state, proteins offer direct insights into essential biological processes, ranging from cell-cell communication to immune diversity and intratumoral heterogeneity. While there is notable correlation between transcriptome and proteome level measurements for some species and under certain conditions, such alignment is not universal. This lack of universality stems from the prevalence of post-transcriptional and post-translational regulations in cells, which introduce complexities and variations [49]. In the following sections, we will focus on the technologies and subsequent computational analyses which were used in this dissertation, as depicted on **Figure 1.4**.

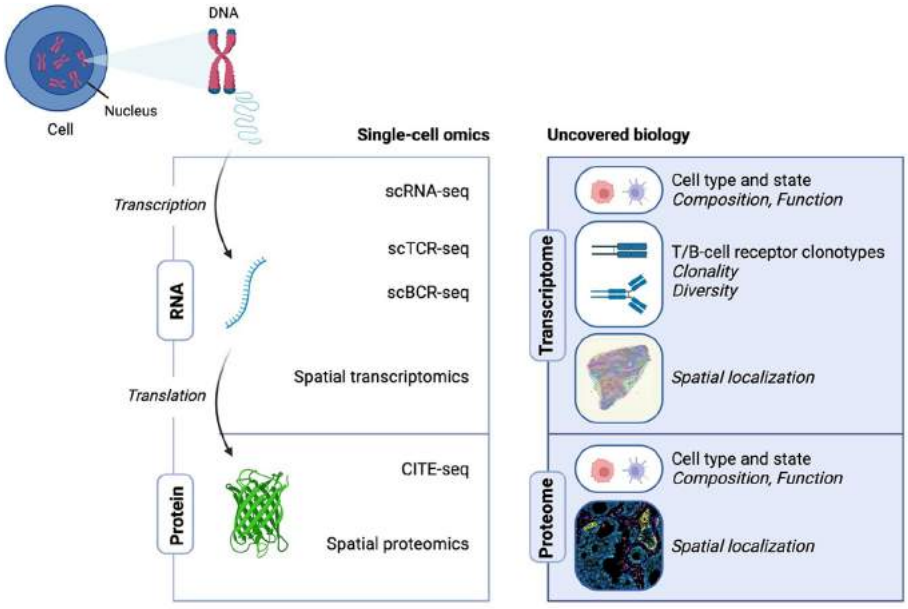

Figure 1.4: Single-cell omics technologies to characterize the transcriptome and proteome of a cell. ScTCR-seq: single-cell T-cell receptor sequencing, scBCR-seq: single-cell B-cell receptor sequencing, CITE-seq: cellular indexing of transcriptomes and epitopes by sequencing.

1.4.1 Unraveling cellular diversity with single-cell technologies

The invaluable power of single-cell analysis - examining individual cells – compared to bulk analysis has been acknowledged for decades [50], evident in the essential role played by immunohistochemistry, *in situ* hybridization, and flow cytometry in exploring variances between normal and cancer cells. Despite their historical value, these traditional methods possess inherent constraints. They often detect only a restricted number of analytes per experiment or test [50], limiting their ability to discern the full spectrum of cellular subtypes and states within the TME. However, in recent years, technologies have advanced tremendously to study tumors in more depth. Nowadays, a considerable fraction of the transcriptome can be measured for thousands of cells at once, making it possible to study gene expression at large scale [51]. This evolution has enabled a more profound dissection of the TME through precise monitoring of cell (sub)type profiles and abundances. After tumor dissociation, individual cells are retrieved for subsequent sequencing. Whereas bulk RNA-sequencing measures the gene expression of all cells collectively, the output will be the average gene expression across all cells derived from a sample. Consequently, it is impossible to distinguish cell types or to know from which cell a certain gene expression profile is derived [50]. **Single-cell RNA-sequencing (scRNA-seq)**, on the other hand, is created to profile single cells separately. This way, one can distinguish cell types in a sample based on its individual expression profile (**Figure 1.5**) [50].

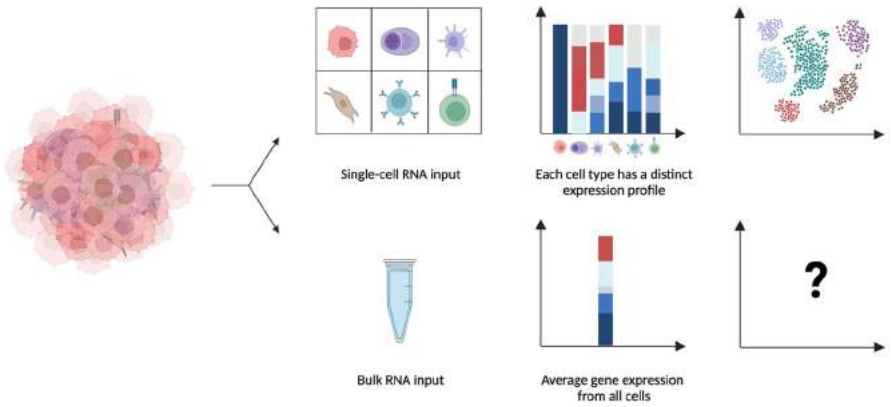

Figure 1.5: Single-cell technologies reveal cellular heterogeneity that is masked by bulk methods. Adapted from Clark *et al.* [52].

Several methods exist to do so, such as the Chromium™ system (10x Genomics®) which unlike traditional methods employs a droplet-based technique to isolate

individual cells and process their genetic material in a high-throughput manner (**Figure 1.6**) [53]. Each droplet contains a barcode (cell identifier), a unique molecular identifier (UMI), and a poly dT sequence, facilitating precise cell identification and transcript quantification for the encapsulated cell. Simultaneously, enzymes, including reverse transcriptase, are included in the droplets to facilitate reverse transcription, converting cellular mRNA into copy DNA (cDNA). The resulting barcoded cDNA is then amplified by polymerase chain reaction (PCR) and the cDNA library is prepared for Illumina sequencing. Briefly, cDNA strands are fragmented into shorter, uniform pieces and end-repaired by adding a complementary nucleobase to pair with the Illumina adapter, ensuring compatibility with the Illumina sequencing platform. Following this, a sample index PCR is performed on these libraries, enabling the pooling of multiple samples for sequencing. Reads are annotated based on their assigned index, allowing the identification of their respective sample origins. Illumina sequencing proceeds utilizing the bridge amplification principle, where cDNA strands are anchored to a flow cell's surface through their Illumina adaptors, initiating local "bridge" amplification to form clusters. Subsequently, fluorescently labelled deoxynucleotide triphosphates (dNTPs) are iteratively added, resulting in robust base calls for each cDNA fragment.

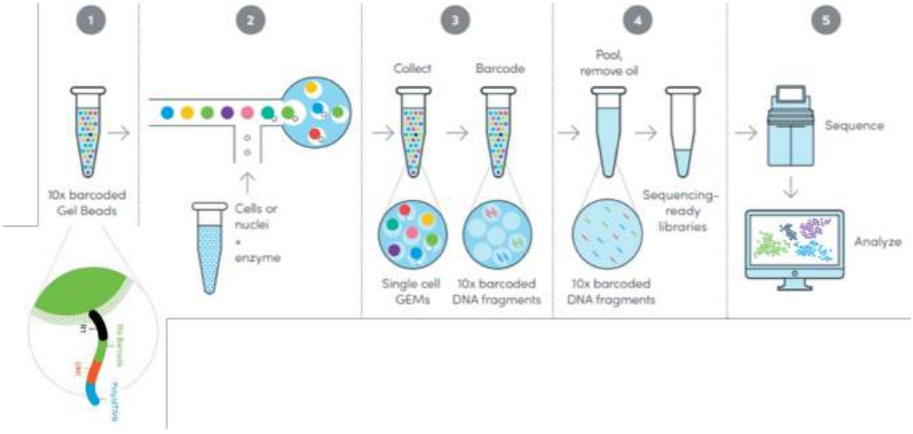

Figure 1.6: The 10x Genomics® Chromium™ system for single-cell RNA sequencing. Adapted from 10x Genomics [54].

Following scRNA-seq experiments, a multi-step computational analysis ensues (**Figure 1.7**) [51]. It begins with aligning sequencing data to a reference genome (here, the human reference genome), yielding a count matrix which depicts the expression levels of genes across individual cells. Quality control measures are then applied to the raw count matrix to exclude cells that could introduce noise or confounding factors. In this manner, subsequent computational analysis

focusses on high-quality, biologically meaningful data. Removal criteria typically include cells with low gene counts (indicative of empty droplets), high gene counts (suggestive of doublets), or aberrant expression patterns (such as elevated mitochondrial gene expression, which may indicate cell stress or damage). Following this, the count matrix undergoes normalization to facilitate a more accurate cellular profile comparison, correcting for variations in gene counts due to cell size or sequencing depth. Gene expression data are then scaled to have a mean of zero and a variance of one, ensuring equitable weighting across all genes, thus enhancing comparability between genes and facilitating the selection of informative ones. While these corrections aim to remove count sampling effects, additional biological and technical variates, such as cell cycle effects, can be regressed out to uncover the underlying biological signal. Moreover, integration techniques can be employed to address potential batch effects, *e.g.* arising from technical differences between samples, safeguarding the integrity of downstream analyses.

To further reduce data noise, alleviate computational burden, and aid data visualization, the dataset's dimensionality is subsequently reduced by selecting only the most variable genes. Next, principal component analysis (PCA) further reduces dimensions by constructing components as linear combinations of gene expression data. This reduction paves the way for K-nearest neighbor graph-based clustering, where cells with similar RNA expression patterns are clustered. To further explore and visualize the data in a two-dimensional space, non-dimensionality reduction techniques like Uniform Manifold Approximation and Projection (UMAP) are used. In subsequent analyses, cells are annotated based on canonical marker genes. Depending on the research questions, further steps may involve testing cell (sub)type abundance, exploring differential gene expression, and conducting gene set enrichment analyses. Trajectory inference can also unveil dynamic processes by pseudotemporal ordering of cells based on gene expression levels.

Similarly, scRNA-seq can be combined with immune receptor profiling by **single-cell T-cell receptor and B-cell receptor sequencing (scTCR-seq and scBCR-seq)**, through selective enrichment of the TCR or BCR region of the amplified cDNA (**Figure 1.8**) [51]. The adaptive immune receptor repertoire is critical for the identification and binding of "non-self" or tumor-specific antigens and unravels insights into the adaptive immune system's response to it. During the early stages of T- and B-cell maturation, V(D)J (variable-(diversity)-joining) recombination takes place, whereby different variable (V) segments are rearranged with diversity (D) and joining (J) segments. This process results in a diverse repertoire of TCRs and immunoglobulins/antibodies in T- and B-cells respectively, enabling recognition of a wide range of epitopes [55]. V(D)J sequencing followed by alignments and chain pairing can identify these

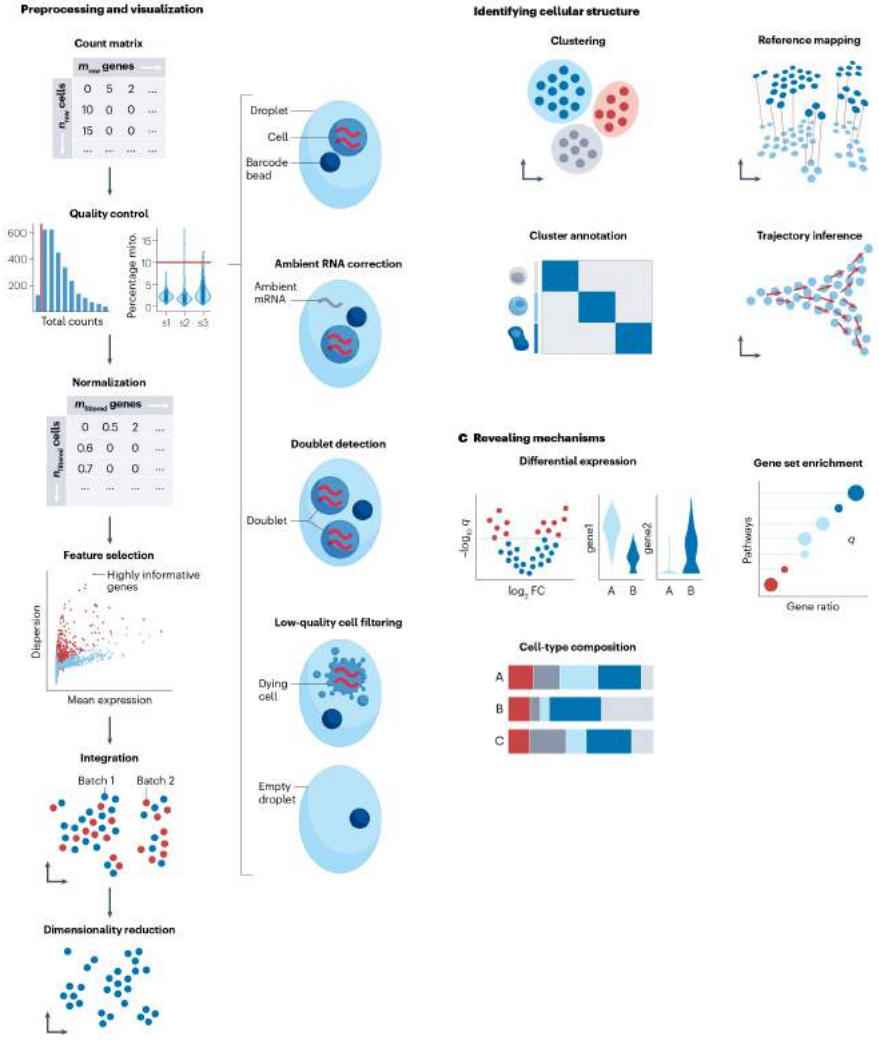

Figure 1.7: Overview of computational analysis steps for single-cell RNA-sequencing data analysis [51]. FC: fold change.

sequences. Measures of clonality and diversity are typically used to study immune responses [56]. Without encountering an antigen, the immune repertoire has diverse receptors and few dominant clones. When faced with a recognized antigen, cells with activated receptors expand, reducing overall diversity but increasing the clonality of specific responding cells. The combined use of scRNA-

seq and scT/BCR-seq is a particularly effective approach for studying both the phenotypic and functional characteristics of T- and B-cells.

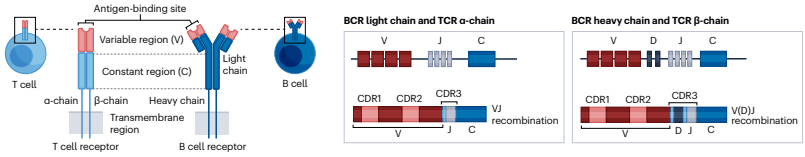

Figure 1.8: Overview of the adaptive immune receptor analysis of T- and B-cells [51]. BCR: B-cell receptor; TCR: T-cell receptor; D: diversity; J: joining; CDR1/2/3: complementarity-determining region 1/2/3.

While transcripts can be relatively easily profiled, offering the potential to yield genome-scale information, the comprehensive profiling of all proteins within a cell poses a bigger challenge. In fact, the entire repertoire of proteins cannot yet be assessed. The human genome is currently estimated to harbor fewer than 20,000 protein-coding genes [57], whereas the total number of human protein products, including splice variants and essential post-translational modifications (PTMs), has been estimated at over one million [58]. Within this dissertation, **cellular indexing of transcriptomes and epitopes by sequencing (CITE-seq)** was performed to simultaneously quantify mRNA and a subset of cell surface proteins in individual cells. Before undergoing scRNA-seq processing, cells are incubated with uniquely barcoded TotalSeq™-A antibodies, facilitating the labeling of the desired cell surface proteins. This technique allows for the simultaneous evaluation of single-cell transcriptomic and proteomic information, providing a notable advantage by enabling protein detection in situations of limited RNA abundance. Consequently, it enhances confidence in identifying specific markers within a given cell type and contributes to its subsequent annotation.

1.4.2 Spatial technologies enable profiling of cells within their tissue context

While single-cell technologies have enhanced our ability to investigate the biological processes within tumors, thanks to their increased throughput and resolution, they come at the cost of losing the spatial localization during single-cell dissociation. In contrast, spatial technologies introduce an additional layer of information, allowing the study of the TME in its native context. An immune-excluded tumor illustrates the importance of not only identifying the function and abundance of cell (sub)types, but also understanding their spatial distribution and intercellular interactions within the TME. While scRNA-seq

will reveal the presence of various cell (sub)types within the sample, the crucial information that some of these cells are unable to infiltrate the tumor bed is lost. **Spatial transcriptomics**, on the other hand, retains the native spatial context of gene expression. Therefore, analyzing the spatial context becomes essential to decipher the unique characteristics of tumors, *e.g.* offering insights into specific dynamics hindering immune cell penetration into the tumor.

Various technologies are available, each with its own set of advantages and disadvantages. For this dissertation, Visium (10x Genomics®) was used, an array-based technology which generates unbiased spatial gene expression data albeit at limited resolution of 55 µm spots (comprising $\sim 1 - 10$ cells/spot; **Figure 1.9**) [59]. Unlike 10x scRNA-seq, Visium technology does not require tissue dissociation. Instead, tissue sections are placed on a slide with barcoded spots. The RNA is subsequently captured locally using spatially barcoded probes, converted to cDNA, and subjected to sequencing. This facilitates the tracing of gene expression data through x and y coordinates that correspond to the spatial locations where RNA was captured. To approach single-cell resolution and gain information about cell (sub)type composition per spot, different deconvolution algorithms exist to calculate the abundance probability of a certain cell (sub)types based on gene expression levels. SPOTlight [60], for instance, is based on a non-negative matrix factorization (NMF) regression framework and leverages the strengths of both scRNA-seq and spatial transcriptomics data to infer the location of cell (sub)types. It compares observed gene expression patterns in spatial transcriptomics data with predefined signatures of gene expression specific to different cell (sub)types derived from scRNA-seq data. The core of its functionality lies in predicting the proportion of each cell (sub)type's presence in each spatial spot. The final output is a visual representation that provides researchers with insights into the detailed spatial distribution of inferred cell types within the analyzed biological sample.

Whereas spatial transcriptomics captures a snapshot of the RNA molecules present within a tissue at a specific point in time, it does not encompass protein degradation, protein-to-protein interactions, or post-translational modifications. These aspects are better characterized by **spatial proteomics** and prove especially valuable in the development of therapies and diagnostic tools [49]. PhenoCycler™ (Akoya Biosciences®) is an imaging-based technology to measure single-cell protein expression in space, enabled by multiplex immunofluorescence (**Figure 1.10**) [62]. The advantages of this technology are single-cell resolution and the potential to increase the multiplex capabilities of spatial analysis to a level of up to 100 marker proteins. All specific marker-antibodies are conjugated to a unique DNA oligonucleotide barcode and a fluorophore, making it possible for all antibodies to remain bound until the end of the experiment. Every cycle, up to three fluorophores can be imaged, followed by fluorophore removal. There

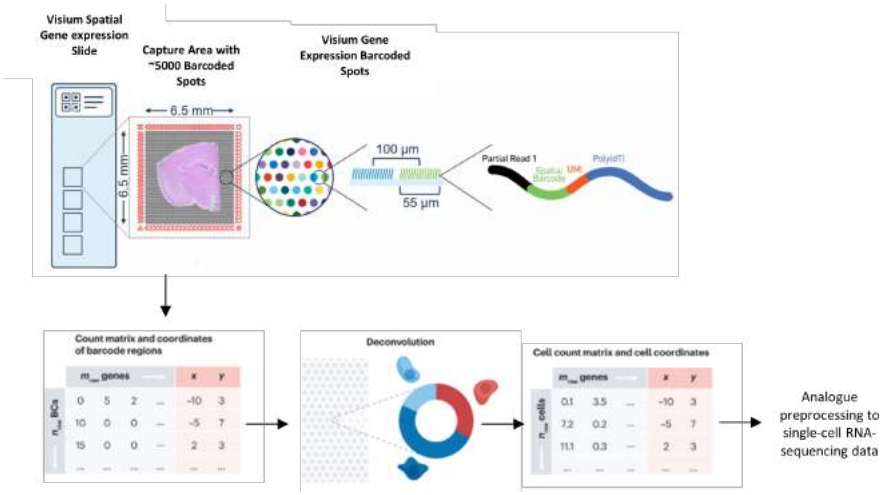

Figure 1.9: The Visium (10x Genomics®) technology for spatial transcriptomics and downstream analysis. Adapted from 10x Genomics [61] and Heumos *et al.* [51]. UMI: unique molecular identifier.

is no need for antibody stripping between cycles, which circumvents the tissue to be damaged.

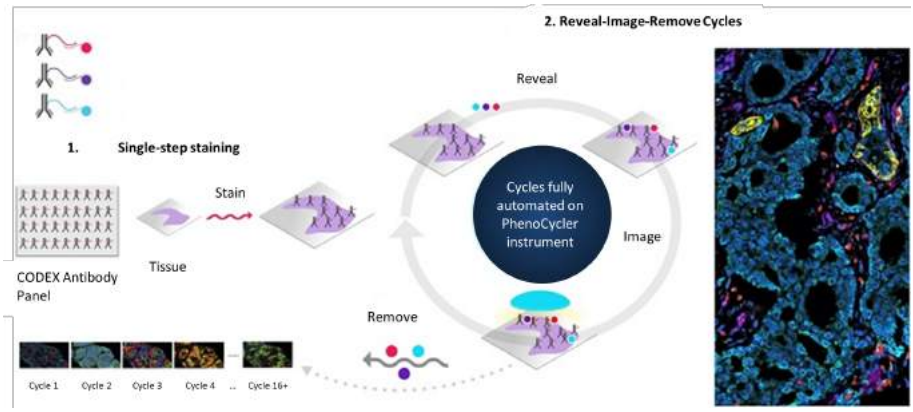

Figure 1.10: The workflow steps of the PhenoCycler™ (Akoya Biosciences®) technology [62].

Describing the single-cell and spatial characteristics of the TME offers valuable insights, but understanding the functions and clinical implications of these

findings is the next crucial step in unraveling mechanisms of ICB response. To address these questions, integrating single-cell and spatial technologies into clinical trials with ICB offers insights in a real-world human setting, allowing the evaluation of treatment effects by examining changes during treatment.

1.5 Immune checkpoint blockade response: insights from single-cell and spatial analyses

The role of the TME in ICB response has been increasingly investigated by single-cell and spatial technologies [63]. Evidence shows how the functional orientation, abundance, and location of cells in the TME play a critical role in the clinical response of cancer patients.

In the context of **aPD-(L)1** response, a recurrent observation is the presence of a pro-inflammatory TME already before treatment initiation, which suggests that aPD-(L)1 reinvigorates pre-existing T-cells [15]. This TME can consist of various immune cell types, including CD4+ T-helper 1 (T_{H1}), CD4+ follicular helper (T_{FH}), CD8+ T_{EM}, and CD8+ exhausted (T_{EX}) T-cells, as well as myeloid cells expressing T-cell homing factors (CXCL9/10) [64]–[67]. Additionally, the organization of these immune infiltrates within intratumoral TLS together with follicular B-cells has been associated with ICB response in various tumor types [66], [68]–[71]. The positive impact of these structures on anti-tumor immunity is likely attributed to the creation of a favorable niche. This environment facilitates T-cells in acquiring their functional roles by fostering increased contact between immune cells, thereby ensuring the swift initiation of an immune response. However, counterbalancing this perspective, accumulating evidence points toward the involvement of a secondary, systemic response mechanism. In mice, activation and proliferation of T-cells in tdLNs and peripheral blood was observed following aPD-1 treatment [72]. The latter was similarly observed in human subjects [24]. Additionally, the identification of exhaustion as an irreversible epigenetic state raises questions about the possibility of inducing a *de novo* immune response in later stages to sustain the anti-tumor immune response [73].

Building on this knowledge, various genes associated with an anti-tumor immune response have emerged as predictive biomarkers. These encompass ICB targets, cytokines, chemokines, and genes involved in neoantigen presentation and immune-related pathways. *PD-L1 expression* was the first biomarker used in clinics to predict aPD-1 response, demonstrating a positive correlation with ICB responsiveness in several cancer types [63]. This correlation can be explained in the context of a pro-inflammatory TME, as PD-L1 can be induced through

immunological signaling pathways, such as IFN signaling [74]. Similarly, IFNγ-signatures and MHC molecules have shown promise as biomarkers. MHC molecules provide insights into the immunogenicity of cancer cells. While the downregulation of MHC class I antigen peptide complexes by cancer cells serves as a mechanism to evade the immune system, MHC class II expression is increasingly being detected on cancer cells and postulated to mediate anti-tumor activity via cytotoxic CD4+ T-cells [75]. However, the predictive value of these biomarkers is variable, likely attributable to the considerable intratumor heterogeneity and absence of spatial context.

The integration of spatial information with the capability to measure the expression levels of multiple genes and/or proteins presents a valuable source of predictive biomarkers, exemplified by the *spatial density* of T cells within the TME. Spatial measurements not only provide insights into spatial relationships but also reveal co-localized expression of various markers, offering highly informative data. For instance, the spatial density of PD-1/PD-L1 has demonstrated the ability to predict responses to aPD-1 therapy [76], potentially surpassing the predictive capabilities of other biomarkers like PD-L1 and gene expression signatures.

With regards to **aCTLA4** mono- or combination therapy, it is less clear which TME characteristics define response. Given that the anti-tumor responses induced by aPD-1 and aCTLA4 operate through distinct cellular mechanisms, it is anticipated that different biomarkers will be predictive [77]. Specifically, aCTLA4 is expected to induce a *de novo* peripheral or systemic effect by acting on a lymph node resident population of CD4+ T-cells. However, despite insights gained from mouse studies, no clear predictive biomarkers have yet emerged from human studies. In mice, it was demonstrated that aCTLA4 primes T_N-cells in lymph nodes, which subsequently migrate to the tumor and undergo clonal expansion [18]. Beyond its early function, CTLA4 is constitutively expressed on T_{REG}-cells and can be upregulated by various T cells, notably CD4+ T cells, post-activation [78], [79]. T_{REG}-cells are expected to suppress anti-cancer T-cells, but the extent to which aCTLA4 depletes T_{REG}-cells remains uncertain [80], [81]. In a recent study comparing neoadjuvant aPD-1 *versus* aPD-1 plus aCTLA4 in HNSCC patients, the response to both ICB treatments was attributed to tumor-infiltrating CD8+ T-cells exhibiting a tissue-resident memory program (T_{RM}; *ITGAE+/ZNF683+/GZMB+*) [82], [83].

Several questions regarding ICB response remain unanswered. The precise location of ICB-mediated T-cell activation - whether it occurs within the tdLNs, tumor, and/or TLS - requires clarification. Additionally, understanding the timing of clonal replacement is crucial for unraveling the dynamics of the immune response. While existing scientific analyses have predominantly centered on T-cell responses, it is imperative to broaden the scope of investigation to include

non-T-cell components within the TME. Profiling these elements concurrently with tumor-specific T-cells, and considering their spatial co-localization, is essential for a comprehensive understanding of the factors influencing anti-tumor immunity.

1.5.1 Window-of-opportunity trials

To study the mechanisms of response to ICB, window-of-opportunity trials are especially valuable. The time between the diagnosis of a medical condition (such as cancer) and the initiation of the standard treatment (such as surgery), referred to as a "window of opportunity", allows to explore the effects of an experimental treatment (such as ICB) on the disease or to gather additional information about the biological processes involved in a real-world clinical setting. Here, neoadjuvant studies offer an optimal setting to investigate response predictors and mechanisms of response, because of the availability of paired samples before and after treatment. Early neoadjuvant trials already identified immune responses to aPD-(L)1 and aCTLA4 at 4-6 weeks post therapy [84], demonstrating that the immunological activity of immunotherapies occurs early in patients.

In the following chapters, we show how we leveraged single-cell and spatial omics technologies within the framework of a window-of-opportunity trial. This facilitates comprehensive investigations into the mechanisms underlying response to ICB mono- *versus* combination therapy, ultimately advancing the identification of robust predictive biomarkers.

Chapter 2

Research Objectives

Immunotherapy has made remarkable advancements in the field of cancer treatment. It has led to clinical improvements, including extended life spans, enhanced quality of life, and even instances of complete remission. A critical limitation, however, is the varying efficacy of immunotherapy across patients. Durable clinical responses are only observed in a small fraction of patients, and we are currently unable to accurately predict a patient's response upfront. This lack of predictability may entail non-responding patients enduring severe immune-related side effects of the therapy and losing valuable time before exploring alternative treatments that might prove more effective. Fortunately, there is potential to augment the clinical benefits of immunotherapy by developing combination therapies, with numerous ongoing clinical trials dedicated to this pursuit. Nonetheless, the challenge frequently arises from the lack of a clear scientific rationale for these combinations. A deeper understanding of the mechanisms governing the response to immunotherapies could provide the knowledge needed for making more informed decisions about the strategic combination of therapies.

The **central goal** of this doctoral research project was to comprehensively characterize immunotherapy response within the context of a neoadjuvant clinical trial, thereby comparing aPD-L1 monotherapy *versus* aPD-L1 combined with aCTLA4. Tumor biopsies, tdLNs, and peripheral blood samples were prospectively collected from patients with locally advanced HNSCC before and/or after one cycle of aPD-L1 or aPD-L1 plus aCTLA4. Subsequently, these samples were subjected to single-cell omics technologies to profile the cellular heterogeneity of the TME, *i.e.* scRNA-seq, scT/BCR-seq, CITE-seq, spatial transcriptomics, and spatial proteomics.

In the **short term**, this approach allowed us to closely monitor the early changes in the TME during the administration of ICB therapy at an unprecedented level of detail, thereby providing valuable insights into the mechanisms underlying response to mono- or combination therapy in HNSCC patients. In the **long term**, this knowledge holds potential to identify more informative predictive biomarkers for early ICB response. Moreover, these findings could influence clinical decision-making, paving the way for personalized therapy tailoring in cancer patients to optimize efficacy.

Chapter 3

Methodology & materials

Adapted and edited from:

> A. Franken, M. Bila, A. Mechels, S. Kint, J. Van Dessel, V. Pomella, S. Vanuytven, G. Philips, O. Bricard, J. Xiong, B. Boeckx, S. Hatse, T. Van Brussel, R. Schepers, C. Van Aerde, S. Geurs, V. Vandecaveye, E. Hauben, V. Vander Poorten, S. Verbandt, K. Vandereyken, J. Qian, S. Tejpar, T. Voet, P. M. Clement, D. Lambrechts, "CD4+ T cell activation distinguishes response to anti-PD-L1+anti-CTLA4 combination therapy from aPD-L1 monotherapy", Immunity (2024), 57: 541-558.

In this chapter, we describe the methodology and materials employed in our study, building upon the technologies and study design introduced in Sections 1.4 and 1.5.1.

3.1 Experimental model and study participant details

3.1.1 Patients

A single center, window-of-opportunity phase I/II study named DUTRELASCO (DUrvalumab with or without Tremelimumab in REsectable Locally Advanced Squamous cell Carcinoma of the Oral cavity) was set up and approved by the local medical ethics committee of the University Hospitals Leuven

(NCT03784066; S60379). The prospective study was conducted according to EU legislation regarding ethical regulations and was registered online (2017-000577-36). All 20 patients provided written informed consent. Only patients with a newly diagnosed resectable locally advanced HNSCC of the oral cavity were included. All patients were HPV-negative, as assessed by PCR-based genotyping using DNA isolated on the formalin-fixed paraffin-embedded (FFPE) blocks. Patients were treated with a single dose of 1500 mg durvalumab alone (aPD-L1; arm A; n=10) or 1500 mg durvalumab combined with 75 mg tremelimumab (aCTLA4; arm B; n=10) 14 days before surgery and 6 cycles adjuvant (**Figure 3.1**). Tumor shrinkage was evaluated by magnetic resonance imaging (MRI) at the time of therapy onset and two weeks after start of treatment.

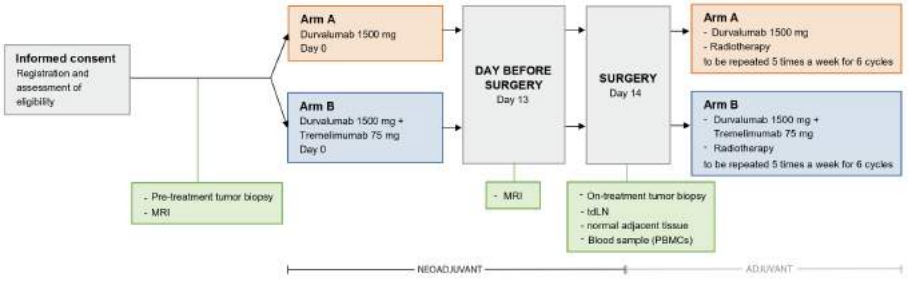

Figure 3.1: DUTRELASCO CONSORT diagram.

3.2 Method details

3.2.1 Sample collection and processing

Fresh tumor tissue was harvested at diagnosis (pre-treatment), and during surgery (on-treatment). Up to 20 pairs of matched pre- and on-treatment tumor biopsies were collected, in addition to blood (n=16), normal adjacent tissue of the oral cavity (n=16), and tdLNs (n=17) at the time of surgery. TdLNs (levels I to IV in case of nodal status N0/N1, or I to V in case of nodal status N2) were removed from the ipsilateral side of the neck and pathologically staged to confirm absence of cancer cells. Adjacent tissue was required to be more than 0.5 cm away from the tumor and defined as being free of disease morphology at the discretion of the pathologist. From each patient enough tissue was sampled to both, assess standard histopathology after fixation with formalin and embedding it in paraffin, and perform scRNA-seq. For the latter, tissue samples were immediately subjected to single-cell dissociation on ice; first mechanically,

using a scalpel, and subsequently enzymatically in digestion medium (2 mg/mL Collagenase P (Sigma Aldrich) and 0.2 mg/ml DNAse I (Roche) in Dulbecco's Modified Eagle Medium (DMEM; Thermofisher scientific)). Red blood cells were removed from the cell suspension using red blood cell lysis buffer (Roche), and cells were filtered using a 40 µm Flowmi tipstrainer (VWR). Next, the number of living cells were determined using a LUNA automated cell counter (Logos Biosystems). Peripheral blood mononuclear cells (PBMCs) were extracted from on-treatment blood samples using SepMate tubes (Stemcell Technologies) and Histopaque-1077 density gradient medium (Sigma). Cells were stored at -80°C (in fetal bovine serum (FBS)+10% dimethylsulfoxide (DMSO)). When PBMC samples were thawed, DMEM was added and cells were filtered using a 40 µm Flowmi tip strainer (VWR) and the number of living cells was counted again using a LUNA automated cell counter (Logos Biosystems) using AO/PI Cell viability kit (Westburg).

3.2.2 Single-cell RNA/TCR/BCR and CITE-sequencing

We performed single-cell TCR-seq, BCR-seq, 3' and 5' gene expression profiling on the same single-cell suspension using the Chromium™ Single Cell V(D)J Solution from 10x Genomics according to the manufacturer's instructions. Up to 5,000 cells were loaded on a 10x Genomics cartridge for each sample. Cell-barcoded 5' gene expression libraries were sequenced on an Illumina NextSeq or/and NovaSeq6000, and mapped to the GRCh38 human reference genome using CellRanger (10x Genomics, v3). V(D)J enriched libraries were sequenced on an Illumina HiSeq4000 PE 300 cycles and TCR/BCR alignment and annotation was achieved with CellRanger VDJ (10x Genomics). Additionally, TotalSeqA-based CITE-seq was performed as described before [65].

3.2.3 Cell (sub)clustering, abundance testing, and gene expression analysis

Raw gene expression matrices were analyzed using the Seurat v4 R package [85]. All cells expressing < 200 or > 6000 genes were removed, as well as cells that contained < 400 UMIs and $> 15\%$ mitochondrial counts. Samples were merged and log normalized. Default parameters of Seurat were used, unless mentioned otherwise. Briefly, for the clustering of all cell types, 2000 variable genes were identified and principal component analysis (PCA) was applied to the dataset to reduce dimensionality after regressing for percentage mitochondrial DNA. The 20 most informative principle components (PCs) were used for clustering and UMAP [61], [62] reduction. Clusters in the resulting two-

dimensional UMAP representation consisted of distinct cell types, which were identified based on the expression of marker genes. Differentially expressed genes that functionally characterized the clusters were defined by the Model-based Analysis of Single-cell Transcriptomics (MAST) test implemented in the FindAllMarkers function from Seurat. To subcluster cell types from different scRNA-seq technologies (5' *versus* 3'), we used the canonical correlation analysis (CCA)-integration pipeline of Seurat. Importantly, following CCA, 5'- and 3'-scRNA-seq data were combined to cluster and annotate cell clusters, but all downstream analyses (*e.g.*, abundance, gene expression, and T-cell expansion analyses) were solely performed on the 5'-scRNA-seq data while using the scaled RNA data assay. We regressed for the following confounding factors: number of UMIs (counts), percentage of mitochondrial RNA, and individual samples. For T-cell subclustering, additional regression for IFN response and cell cycle score was needed since failure to regress for it revealed a cluster driven by high IFN or cell cycle signaling respectively, which consisted of multiple heterogeneous T-cell (both CD4+ and CD8+) subclusters which makes it difficult to annotate them accurately. An IFN response score was calculated by the *AddModuleScore* function in Seurat using the gene set BROWNE_INTERFERON_RESPONSIVE_GENES from the Molecular Signatures Database or MSigDB v6.2. S and G2M scores calculated by the *CellCycleScoring* function in Seurat. Similarly for myeloid cells, regression for hypoxia was necessary. The score was calculated based on the hypoxia-associated gene signature from Zhang *et al.* [86] (*VEGFA, PGAM1, ENO1, LDHA, TPI1, P4HA1, MRPS17, ADM, NDRG1, TUBB6, ALDOA, MIF, SLC2A1, CDKN3, ACOT7*). For B-cell subclustering, variable genes of the BCR (IGLVs, IGKVs, IGHVs) were excluded to avoid somatic hypermutation associated variances.

To circumvent the limitation of sample sizes and the need to divide patients into discrete groups, we performed a spearman correlation between relative cell (sub)type abundances or gene expression levels and the number of expanded T-cell clonotypes per patient. This allowed us to leverage the scRNA-seq and scTCR-seq data in a continuous axis, thereby detecting positive and negative correlating patterns among cell (sub)type abundance or gene expression profiles and T-cell expansion in all patients. Per sample, the cellular proportions of subclusters were calculated as their relative fraction within the respective cell type.

To identify tissue-specific subpopulations, we performed compositional analysis between T-cell subclusters from tdLNs and tumor tissue (both, pre- and on-treatment), using a tool for differential abundance testing on k-nearest neighbor (KNN) graph neighborhoods, implemented in the R package miloR (v1.6.0) [87].

With regards to gene expression analyses, genes with less than 10 reads in total were filtered out from the correlation analysis. Differentially expressed genes

were identified using the MAST test with *FindMarkers* and *FindAllMarkers* functions in Seurat without a threshold for logFC and for expression in a minimum fraction of cells. The R package hypeR was used for GSEA on genes correlating with T-cell expansion. For this analysis the GO:BP ('C5') gene sets were used from the MSigDB v6.2 and were exported using the R package GSEABase. Only significant genes (Bonferroni-adjusted p-value<0.05) and genes with a correlation coefficient r higher than 0.5 were used. Additional scores were calculated by the *AddModuleScore* function in Seurat using the respective gene set. Scores for pro-inflammatory and anti-inflammatory myeloid cells were based on gene signatures from Martinez *et al.* [88].

3.2.4 Assessing the TCR and BCR repertoire using V(D)J analysis

Since every cell has a unique barcode, scRNA-seq data could be linked with the scTCR-seq and scBCR-seq data. By scTCR-seq, we identified TCR alpha and beta chain sequences for 82,832 of the 99,058 (83.62%) T-cells annotated by scRNA-seq. We only considered productive T/BCRs, meaning that they could be joined in the proper reading frame by V(D)J recombination without premature stop codons, enabling expression of paired chains for downstream analysis (IGH and IGL/IGK for BCRs, TRA and TRB for TCRs). T/BCR clonotypes were defined as T/BCRs with the same complementarity-determining region 3 (CDR3) nucleotide sequences for TCRs or V gene usages for BCRs. T-cell clonality was calculated per sample by using the STARTRAC (v0.1.0) R package [89]. The clonotype equality of a sample was measured by the Gini coefficient, as calculated by the Gini() function from the DescTools package, where zero expresses perfect equality and one expresses maximal inequality among clonotypes.

When examining the TCR sequences of T-cell clonotypes pre- and on-treatment, we considered a clonotype undergoing expansion when *i*) there was an increase in proportion (*i.e.*, frequency normalized for number of cells in a sample with a TCR detected) on- *versus* pre-treatment and *ii*) a frequency on-treatment > 2. The number of expanded clonotypes upon treatment defined by these criteria was calculated per patient. Clonotypes not detected pre-treatment, but clonal on-treatment (frequency > 2) were also considered as expanded clonotypes. For differential gene expression analysis, an increase in proportion on- *versus* pre-treatment and a frequency on-treatment > 2 was used to define expanding T-cells. The same critera were used to define expanding B-cell clonotypes, while only considering cells containing both, scRNA-seq and scBCR-seq data. This was done to prevent the inclusion of signals captured after non-specific binding

of scBCR-seq primers, as suggested by the lower overlap between scBCR-seq and scRNA-seq data (53.33%).

TCR sharing was calculated as the number of unique TCRs shared between sample types (exact CDR3 nucleotide match). Data were visualized using the ggalluvial R package. Whereas the stacked bar graphs represent the relative proportion of T-cell subclusters with unique shared TCRs within the respective sample type (pre-treatment tumor, on-treatment tumor, tdLN or PBMCs), the horizontal splines (alluvia) represent the shared TCRs between the different sample types.

3.2.5 Trajectory inference analysis

The R package Slingshot [90] was used to explore pseudotime trajectories/potential lineages in CD4+ T-cells. CD4+ $T_{N/CM}$-cells were considered as the root state when calculating trajectories and the pseudotime. CytoTRACE [91] was used within the CellRank [92] workflow to validate the results retrieved from Slingshot, by giving each cell a score according to their differential status (a higher score reflects a higher differential potential).

To investigate potential differences across the trajectories between treatment arms (aPD-L1 *versus* aPD-L1/aCTLA4) or sample types (pre- *versus* on-treatment tumor samples), density plots were created from the ordered pseudotime distributions (scaled from 0 to 100). To determine whether pseudotime distributions differed at the end of the trajectories between treatment arms or sample types, a Kolmogorov-Smirnov (KS) test was performed while only considering the terminal subcluster of interest (CD4+ T_{H1}, CD8+ T_{EX}, or CD8+ T_{RM}).

3.2.6 Spatial transcriptomics

Tissue preparation and sectioning was performed according to 10x Genomics recommendations (Visium Spatial Protocols – Tissue Preparation Guide, CG000240, RevC). After dissection, tissue was washed with 1x DPBS and snap-frozen in liquid nitrogen chilled isopentane. Frozen samples were embedded in chilled optimal cutting temperature compound and immediately transferred to dry ice and stored in −80ºC until further use. 10 µm sections were cut in a cryostat at −20ºC and immediately placed onto the Visium Spatial Gene Expression Slide in the cryostat. Slides containing sections were stored at -80ºC for a maximum of 1 week before use.

Fixation, staining, imaging, and construction of cDNA libraries was done according to the manufacturer's instructions (Visium Spatial Gene Expression User Guide_Rev D; 10x Genomics, CG000239) using the Visium Spatial Gene Expression Slide & Reagent Kit (10x Genomics, Cat#PN-1000184). Briefly, sections were fixed in chilled methanol for 30 minutes at -20ºC and hematoxylin and eosin (H&E) stained, followed by imaging on a Nikon-Marzhauser Slide Express 2 whole-slide scanner at 10x magnification. Subsequently, sections were permeabilized for 24 minutes at 37ºC, as determined using the Visium Spatial Tissue Optimization Slide & Reagent Kit (10x Genomics, PN-1000193) following the manufacturer's instructions (Visium Spatial Gene Expression Reagent Kits - Tissue Optimization_Rev A, 10x Genomics, CG000238). After permeabilization, on-slide reverse transcription was performed at 53ºC for 45 minutes, followed by on-slide second strand synthesis for 15 minutes at 65ºC. All on-slide reactions were performed in a thermocycler (Bio-rad, C1000 Touch) with a metal slide adapter plate (10x Genomics). Following second strand synthesis, samples were transferred to tubes for cDNA amplification, clean-up, and library preparation. cDNA and library quality was assessed using an Agilent Technologies Bioanalyzer High Sensitivity kit (Agilent Technologies, Cat#5067-4626). Visium libraries were sequenced on Illumina NextSeq2000. The sequencing depth was determined by the amount of Visium spots covered by tissue (50.000 reads per spot). The overall organization of each tumor and presence and localization of mononuclear infiltrates were first annotated by a trained pathologist after H&E staining of the sections.

The FASTQ files were processed using Space Ranger (10x Genomics, v1.1.0) in manual alignment mode with the GRCh38-3.0.0 reference genome. The filtered gene-barcode matrices obtained were filtered for spot barcodes with fewer than 300 genes and/or 500 detected UMIs, as well as genes with fewer than 10 counts and/or detected in fewer than 5 spots. The Seurat v4 R package was subsequently used with default parameters to perform log-normalization, dimensionality reduction (using the top informative principal components determined by bootstrapping), and clustering. To map expanded and non-expanded T-cells back to their spatial coordinates, we applied CellTrek [93] to our spatial transcriptomics dataset while using the differentially expressed genes of these cells from the scRNA-seq data as a training set. Subsequently, spots were annotated as expanded, non-expanded, or random, based on the presence of expanded T-cells, non-expanded T-cells, or the absence of both, respectively. To then quantify the difference in gene expression between annotated spots, a Wilcoxon test was used.

To study the TME spatially, we deconvoluted spatial transcriptomics spots into proportions of different cell types using SPOTlight [60]. To train the model, markers genes for each cell type were obtained from the scRNA-seq data using

the MAST test implemented in the *FindAllMarkers* function from Seurat and Bonferroni adjusted. The probability of cell type co-location was calculated by multiplying the proportion of the respective cell types per spot.

3.2.7 Spatial proteomics

The PhenoCycler-Fusion platform (Akoya Biosciences) was used to perform single-cell spatial protein profiling of HNSCC FFPE slides. Six tissue sections (10 µm thick) from six different patients included in the DUTRELASCO study were stained with a 62-plex antibody panel and the standard protocol was followed for coverslip preparation, tissue staining, and imaging in accordance with PhenoCycler manufacturer instructions (Akoya Biosciences User Manual, Revision-C).

Computational image analysis involved DAPI-based cell segmentation using StarDist extension (0.5 µm) [94] after QPTIFF files were imported in QuPath (v0.4.2) [95]. Subsequently a model was trained in QuPath to annotate cells adequately based on the combination of key immune markers, including proliferating (Ki67+) CD4+ and CD8+ T-cells (CD3+), T_{H1} cells (CD3+ CD4+ Tbx21+), activated (CD40+) DCs (CD68+ CD11c+), B-cells (CD79a+ or CD20+), and plasma cells (CD138+). A data matrix containing the cell (sub)type annotation as well as the x and y coordinates was exported from QuPath and further manipulated in R to calculate inter-cellular distance using the kdist() function from the R package CellTrek [96].

3.2.8 Quantification and statistical analysis

All statistical analyses were performed using GraphPad Prism 9. All comparisons between two groups were performed using either a two-tailed unpaired Student's t-test or Mann-Whitney test, depending on the normality of distribution. Gene expression correlation analyses and TCR sharing analyses were Bonferroni corrected for the number of genes or T-cell phenotypes compared, respectively. When analyzing a small number of samples, more precisely to compare treatment arms for the number of shared TCRs expressed by expanded T-cells across tissue compartments, a Fisher's exact test was performed.

Chapter 4

Results

Adapted and edited from:

> A. Franken, M. Bila, A. Mechels, S. Kint, J. Van Dessel, V. Pomella, S. Vanuytven, G. Philips, O. Bricard, J. Xiong, B. Boeckx, S. Hatse, T. Van Brussel, R. Schepers, C. Van Aerde, S. G., V. Vandecaveye, E. Hauben, V. Vander Poorten, S. Verbandt, K. Vandereyken, J. Qian, S. Tejpar, T. Voet, P. M. Clement, D. Lambrechts, "CD4+ T cell activation distinguishes response to anti-PD-L1+anti-CTLA4 combination therapy from aPD-L1 monotherapy", Immunity (2024), 57: 541-558.

This chapter presents the results obtained after applying the methodology and materials described in Section 3, with a focus on distinguishing the mechanisms between combined therapy with aCTLA4 and aPD-L1 from aPD-L1 monotherapy in HNSCC.

Single-cell profiling before and after one dose of immune checkpoint blockade

Patients with locally advanced HNSCC of the oral cavity were treated with a single dose of durvalumab (aPD-L1; arm A; n=10) or durvalumab combined with tremelimumab (aPD-L1/aCTLA4; arm B; n=10) 14 days before surgery, as part of a window-of-opportunity phase I/II study (DUTRELASCO, NCT03784066; **Figure 3.1**). A first tissue biopsy was harvested at diagnosis (pre-treatment), while a second biopsy was harvested during surgery (on-treatment). 20 pairs of matched pre- and on-treatment tumor biopsies were collected, in addition

to blood (for PBMCs; n=17), adjacent tissue of the oral cavity (n=16) and tdLNs (n=17) at the time of surgery. All 90 tissue samples were digested into a single-cell suspension and unbiasedly processed for 5'-scRNA-seq and immune repertoire profiling (scTCR-seq and scBCR-seq). Additionally, when sufficient tissue was available (n=23), we subjected cells to 3'-scRNA-seq and TotalSeqA. We combined 5'- and 3'-scRNA-seq data from all tissues to cluster and annotate cells. All downstream analyses were performed using 5'-scRNA-seq data alone, while TotalSeqA alongside 3'-scRNAseq data were only used to confirm gene expression data at protein level. Overall, we obtained 313,626 cells by 5'-scRNA-seq with on average expression of 1,055 genes/cell. Based on marker genes, we identified several cell type clusters, which could be assigned to immune cell populations, ECs, fibroblasts, muscle, and epithelial cells (**Figure 4.1A**).

T-cell expansion as a surrogate for early treatment response

Since patients received a single dose of ICB prior to undergoing surgery, we could not consider RECIST or pathological complete response at surgery as measures of treatment response, as they are typically determined after multiple cycles of ICB treatment. However, since T-cell clonotype expansion after one dose of ICB translates into clinical response based on RECIST after multiple cycles of ICB treatment [97]–[100], we used clonotype expansion as a surrogate of response. All T-cell clonotypes with a TCR frequency > 2 in on-treatment tumor samples were considered and T-cell expansion was quantified as the number of clonotypes that proportionally increase when comparing on- *versus* pre-treatment samples [65]. A positive correlation between T-cell expansion and radiologic tumor shrinkage after one cycle of ICB was observed ($r = 0.759$, $p < 0.001$; **Figure 4.1B**). A high percentage of T-cells pre-treatment did not predict T-cell expansion on-treatment ($r = 0.416$, $p = 0.068$), while also tumor-infiltrating lymphocyte (TIL) scores by histopathology did not correlate with expansion ($r = 0.427$, $p = 0.080$; data not shown). Interestingly, 49,27% of clonotypes on-treatment (range between patients: 0-81%) were not detected pre-treatment, which could be due to sampling bias (because pre- and on-treatment biopsies are taken from different tumor regions) or the recruitment of novel clonotypes during treatment. T-cell expansion was tumor-specific, as the number of clonotypes in normal adjacent tissue was low and did not correlate with those detected in tumors ($r = -0.109$, $p = 0.749$; **Figure 4.1C**). When performing differential gene expression analysis comparing expanding *versus* non-expanding T-cells in on-treatment tumors, we observed increased expression of cytotoxicity/T-cell activation (*IFNG, PRF1, GNLY, GZMA/B/H/K, NKG7*) and immune cell homing markers (*CCL3/4/5, CCL4L2, CXCL13*) in expanding T-cells, but lower expression of naïve (*IL7R, LEF1, CCR7, SELL*) and immune

regulatory (*FOXP3, TNFRSF4*) markers (**Figure 4.1D**). These differences support the notion that T-cell expansion reflects ongoing immune responses upon ICB.

Subsequently, we explored which cells in tumor biopsies express the molecules targeted by aPD-L1 or aCTLA4. As expected, *CD274* (PD-L1) was predominantly expressed by epithelial cells and a subset of myeloid cells, while its receptor *PDCD1* (PD-1) was confined to T-cells (**Figure 4.1E**). Likewise, *CTLA4* was predominantly expressed by T-cells, while its ligands *CD80* (B7-1) and *CD86* (B7-2) were confined to myeloid cells (**Figure 4.1E**). When analyzing both treatment arms separately, *PDCD1* expression by T-cells in pre-treatment biopsies was not correlated with T-cell expansion upon aPD-L1 monotherapy ($r = 0.109$, $p = 0.765$), but its specific expression in CD8+ T-cells did correlate with expansion ($r = 0.936$, $p < 0.001$; **Figure 4.1F**). *CD274* expressed on myeloid and epithelial cells was also correlated with T-cell expansion, albeit not significantly ($r = 0.584$, $p = 0.082$). In the aPD-L1/aCTLA4 arm, both *CD274* and *CD80* on myeloid cells correlated with T-cell expansion ($r = 0.829$, $p = 0.005$ and $r = 0.896$, $p < 0.001$, respectively; **Figure 4.1G**). The observed correlations for both *CD274* and *CD80* suggest that the PD-1 and CTLA4 pathways were both effectively targeted in the combination arm.

CD4+ T-cell expansion is enhanced upon aPD-L1/aCTLA4 versus aPD-L1

To assess which T-cell subclusters expanded upon treatment, we subclustered intra-tumor T-cells 6 CD4+ and 5 CD8+ subclusters based on marker gene expression, as described previously (**Figure 4.2A**) [17]. We observed that T_N-cells (CD45RA+/CD45RO-) and T_{CM}-cells (CD45RA-/CD45RO+) clustered together either as CD4+ or CD8+ $T_{N/CM}$-cells, as confirmed at protein level by analyzing 3'-scRNA-seq and TotalSeqA data (**Figure 4.2B**). We also identified CD8+ T_{EM} (*GZMK+/EOMES+*), T_{RM} (*ZNF683+/ITGA1+*), T_{EX} (*PDCD1+/GZMB+*), and effector memory re-expressing CD45RA (T_{EMRA}; *FCGR3A+/CX3CR1+*) T-cell subclusters, whereas in the CD4+ compartment T_{REG} (*FOXP3+/IL2RA+*), T_{EM} (*CD44+/IL7R+*), T_{H1}-cells (*TBX21+/PDCD1+*), T-helper 17 (T_{H17}-cells; *RORC+/IL17A+*), and T_{FH} *(BCL6+/CXCR5+*) cell subclusters were detected.

Pre-treatment, expanded T-cells predominantly belonged to CD8+ T_{EM}-(45.21%), T_{RM}- (19.33%), and T_{EX}-cell (6.54%) subclusters in the aPD-L1 arm. On-treatment, they mapped to similar T-cell subclusters (49.38%, 23.88%, 11.50%, respectively), although a small subset also consisted of CD4+ T_{H1}-cells (4.50%; **Figure 4.2C**). In the aPD-L1/aCTLA4 arm, although the same CD8+ T-cell subclusters expanded as in the aPD-L1 arm, CD4+ T-cell subclusters

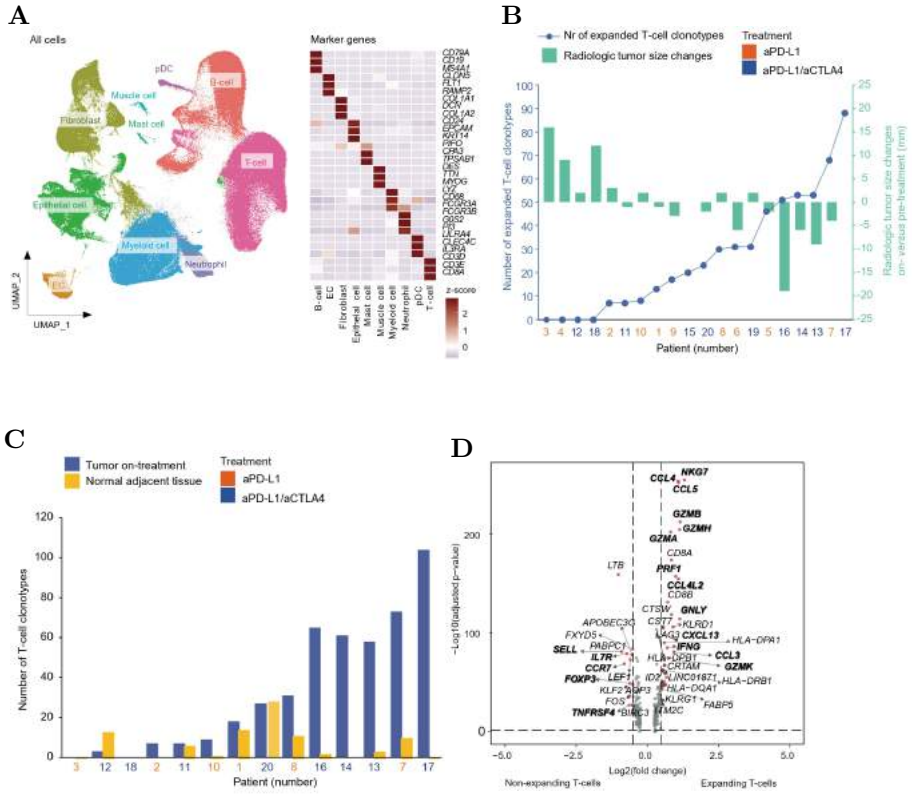
A
All cells
pDC
B-cell
Muscle cell
Fibroblast
Mast cell
T-cell
Epithelial cell
Myeloid cell
Neutrophil
Endothelial cell
UMAP_2
UMAP_1
Marker genes
B-cell
EC
Fibroblast
Epithelial cell
Mast cell
Muscle cell
Myeloid cell
Neutrophil
pDC
T-cell
z-score
B
Nr of expanded T-cell clonotypes
Radiologic tumor size changes
Treatment
aPD-L1
aPD-L1/aCTLA4
Number of expanded T-cell clonotypes
Radiologic tumor size changes on- versus pre-treatment (mm)
Patient (number)
C
Tumor on-treatment
Normal adjacent tissue
Treatment
aPD-L1
aPD-L1/aCTLA4
Number of T-cell clonotypes
Patient (number)
D
-Log10(adjusted p-value)
Log2(fold change)
Non-expanding T-cells
Expanding T-cells
NKG7
CCL4
CCL5
GZMB
GZMH
GZMA
CD8A
LTB
PRF1
CCL4L2
CD8B
CTSW
GNLY
CST7
KLRD1
APOBEC3C
LAG3
CXCL13
FXYD5
HLA-DPA1
PABPC1
IFNG
SELL
IL7R
HLA-DPB1
CCL3
CCR7
CRTAM
GZMK
FOXP3
LEF1
ID3
LINC01871
HLA-DRB1
KLF2
S1PR1
HLA-DQA1
FOS
KLRG1
FABP5
TNFRSF4
BIRC3
TM2C
E
PDCD1
CD274
Min
Max
CTLA4
CD80
CD86

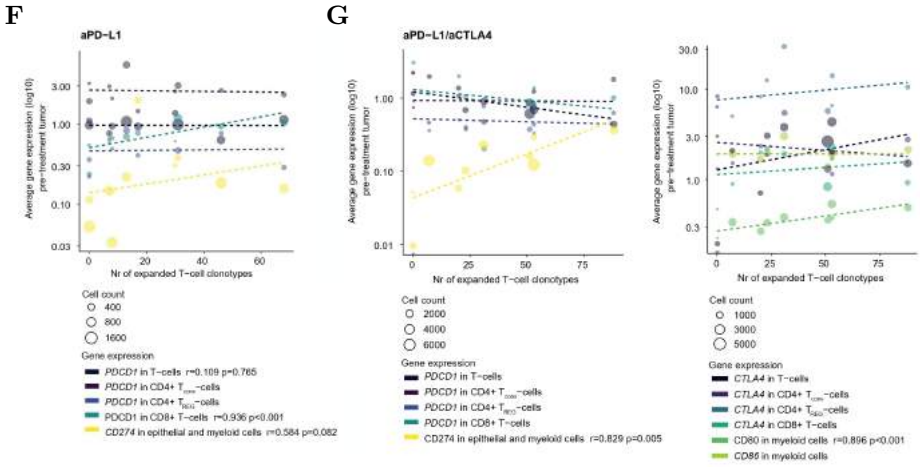

Figure 4.1: Single-cell profiling before and after one dose of immune checkpoint blockade

(A) UMAP and heatmap depicting clustering of main cell types derived from 5'-scRNA-seq data of tissue samples (tumors pre- and on-treatment biopsies, tdLNs, and normal adjacent tissues; 313,626 cells), based on their marker gene expression. **(B)** Radiological tumor size changes (mm: millimeter; green) compared to the number of expanded T-cell clonotypes in on- versus pre-treatment tumor biopsies (increase in proportion and on-treatment frequency >2) after one cycle of treatment per patient (blue) upon aPD-L1 (orange) and aPD-L1/aCTLA4 (blue). **(C)** The number of T-cell clonotypes (frequency >2) in the tumor biopsy on-treatment (blue) compared to normal adjacent tissue (yellow) per patient. **(D)** Volcano plot depicting differentially expressed genes (red dots: $p<0.05$ and absolute log2(fold change)≥ 0.5, gray dots: p=non-significant) between expanding T-cells (n=4,837) and non-expanding T-cells (n=75,118). Bonferroni-adjusted P-values by MAST (Model-based Analysis of Single-cell Transcriptomics) test and were. **(E)** Density plots showing *PDCD1* (PD-1), *CD274* (PD-L1), *CTLA4*, *CD80*, and *CD86* expression across all cells. **(F-G)** Spearman correlation between the average expression of the indicated gene in a cell (sub)type and the number of expanded T-cell clonotypes per patient from the aPD-L1 arm (F) and aPD-L1/aCTLA4 arm (G). EC: endothelial cell, pDC: plasmacytoid dendritic cell.

accounted for a larger proportion of expanding clonotypes both pre- and on-treatment (36% and 31%, respectively; **Figure 4.2C**). When analyzing patients covering >90% of expanding TCRs (expanders; n=6 for both treatment arms), we noticed that on-treatment 28.18% of expanding T-cells represented CD4+ T-cells in the aPD-L1/aCTLA4 arm (*versus* 19.13% in the aPDL1 arm; p = 0.044). Interestingly, expanding CD4+ T-cells in pre-treatment biopsies from the aPD-L1/aCTLA4 arm mainly consisted of poorly differentiated CD4+ T-cell phenotypes, *i.e.* CD4+ $T_{N/CM}$-cells (22.83% of expanding CD4+ T-cells), whereas on-treatment, we observed an increase in expanding CD4+ T_{EM}- and T_{H1}-cells (16.50% and 48.54%, respectively).

Subsequently, we used Slingshot [90] and CytoTRACE [91], two independent tools to infer trajectories from pseudotime ordered single-cell data. We hereby focused on reconstructing trajectories involving the subclusters that contain expanding T-cells. Particularly, we reconstructed a CD4+ T_{H1} trajectory, starting from CD4+ $T_{N/CM}$-cells, connected to T_{EM}-cells and followed by T_{H1}-cells as terminal state (**Figure 4.2D**). Likewise, CD8+ trajectories were constructed, starting from CD8+ $T_{N/CM}$-cells, connected to CD8+ T_{EM}-cells and branching into CD8+ T_{EX}-cells and T_{RM}-cells, as reported previously [65]. These trajectories were supported by marker gene expression along pseudotime and increased TCR sharing between subsequent subclusters (data not shown). Next, to explore whether T-cell phenotypes in tumors changed upon treatment, we visualized the proportion of shared TCRs between subsequent T-cell subclusters according to these trajectories. We observed that pre-treatment CD4+ $T_{N/CM}$-cells shared more TCRs with on-treatment CD4+ T_{EM}- and T_{H1}-cells upon aPD-L1/aCTLA4 *versus* aPD-L1 alone. Particularly, this was observed in expanders ($p < 0.05$ after Bonferroni-adjustment for all subcluster comparisons; see boxed T-cell subclusters on **Figure 4.2E**), but not in non-expanders (covering <10% of expanding TCRs; n=4; data not shown). Notably, although the proportion of these shared TCRs was small, 80% of them represented an expanding clonotype upon aPD-L1/aCTLA4, while none were expanded upon aPD-L1 ($p = 0.008$; **Figure 4.2E**), suggesting that expansion of CD4+ $T_{N/CM}$-towards T_{EM}- or T_{H1}-cells was induced by the combination treatment. In both treatment arms, we observed substantial TCR sharing on-*versus* pre-treatment between T_{REG}-cells, but this was unlikely to be driven by T-cell expansion since very few T_{REG}-cells had expanded on-treatment in both treatment arms (**Figure 4.2E**). We performed a similar analysis comparing proportions of shared TCRs between CD8+ T-cell subclusters along the different trajectories. However, this did not differ significantly between treatments arms for any of the CD8+ T-cell subclusters compared (**Figure 4.2E**).

Finally, to confirm that CD4+ T-cell activation varied between treatment arms, we calculated T-cell density distributions along the CD4+ T_{H1} trajectory. In on-

treatment tumors, CD4+ T-cells clearly shifted towards the end of the trajectory after aPD-L1/aCTLA4, but not aPD-L1 ($p < 0.001$ for Slingshot; **Figure 4.2F**, and CytoTRACE trajectories (data not shown)). This was confirmed by comparing expanded CD4+ T-cells between on- *versus* pre-treatment biopsies, demonstrating significant differences in the aPD-L1/aCTLA4 ($p < 0.001$), but not the aPD-L1 arm ($p = 0.954$). In contrast, in the CD8+ T_{EX} and T_{RM} trajectories, no differences in T-cell density in on-treatment tumors were observed between treatment arms ($p = 0.273$ and $p = 0.226$, respectively), while also the comparisons of expanded CD8+ T-cells in on- *versus* pre-treatment tumors were not significant, neither for aPD-L1 nor aPD-L1/aCTLA4 ($p = 0.112$ and $p = 0.923$ for T_{EX}-, $p = 0.166$ and $p = 0.448$ for T_{RM} trajectories). Overall, this confirms increased T-cell activation along the CD4+ T_{H1} trajectory upon aPD-L1/aCTLA4, whereas for CD8+ T-cells the T_{EM}-, T_{RM}-, and T_{EX}-cell subclusters expanded, but did not seem to shift towards a more differentiated T-cell phenotype, neither upon aPD-L1 nor aPD-L1/aCTLA4.

The pre-treatment T-cell landscape predicts expansion upon aPD-L1, but not aPD-L1/aCTLA4

Next, we analyzed whether the relative abundance of T-cell subclusters was associated with T-cell expansion. We found that pre-treatment CD8+ T_{EM}-, T_{RM}-, T_{EX}-, and CD4+ T_{H1}-, T_{FH}-cell abundances were all significantly correlated with T-cell expansion upon aPD-L1 ($p < 0.05$; **Figure 4.3A**). These subclusters contained the majority of expanding T-cells and expressed the highest levels of *PDCD1* (**Figure 4.2A**, consistent with the notion that inhibition of PD-1 signaling on T-cells fosters their expansion. *Vice versa*, CD4+ $T_{N/CM}$-cells correlated negatively with expansion ($p = 0.004$). In addition to cell type abundance, we also explored which genes expressed in all T-cells were associated with T-cell expansion. Pre-treatment expression of T-cell activation/cytoxicity (*IFNG, GZMB, NKG7, HLA-DPB1*) and B-cell homing (*CXCL13*) markers correlated with T-cell expansion (**Figure 4.3B**. These genes were all highly expressed by the subclusters positively associated with T-cell expansion (**Figure 4.3B**. Overall, given the fact that both CD4+ T_{H1}- and various effector CD8+ T-cell subclusters correlated with expansion, our results indicate the presence of a pre-existing type 1 immune response in patients with T-cell expansion upon aPD-L1 [101].

In contrast, in the aPD-L1/aCTLA4 arm, associations between relative abundance of T-cell subclusters and T-cell expansion revealed few significant associations. Only CD8+ T_{EX}-cells correlated positively with expansion, albeit not significantly ($p = 0.058$; **Figure 4.3A**. Also at gene expression level, no

genes involved in T-cell mediated immunity were significantly correlated with expansion (**Figure 4.3B**, suggesting that, in contrast to aPD-L1 alone, a pre-treatment TME characterized by a type 1 immune response may not be crucial for aPD-L1/aCTLA4 to induce anti-tumor immunity.

On-treatment, correlations with T-cell expansion were similar between aPD-L1 *versus* aPD-L1/aCTLA4 (**Figure 4.3A**, as both CD8+ T_{EX}- ($p = 0.015$ and $p = 0.038$, respectively) and CD4+ T_{H1}-cell ($p=0.030$ and $p=0.046$, respectively) abundances correlated with expansion in both treatment arms. This was also reflected in the gene expression data, which revealed genes involved in T-cell activation/cytotoxicity (HLA class II genes and *GZMB* in both arms; *ITGAE,*

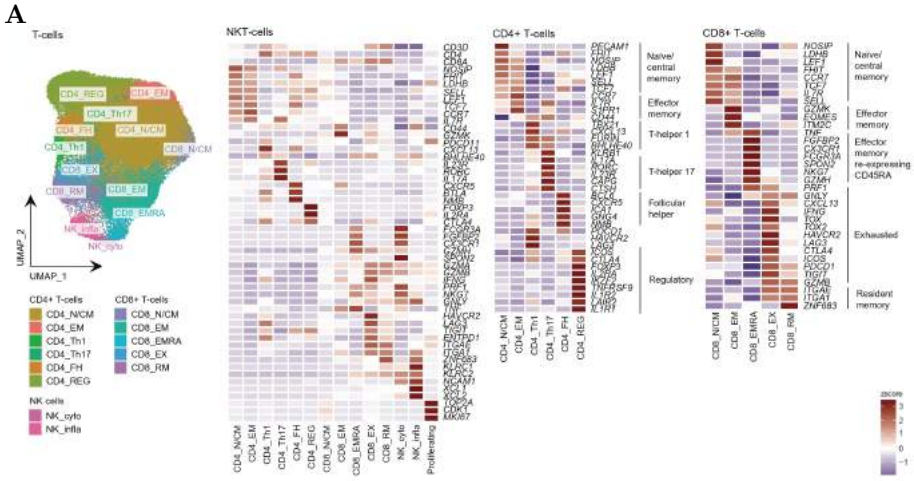

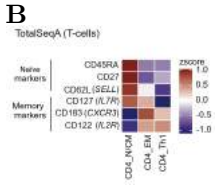

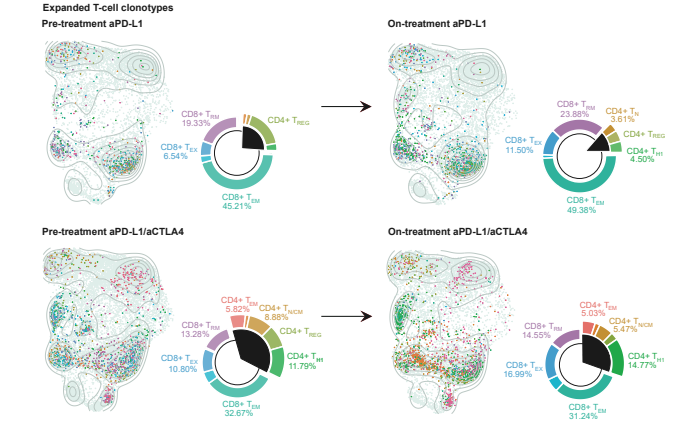

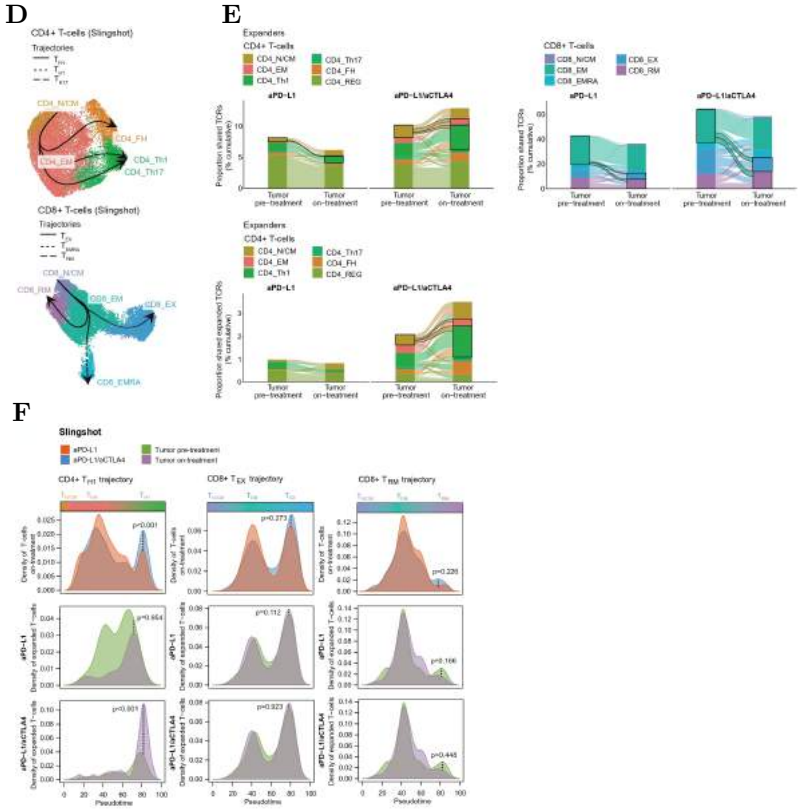

Figure 4.2: Increased CD4+ T-cell expansion upon aPD-L1/aCTLA4 *versus* aPD-L1

(A-B) UMAP of 223,309 T-/NK-cells subclustered into 13 subclusters based on marker gene (A) and protein (B) expression. **(C)** UMAP of T-cells color-coded for unique expanded clonotypes detected in tumors pre- and on-treatment for aPD-L1 (upper panels) and aPD-L1/aCTLA4 (lower panels). Pie charts showing the relative proportion of expanded T-cell subtypes, calculated across all expanded T-cells per patient. **(D)** Slingshot on T-cells derived from pre- and on-treatment tumor biopsies, revealing three CD4+ T-cell trajectories: T_{H1}, T_{FH}, and T_{H17} (left) and three CD8+ T-cell trajectories: T_{EX}, T_{EMRA}, and T_{RM} (right). **(E)** Alluvial plots showing the proportion of all (upper panels) or expanded (lower panel) shared unique TCRs between pre-treatment and on-treatment CD4+ or CD8+ T-cells in expanders (n=6 for both treatment arms). Boxed areas highlight CD4+ T_N-cells pre-treatment that share TCR sequences with CD4+ T_{EM}- or T_{H1}-cells on-treatment. **(F)** Density plots showing the distribution of T-cells (upper panels) or expanded T-cells (middle and lower panels) along the CD4+ T_{H1}, CD8+ T_{EX}, and T_{RM} trajectories as calculated by Slingshot, while stratifying for treatment arm (upper panels) or sample type (middle and lower panels). The overlapping area between treatment arms is gray. Differences in distributions were calculated by the KS test (see **Methods**). $T_{N/CM}$: naïve/central memory T-cell, T_{EM}: effector/memory T-cell, T_{H1}: T-helper 1 cell, T_{H17}: T-helper 17 T-cell, T_{FH}: follicular helper T-cell, T_{REG}: regulatory T-cell, T_{EMRA}: effector memory re-expressing CD45RA T-cell, T_{EX}: exhausted T-cell, T_{RM}: tissue-resident memory T-cell, NK_{infla}: inflammatory natural killer cell, NK_{cyto}: cytotoxic natural killer cell, Exp: expanded.

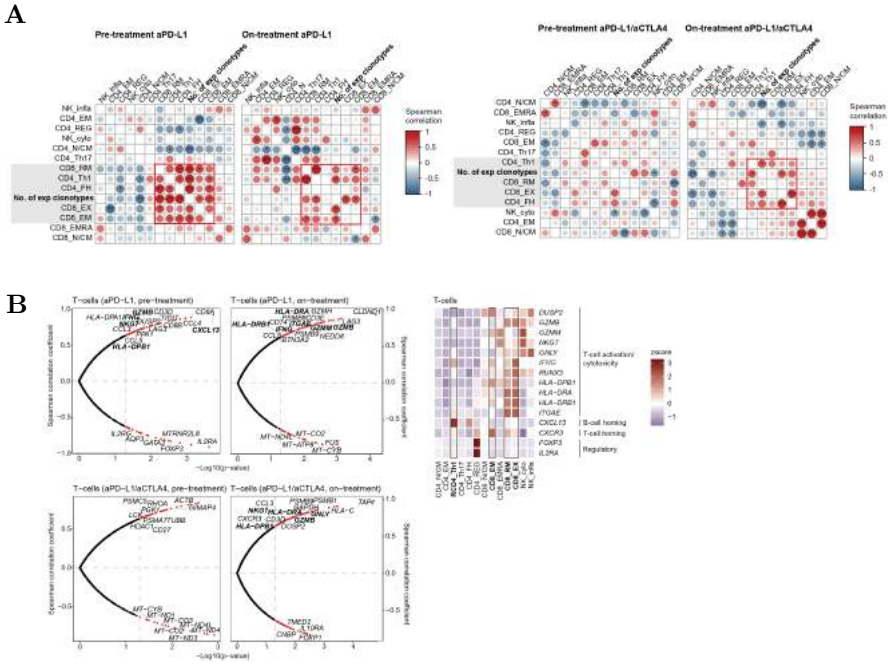

Figure 4.3: The pre-treatment T-cell landscape predicts expansion upon aPD-L1, but not aPD-L1/aCTLA4

(A) Heatmaps showing the spearman correlation between relative T-cell subcluster abundance and the number of expanded T-cell clonotypes per patient pre- and on-treatment for aPD-L1 (left panels) or aPD-L1/aCTLA4 (right panels). **(B)** Genes positively and negatively correlating with T-cell expansion in T-cells from tumors pre- and on-treatment for aPD-L1 (upper panels) or aPD-L1/aCTLA4 (lower panels); Bonferroni-adjusted p-value, black dots: p=non-significant, red: $p < 0.05$. Heatmap depicting the genes (anti-)correlating with T-cell expansion in the different T-cell subclusters (right panel). * $p < 0.05$, ** $p < 0.01$, *** $p < 0.001$ (see legend of **Figure 4.2** for abbreviations).

GZMM, IFNG upon aPD-L1; *NKG7, GNLY* upon aPD-L1/aCTLA4; **Figure 4.3B** to be correlated with T-cell expansion, all of which were highly expressed in CD8+ T_{EX} and CD4+ T_{H1} subclusters.

Spatially co-localized CD4+ and CD8+ T-cells expand upon aPD-L1/aCTLA4

To gain insights in the spatial organization of the TME associated with T-cell expansion, we performed spatial transcriptomics (Visium, 10x Genomics), which generates unbiased spatial gene expression data at limited resolution (55 µm spots comprising $\sim 1-10$ cells/spot). Based on tissue availability and quality control, we selected on-treatment sections from expanders and non-expanders (n=3 and 4 patients, respectively). Deconvolution of Visium spots based on differentially expressed genes in expanding T-cells *versus* other cells in scRNA-seq data, confirmed that T-cell expansion estimated by Visium, correlates with T-cell expansion scored by scTCR-seq (**Figure 4.4A**). Next, we annotated individual spots across all 7 on-treatment sections either as 'expanded' (8.3 ± 5.5 spots per section from expanders only), 'non-expanded' (9.4 ± 7.7 spots per section from both expanders and non-expanders), or 'random' spots (10 per section) based on the presence of expanded or non-expanded T-cells, or absence of both, respectively (**Figure 4.4B**). Notably, we observed that the average distance between expanded spots was smaller compared to distances between 'expanded to non-expanded' or 'expanded to random spots', confirming T-cell expansion to be spatially confined to specific areas (**Figure 4.4C**). We subsequently explored whether expanded spots contained CD4+ or CD8+ T-cells, or a combination of both. Interestingly, the majority of expanded spots (*i.e.*, 72%) showed both *CD3D/CD3E/CD4* and *CD3D/CD3E/CD8A/CD8B* expression. However, when comparing aPD-L1 *versus* aPD-L1/aCTLA4, 50% *versus* 92.3% of expanded spots were positive for both *CD4* and *CD8A/B* ($p = 0.019$; **Figure 4.4D**).

Since *CD4* is not only expressed by T-cells, we cannot exclude that *CD4*, even though it colocalizes with *CD3D/E*, in these expanded spots is expressed by other cell types, *e.g.* myeloid cells [102]. We therefore validated our findings using spatial proteomics in on-treatment tumor sections (PhenoCycler, Akoya Biosciences; n=3 for both treatment arms). We included antibodies against CD3e, CD4, CD8 and CD68 to discern CD3e+/CD4+ and CD3e+/CD8+ T-cells from CD4+/CD68+ myeloid cells, as well as the proliferation marker Ki67 to identify proliferating/expanding T-cells. Although CD4 in some instances was indeed expressed by CD68+ myeloid cells, we mostly confirmed CD4 expression by T-cells, especially in expanded spots. Additionally, we could confirm that expanding CD4+ (CD3e+/CD4+/Ki67+) and CD8+ T-cells (CD3e+/CD8+/Ki67+) were co-localized in tumors receiving aPD-L1/aCTLA4, more than in those receiving aPD-L1 alone ($p < 0.001$; **Figure 4.4E**). Interestingly, within Ki67+/CD3e+/CD4+/CD8+ areas, we mostly detected CD4+/Tbx21+/PD-1+ and CD8+/IFNG+ or CD8+/IFNG+/PD-1+

T-cells (**Figure 4.4F**). CD4+ T_{H1}-, CD8+ T_{EM}-, and CD8+ T_{EX}-cells express *TBX21/PDCD1*, *IFNG*, and *IFNG/PDCD1* as marker genes, respectively, thereby confirming scRNA-seq data showing expansion of CD4+ T_{H1}-, CD8+ T_{EM}-, and T_{EX}-cells. Overall, our spatial data recapitulate the scRNA-seq findings by confirming that upon aPD-L1 expanding T-cells consist mainly of CD8+ T-cells, whereas upon aPD-L1/aCTLA4 also CD4+ T-cells expand, while being located in close vicinity to expanding CD8+ T-cells.

DCs expressing antigen-presentation and T-cell homing genes correlate with T-cell expansion

Next, we subclustered immune cell types residing in the TME and explored their involvement in T-cell expansion. For dendritic cells (DCs), we identified 5 subclusters, including two migratory DC (migDC) populations: a transcriptionally-active population expressing a regulatory signature (*CD274+/CD80+*) [103] and

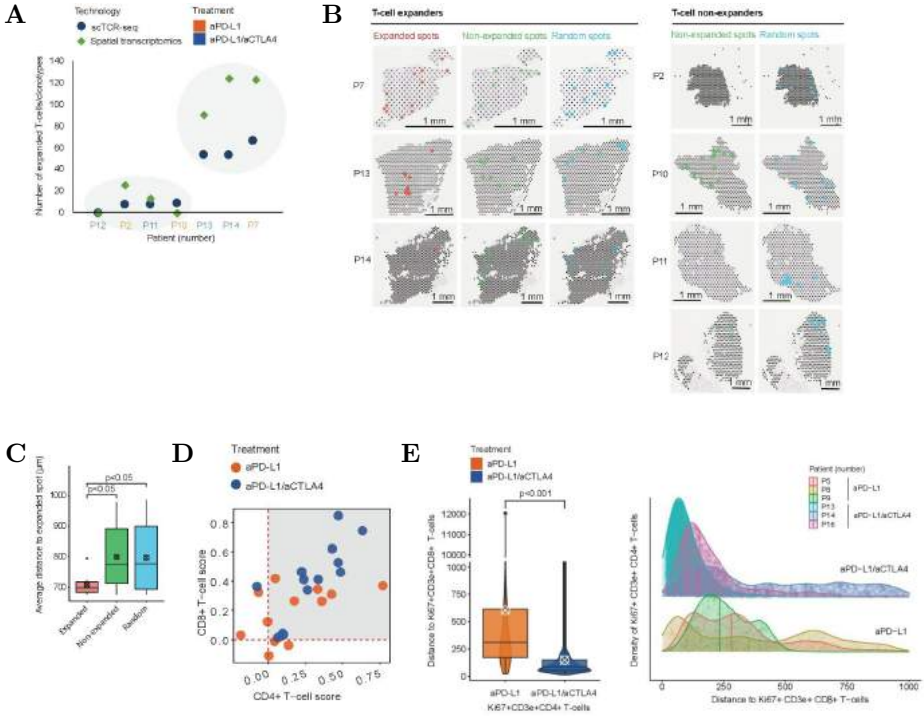

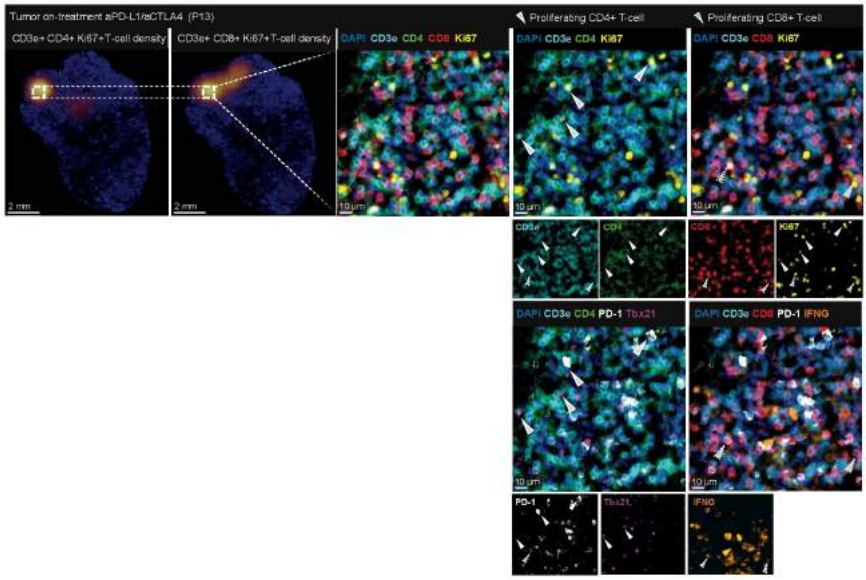

Figure 4.4: Expanded CD4+ and CD8+ T-cells are co-localized upon aPD-L1/aCTLA4

(A) Spearman correlation between the number of expanded T-cell clonotypes per patient, calculated based on scTCR-seq data (blue) and deconvolution of expanded T-cells from spatial transcriptomics data (green) on on-treatment tumor sections after aPD-L1 (orange) and aPD-L1/aCTLA4 (blue; r=0.771, p=0.052). **(B)** Expanded (red), non-expanded (green), and random spots (blue) selected based on the presence of deconvoluted expanded T-cells, non-expanded T-cells, or absence of both, respectively, in tumor sections from patients exhibiting clear T-cell expansion (expanders; n=3) or no T-cell expansion (non-expanders; n=4) across treatment arms. **(C)** Bar plot showing the average distance of expanded, non-expanded, and random spots to expanded spots (µm) across all tissue sections. **(D)** Scatterplot showing the expression of a signature score for CD4+ and CD8+ T-cells per expanded spot derived from tumor sections upon aPD-L1 (orange) and aPD-L1/aCTLA4 (blue). The gray area consists of expanded spots co-expressing the CD4+ and CD8+ signature score (50% of expanded spots upon aPD-L1 versus 92.3% upon aPD-L1/aCTLA4; p=0.019). **(E)** Violin/boxplot (left) and ridge plot (right) showing the distance of Ki67+CD3+CD8+ T-cells to Ki67+CD3+CD4+ T-cells in PhenoCycler-stained tumor sections upon aPD-L1 (n=3) and aPD-L1/aCTLA4 (n=3). **(F)** Images of a PhenoCycler-stained tumor section upon aPD-L1/aCTLA4. Regions with a high density of proliferating (Ki67+) CD4+ and CD8+ T-cells were further characterized for T-cell markers (Tbx21, IFNG, PD-1).

a population expressing T-cell recruiting chemokines (*CXCL9/10/11+*; **Figure 4.5A**). Myeloid cells were subclustered into classical monocytes, neutrophils, and 6 macrophage subclusters (**Figure 4.5B**). While Mac_CCR2 monocyte-derived macrophages and Mac_MTG1 macrophages were polarized towards pro-inflammatory macrophages, other subclusters, including Mac_TREM2 and perivascular Mac_LYVE1 macrophages were polarized towards anti-inflammatory macrophages (based on gene signature scores by Martinez *et al.* [88]). Subclustering of B-cells revealed 4 follicular B-cell (*MS4A1+/CD19+*) and 5 plasma cell (*MZB1+/SDC1+*) subclusters (**Figure 4.5C**). Within these, we observed mature-naïve (*CD27+*) B-cells that give rise to activated-memory (*CD27+/IGHM+*) IgM+ B-cells upon antigen encounter in the germinal centers (GC), which reside in follicles of peripheral lymphoid organs (*e.g.*, lymph nodes, spleen) but also in tumors in ectopic lymphoid formations called tertiairy lymphoid structures (TLS) [104]. Subsequently, B-cells proliferate and may undergo immunoglobulin class switching, to give rise to plasmablasts (*IGHM-*), which upon leaving the GC terminally differentiate into IgA+ (*IGHA+*) or IgG+ (*IGHG+*) plasma cells. Functionally, plasma cells are the main antibody-secreting cells, while memory B-cells are best equipped for antigen presentation [105].

We then characterized which TME subclusters were associated with T-cell expansion. Pre-treatment, abundance of *CXCL9/10/11+* recruiting migDCs correlated with T-cell expansion upon aPD-L1 (p=0.009; **Figure 4.5D**). Interestingly, the receptor of *CXCL9/10/11* (*i.e., CXCR3*) was most prominently expressed by CD8+ T_{EM}-, T_{RM}-, and T_{EX}-cell subclusters (**Figure 4.3B**), suggesting interaction between migDCs and expanding T-cell subclusters. Gene expression analysis of all myeloid cells revealed increased expression of genes involved in MHC class I antigen processing and presentation (*e.g., HLA-A/C, IRF1*) in patients exhibiting T-cell expansion upon aPD-L1 (**Figure 4.5E**). Notably, expression of these genes was high in migDCs, hence confirming their association with T-cell expansion (**Figure 4.5A**). Overall, these data suggest that migDCs reciprocally interact with activated T-cells to promote an anti-tumor type 1 immune response [106]. In contrast, none of the pre-treatment TME subclusters or no MHC class I or T-cell homing genes were correlated positively with T-cell expansion upon aPD-L1/aCTLA4 (**Figure 4.5E**).

On-treatment, migDCs correlated positively with expansion in both treatment arms (p=0.001 and p=0.014 for aPD-L1 and aPD-L1/aCTLA4, respectively; **Figure 4.5H-I**). A positive correlation between CD8+ T_{EX} and migDCs was also evident in both treatment arms ($p < 0.05$). *CXCL9/10* expression across all myeloid cells correlated with T-cell expansion in both treatment arms (**Figure 4.5E-G**), in addition to genes involved in MHC class I antigen processing and presentation (*IRF1, TAP1*, and HLA class I genes in both arms).

These are genes known to be upregulated in response to IFN type-I and IFN-γ signaling [107], [108], pathways that are most active in CD4+ T_{H1}- and CD8+ T_{EX}-cells (**Figure 4.2A**). Hence, most features of a T-cell expanded TME were shared between both arms, including a TME mediated by type 1 immunity, consisting of CD4+ T_{H1}- and CD8+ T_{EX}-cells, a myeloid cell compartment characterized by antigen processing and presentation, and genes mediating T-cell chemotaxis.

T-cell expansion is associated with the expansion of IgG+ plasma cells

We also noticed that T-cell expansion was positively correlated with expression of genes involved in a B-cell driven anti-tumor immune environment. Particularly, both upon aPD-L1 and aPD-L1/aCTLA4, expression of immunoglobulin variable genes (*IGHV, IGLV, IGKV*) as well as IgG (*IGHG*) genes in B-cells correlated with T-cell expansion ($p<0.05$; **Figure 4.6A**). These genes were mainly expressed by IgG-antibody-producing plasma cells (**Figure 4.5C**). The abundance of these cells was also positively correlated with T-cell expansion, albeit not always significantly (*e.g.*, $p=0.017$ for plasmablasts and $p=0.171$ for mature IgG plasma cells upon aPD-L1/aCTLA4; **Figure 4.5I**). To verify whether these signals were also reflected in the scBCR-seq data, we linked BCR light and heavy chain sequences to the scRNA-seq data. Up to 31,183 of the 58,465 B-cells annotated by scRNA-seq could be linked (53.33%), with on average 362 ± 263 unique B-cell clonotypes detected per tumor. Most BCR clonotypes in the tumor were derived from plasma cells (90,70%), the majority of which had an IgG heavy chain isotype (IgG1 comprised 56,67% of the total IgG; **Figure 4.6B**). When assessing the number of expanded B-cell clonotypes on-*versus* pre-treatment upon aPD-L1, we observed that B-cell expansion correlated significantly with T-cell expansion ($r=0.892$, $p=0.001$; **Figure 4.6C-D**). As expected, expanded B-cells mainly represented IgG-antibody-producing plasma cells, in line with the gene(set)s correlating with T-cell expansion. Fewer B-cell clonotypes were detected in the combination arm (126 ± 89), making it difficult to explore B-cell expansion upon aPD-L1/aCTLA4.

Expression of gene sets correlating with expansion is spatially co-localized with expanding T-cells

Next, we explored the TME characteristics of T-cell expansion in a spatial context. Since Visium does not provide single-cell resolution data, we first identified gene sets/pathways whose expression in T-cells, myeloid cells and B-cells correlated with T-cell expansion in the scRNA-seq data (data not

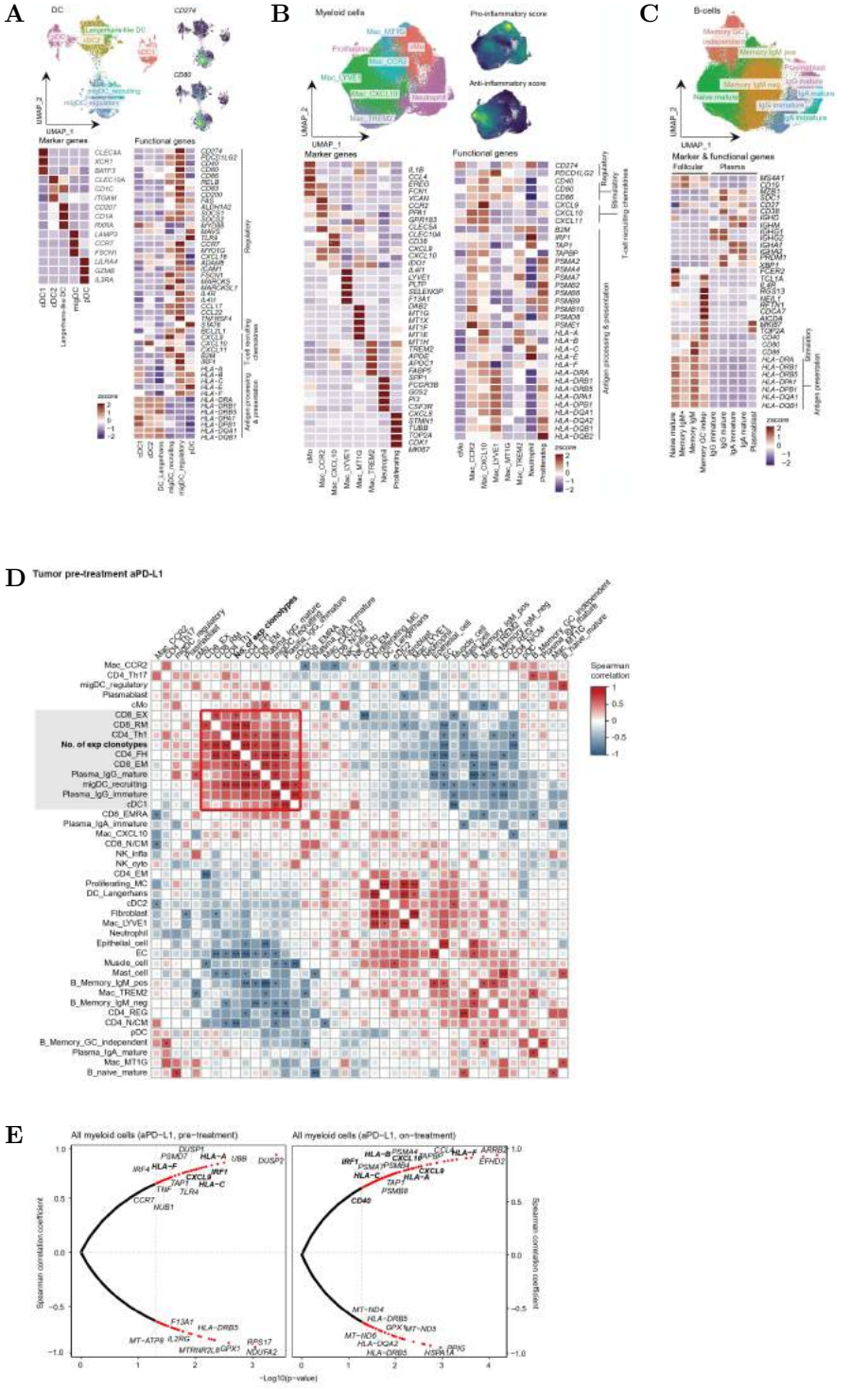
A
DC
Langerhans-like DC
cDC1
cDC2
migDC_recruiting
migDC_regulatory
CD274
CD80
UMAP_1
UMAP_2
Marker genes
Functional genes
cDC1
cDC2
Langerhans-like DC
migDC
pDC
DC_Langerhans
migDC_recruiting
migDC_regulatory
Regulatory
T-cell recruiting chemokines
Antigen processing & presentation
B
Myeloid cells
Mac_MT1G
Proliferating
cMo
Mac_CCR2
Mac_CXCL10
Mac_LYVE1
Mac_MT1G
Mac_TREM2
Neutrophil
Pro-inflammatory score
Anti-inflammatory score
C
B-cells
Memory GC independent
Memory IgM pos
Proliferating
Memory IgM neg
IgA mature
Naive mature
IgG immature
IgA immature
Marker & functional genes
Follicular
Plasma
Naive mature
Memory IgM
Memory GC indep
IgG immature
IgA immature
Plasmablast
Stimulatory
Antigen presentation

D
Tumor pre-treatment aPD-L1
No. of exp clonotypes
Spearman correlation
Msc_CCR2
CD4_Th17
migDC_regulatory
Plasmablast
cMo
CD8_EX
CD8_RM
CD4_Th1
CD8_EM
Plasma_IgG_mature
migDC_recruiting
Plasma_IgG_immature
cDC1
CD8_EMRA
Plasma_IgA_immature
Mac_CXCL10
CD8_N/CM
NK_infla
NK_cyto
CD4_EM
Proliferating_MC
DC_Langerhans
cDC2
Fibroblast
Mac_LYVE1
Neutrophil
Epithelial_cell
EC
Muscle_cell
Mast_cell
B_Memory_IgM_pos
Mac_TREM2
B_Memory_IgM_neg
CD4_REG
CD4_N/CM
pDC
B_Memory_GC_independent
Plasma_IgA_mature
Mac_MT1G
B_naive_mature

E
All myeloid cells (aPD-L1, pre−treatment)
All myeloid cells (aPD−L1, on−treatment)
Spearman correlation coefficient
−Log10(p−value)
DUSP1
PSMD7
HLA-A
UBB
DUSP2
IRF4
HLA-F
IRF1
CXCL9
TAP1
TNF
TLR4
HLA-C
CCR7
MUB1
F13A1
HLA-DRB5
MT-ATP8
IL2RG
MTRNR2L8
GPX1
RPS17
NDUFA2
CXCL10
ARRB2
EFND2
PSMA4
CD40
MT-ND4
MT-ND5
MT-ND6
HLA-DQA2
HSPA1A

F Tumor pre-treatment aPD-L1/aCTLA4

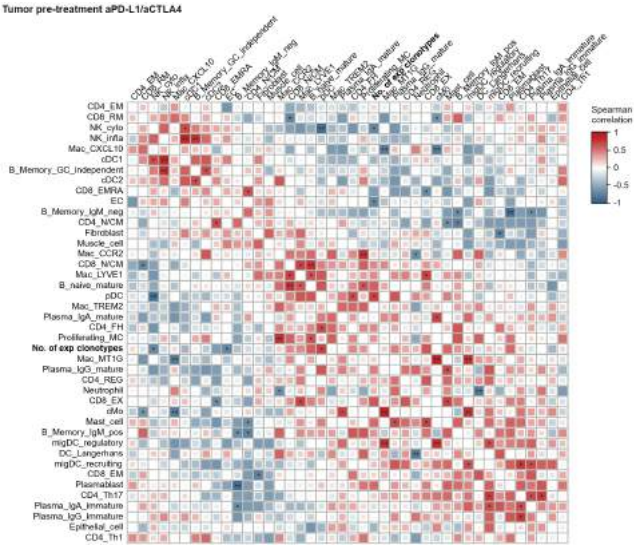

G

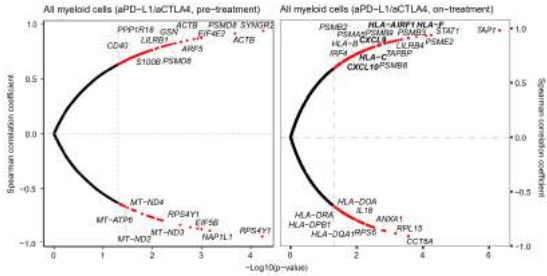

H Tumor on-treatment aPD-L1

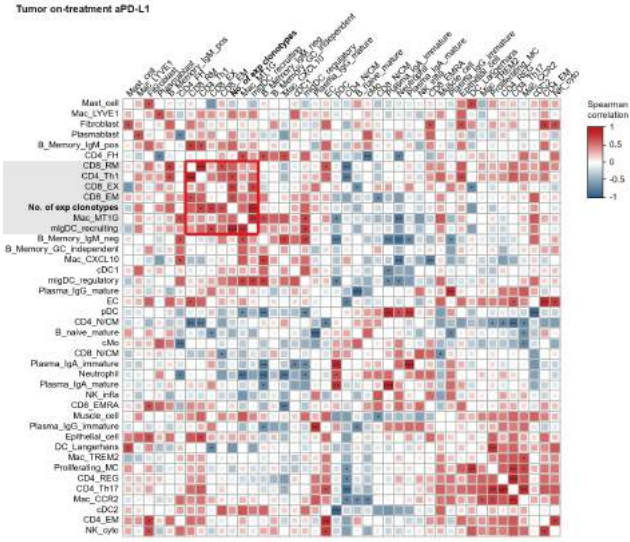

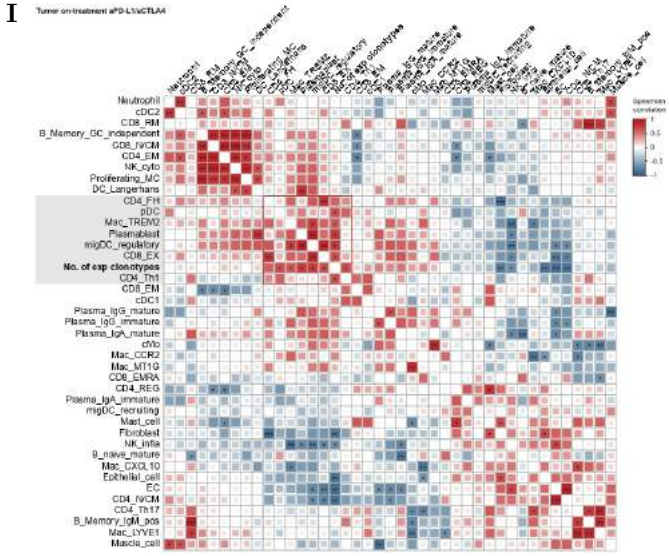

Figure 4.5: A type 1 immune response predicts T-cell expansion upon aPD-L1 **(A-C)** UMAPs showing subclustering of dendritic cells (DC; A), other myeloid cells (B), and B-cells (C), and their annotation based on marker and functional gene expression depicted in the heatmaps across all tissue types (tumor tissues, tdLNs, and normal adjacent tissues) and treatment arms. Density plots (A-B) show the average expression of *CD274* (PD-L1) and *CD80* in DC subclusters (A), and a pro-inflammatory and anti-inflammatory signature in myeloid subclusters (B). **(D, F, H, I)** Heatmaps showing the spearman correlation between relative (sub)cluster abundances and the number of expanded T-cell clonotypes per patient in tumors pre-aPD-L1 (D) and pre-aPD-L1/aCTLA4 (F), on-aPD-L1 (H), and on-aPD-L1/aCTLA4 (I). **(E, G)** Genes positively and negatively correlating with T-cell expansion across DC and other myeloid cells from tumors pre- and on-treatment for aPD-L1 (h) and aPD-L1/aCTLA4 (i). * $p<0.05$, ** $p<0.01$, *** $p<0.001$. Exp: expanded, EC: endothelial cell, DC: dendritic cell, cDC1/2: conventional type 1/2 DC, pDC: plasmacytoid DC, migDC: migratory DC, cMo: classical monocyte (see legend of **Figure 4.2** for additional abbreviations).

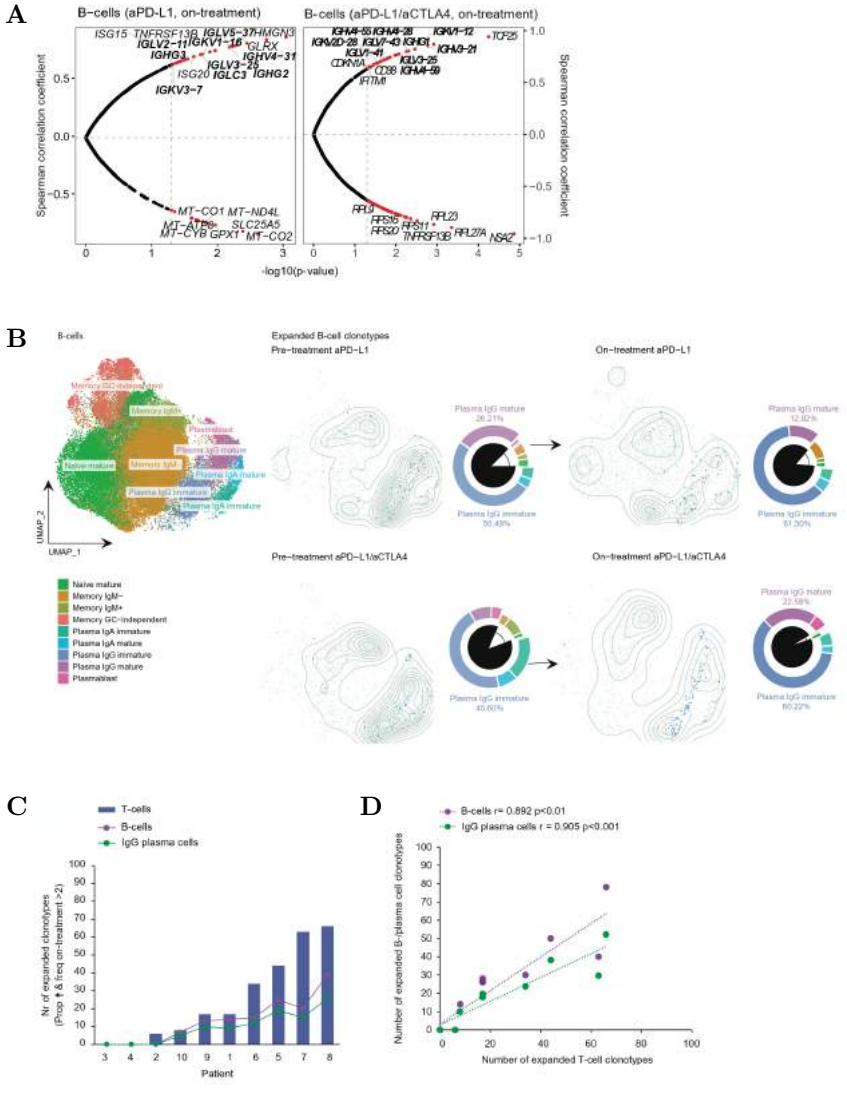

Figure 4.6: T-cell expansion is associated with the expansion of IgG+ plasma cells

(A) Genes positively and negatively correlating with T-cell expansion across B-cells from tumors upon aPD-1 (left panel) and aPD-L1/aCTLA4 (right panel). **(B)** UMAPs of 65,989 B-cells clustered into 9 subclusters based on marker gene expression (left; see also **Figure 4.5C**) and B-cells color-coded for unique expanded clonotypes detected in tumors pre- and on-treatment for aPD-L1 (upper panels) and aPD-L1/aCTLA4 (lower panels). Pie charts showing the relative proportion of expanded B-cell subtypes, calculated across all expanded B-cells per patient. **(C)** Bar plot showing the number of expanded clonotypes for T-cells (blue), all B-cells (purple) and IgG plasma cells (green) per patient upon aPD-L1. **(D)** Spearman correlation between the number of expanded T-cell clonotypes and all B-cell or IgG plasma clonotypes per patient upon aPD-L1. GC: Germinal center.

shown). Subsequently, we studied whether spatial expression of these gene sets/pathways overlapped with areas characterized by the presence or absence of T-cell expansion. We observed these pathways to be consistently upregulated in on-treatment sections from expanders *versus* non-expanders (**Figure 4.7A**). Similarly, they were increased in expanded (*versus* non-expanded or random) spots (**Figure 4.7B**). For instance, T-cell activation and cytotoxicity pathways in T-cells, as well as MHC class I antigen presentation and T-cell attraction pathways in myeloid cells were upregulated in expanded spots, suggesting co-localization of myeloid cells and T-cells. By calculating cell type proportions for each spot using SPOTlight [60] and analyzing co-occurrence by correlating the observed proportions per spot, we observed a correlation between and T-cell proportions among expanders, suggesting their concurrent presence (**Figure 4.7C**).

Next, we confirmed colocalization of expanding T-cells, myeloid cells, and plasma cells in on-treatment sections subjected to spatial proteomics. We observed that within regions containing expanded T-cells (CD3e+/CD4+/CD8+/Ki67+), myeloid/dendritic cells (CD68+/CD11c+) were more frequent (**Figure 4.7D**). The latter expressed HLA-A, CD40, as well as PD-L1, which in our scRNA-seq data were highly expressed in migDCs compared to other DC subclusters (**Figure 4.5A**). Overall, this is in line with our scRNA-seq data, in which migDC abundance correlated with T-cell expansion in both treatment arms. Interestingly, we also found areas with co-localized expansion of T-cells and plasma cells (Ki67+/CD79a+/CD138+) in both treatment arms, further corroborating the positive correlation between T-cell and B-cell expansion (**Figure 4.7E**). These hubs of expanding T-cells and plasma cells were detected in the vicinity of TLS. The latter comprised PD-1+ T-cells (CD3e+/CD4+), PD-1+ B-cells (CD79a+/CD20+), and PD-L1+ DCs (CD68+/CD11c+), allowing the production of high-affinity antibody secreting plasma cells, which subsequently travel into the tumor beds [109]. Moreover, tumors with a high TLS expression signature have been shown to express high levels of immunoglobulin variable genes (IGHV, IGLV) [110], confirming our scRNA-seq data. In conclusion, we observed that gene sets associated with T-cell expansion in the scRNA-seq data were also spatially confined to expanding T-cells.

aPD-L1/aCTLA4 induces $T_{N/CM}$-cell recruitment from tumor-draining lymph nodes to the tumor

Finally, we focused on scRNA-seq data generated from tdLNs. These tdLNs were removed during surgery and were pathologically staged to confirm absence of cancer cells. In total, tdLNs were collected on-treatment from 17 patients,

of which 7 received aPD-L1 and 10 aPD-L1/aCTLA4. Given that T-cells constituted the predominant cell type within tdLNs (52,63%; data not shown), we focused on comparing T-cell subcluster abundances. Within the T-cell population, a significant majority comprised CD4+ $T_{N/CM}$-cells (73%; **Figure 4.8A**). This did not differ between aPD-L1 *versus* aPD-L1/aCTLA4, but clearly deviated from tumors, which contained more activated T-cell subclusters. Next, we compared expression of *CTLA4, CD28, CD274* (PD-L1) and *PDCD1* (PD-1) between tdLNs and tumors. While expression of *CTLA4* did not differ (p=0.752), the co-stimulatory receptor *CD28* was increased in T-cells from tdLNs compared to tumors (p<0.001; **Figure 4.8B**). On the contrary, expression of *PCDC1* (PD-1) and its ligand *CD274* (PD-L1) were significantly lower in tdLNs than tumors (p=0.031 and p<0.001, respectively; **Figure 4.8B**). This suggests that aCTLA4, rather than aPD-L1, might directly affect cells residing within tdLNs.

To explore this, we calculated various TCR metrics (clonality, Gini coefficient,

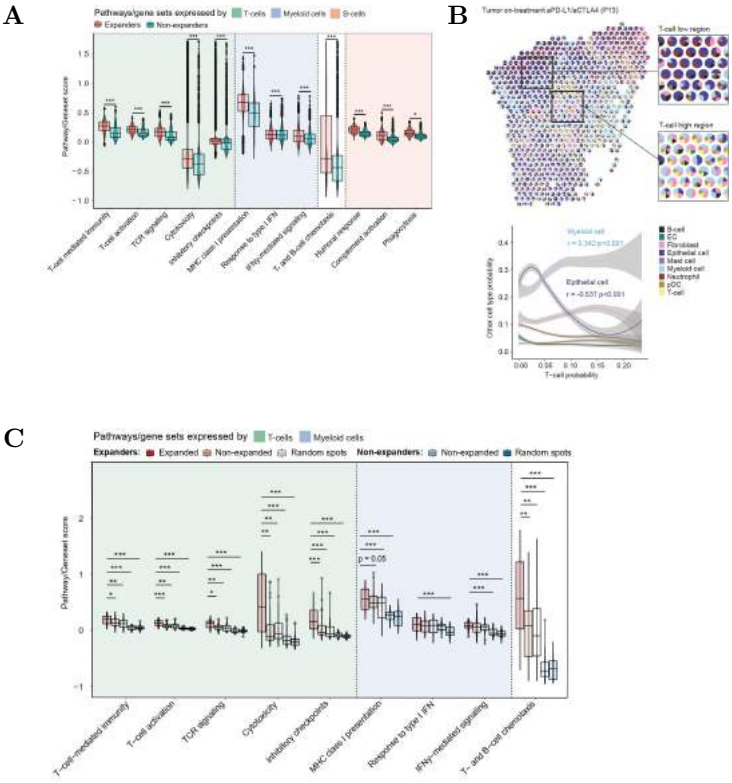

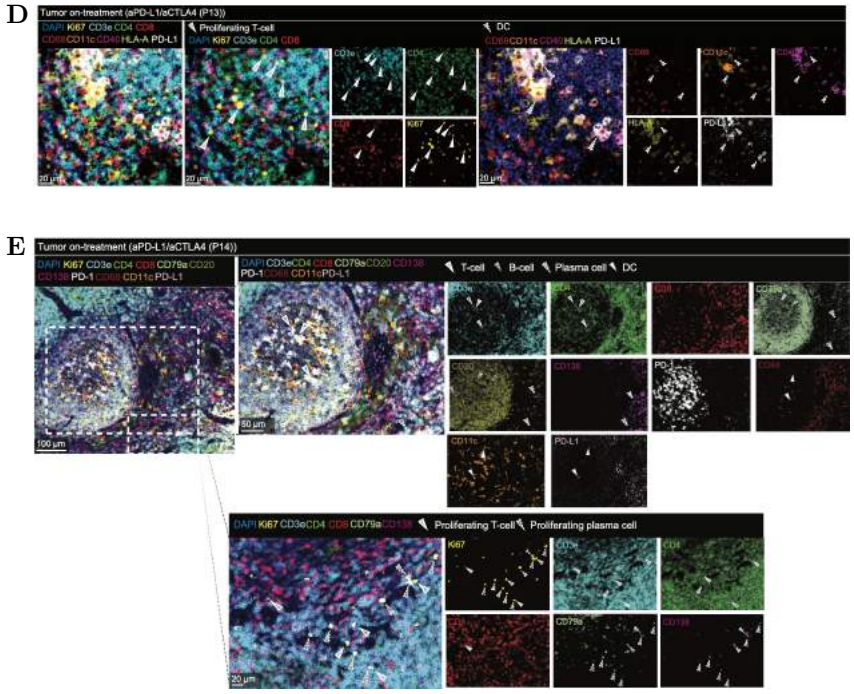

Figure 4.7: Cell types and gene sets correlating with T-cell expansion are spatially co-localized with expanding T-cells
(A, C) Violin plots showing relative expression levels of signature scores for pathway/gene sets correlated with T-cell expansion based on the scRNA-seq data of T-cells, myeloid cells, and B-cells. Scores are represented as mean ± SEM of complete tumor sections on-treatment profiled by spatial transcriptomics of expanders versus non-expanders (A; n=3 and 4 patients, respectively) or represent expanded (dark red; n=25), non-expanded (light red; n=37), and random (white; n=30) spots from expanders and non-expanded (light blue; n=28) and random (dark blue; n=30) spots from non-expanders (C; see also **Figure 4.4b**). **(B, D)** Tumor section upon aPD-L1/aCTLA4 from a T-cell expander profiled by spatial transcriptomics (B) and proteomics (D); showing cell type proportions deconvoluted within each spot by SPOTlight (B; upper panel; see **Methods**). Spearman correlation between T-cell and other cell type predicted proportions per spot (B, lower panel). Regions with a high density of proliferating T-cells were further characterized for T-cell (Ki67, CD3e, CD4, CD8) and myeloid/dendritic cell (DC) protein markers (CD68, CD11c, CD40, HLA-A, PD-L1) protein markers (D). **(E)** Tumor section upon aPD-L1/aCTLA4 from an expander profiled by spatial proteomics to study areas with co-localized proliferating T-cells (Ki67+ CD3e+ CD4+/CD8+; full arrows) and plasma cells (Ki67+ CD79a+ CD138+; dashed arrows) in the vicinity of tertiary lymphoid structures. The latter comprised PD-1+ T-cells PD-1+ B-cells, as well as PD-L1+ DCs.

and the number of unique clonotypes with frequency ≥ 2) in tdLNs, pre-, and on-treatment tumor biopsies, and this for both treatment arms separately. Between treatment arms, none of these metrics differed comparing tdLNs, pre- or on-treatment tumors, respectively (**Figure 4.8C-E**). Within treatment arms, the clonality in tdLNs was always lower than in tumors ($p<0.05$; **Figure 4.8C**), consistent with the high abundance of $T_{N/CM}$-cells in tdLNs. The Gini coefficient was higher in pre- and on-treatment tumors compared to tdLNs upon aPD-L1 ($p=0.023$ and $p=0.089$), but this difference arm was no longer significant in the aPD-L1/aCTLA4 arm ($p=0.248$ *versus* $p=0.280$), suggesting that the addition of aCTLA4 may have increased Gini coefficients in tdLNs (**Figure 4.8D**). A similar analysis while stratifying for T-cell subclusters in tdLNs revealed that Gini coefficients of both CD4+ $T_{N/CM}$- and CD8+ $T_{N/CM}$-cells were increased upon aPD-L1/aCTLA4 compared to aPD-L1, albeit non-significantly ($p=0.070$ and $p=0.051$, respectively; **Figure 4.8F**). However, when considering unique clonotypes with frequency ≥ 2 (8% of all TCRs detected in tdLNs), CD4+ $T_{N/CM}$- and CD8+ $T_{N/CM}$-cells had a higher number of unique clonotypes with frequency ≥ 2 in tdLNs upon aPD-L1/aCTLA4 *versus* aPD-L1 ($p=0.024$ and $p=0.028$, respectively; **Figure 4.8G-H**).

Since CD4+ $T_{N/CM}$-cells in tumor biopsies became activated upon aPD-L1/aCTLA4, we analyzed based on TCR sharing, whether the same T-cells were stimulated by aPD-L1/aCTLA4 both in tumors and tdLNs. In expanders, we observed that CD4+ T-cells in tumors exhibited equal proportions of TCR sharing between tdLNs and on-treatment tumors (3.37% upon aPD-L1/aCTLA44 *versus* 1.96% upon aPD-L1; $p=0.730$; **Figure 4.8I**). However, when examining differences in TCR sharing according to the T_{H1} trajectory, increased clonotype sharing between CD4+ $T_{N/CM}$-cells in tdLNs and CD4+ T_{EM}- and T_{H1}-cells in tumors of expanders receiving aPD-L1/aCTLA4 versus aPD-L1 was observed (0.84% *versus* 0.00% in tumors, $p=0.044$; data not shown). A similar analysis was not significant for CD8+ T-cells (16.2% *versus* 12.4%, $p=0.413$), also not when analyzing TCR sharing according to T_{EX} or T_{RM} trajectories (data not shown). Interestingly, 12.2% of these shared TCRs were expanded in the tumor upon aPD-L1/aCTLA4 *versus* 0% upon aPD-L1 ($p < 0.001$), indicating that this increase in TCR sharing was linked to T-cell expansion induced by aPD-L1/aCTLA4. In non-expanders, mainly CD4+ T_{REG}-cells shared TCRs between tumors and tdLNs upon aPD-L1/aCTLA4 (data not shown). Likewise, in the aPD-L1 arm, shared TCRs between tumors and tdLNs mainly involved T_{REG}-cells, both in expanders and non-expanders.

We then analyzed blood samples collected on-treatment by scRNA-seq and scTCR-seq (PBMCs; n=17; n=7 and n=10 for the aPD-L1 and aPD-L1/aCTLA4 arm, respectively). After (sub)clustering and annotation of T-cell subclusters (data not shown), we calculated the proportion of unique TCRs shared between

PBMCs and tumors. This was higher for CD4+ T-cells upon aPD-L1/aCTLA4 than aPD-L1, but differences were non-significant (2.74% *versus* 0.90% on aPD-L1 alone, p=0.262; **Figure 4.8J**). Nevertheless, more CD4+ $T_{N/CM}$-cells in PBMCs with shared clonotypes had differentiated to T_{EM}- or T_{H1}-cells in tumors upon aPD-L1/aCTLA4 *versus* aPD-L1 (1.0% *versus* 0.17%; p=0.024). Between tdLNs and PBMCs, these shared TCRs consistently represented $T_{N/CM}$-cells (see boxed T-cell subclusters on **Figure 4.8J**). In non-expanders, no differences in the proportion of TCRs shared between PBMCs and tumors was observed in aPD-L1/aCTLA4 *versus* aPD-L1 (p=0.354), and almost no sharing specifically between CD4+ $T_{N/CM}$-cells and CD4+ T_{EM} or T_{H1}-cells was seen. Overall, these results suggest that upon aPD-L1/aCTLA4, trafficking of CD4+ $T_{N/CM}$-cells occurs from the tdLNs, via blood towards the tumor, where subsequently these T-cells differentiate into CD4+ T_{EM}- or T_{H1}-cells.

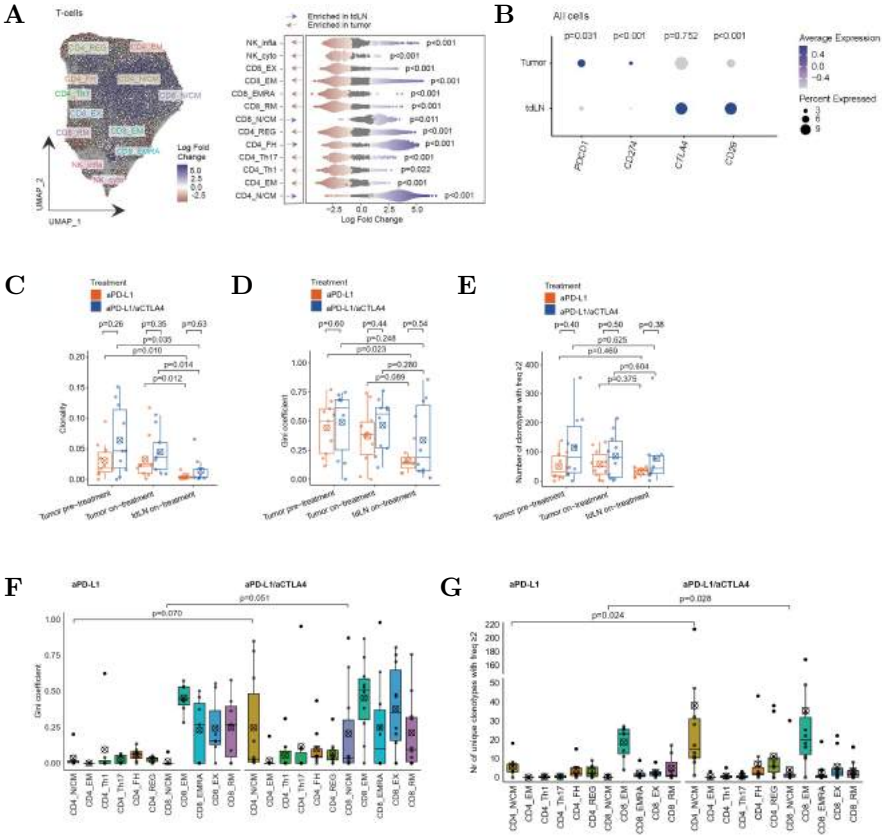

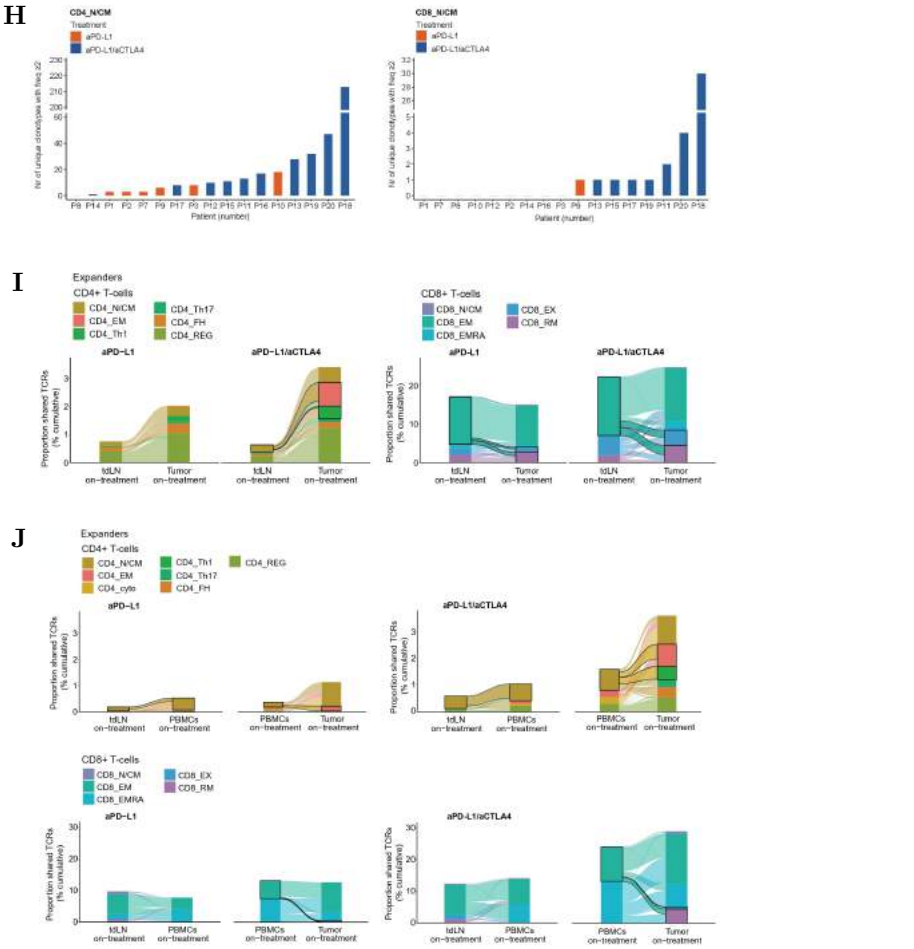

Figure 4.8: aPD-L1/aCTLA4 recruits TN/CM-cells from tumor-draining lymph nodes to the tumor

(A) Milo analysis showing differential T-cell subcluster abundance between tdLNs and tumor tissue (pre- and on-treatment from both treatment arms). **(B)** Average expression of checkpoint receptors and ligands in tdLNs and tumor biopsies (pre- and on-treatment), across cells from both treatment arms. **(C-E)** T-cell clonality (c), Gini coefficient (D), and the number of clonotypes with frequency ≥ 2 (E) in tdLNs compared to tumor biopsies pre- and on-treatment within the aPD-L1 (orange) or aPD-L1/aCTLA4 arm (blue). A cross in each box indicates the mean. **(F,G)** Gini coefficient (F) and the number of clonotypes with frequency ≥ 2 (G) calculated per T-cell subcluster in tdLNs while comparing treatments. **(H)** Bar plots showing the number of unique CD4+ (left) and CD8+ $T_{N/CM}$-cell clonotypes (right) with frequency ≥ 2 in tdLNs per patient. **(I,J)** Alluvial plots showing the proportion of shared unique CD4+ or CD8+ TCRs between tdLNs and tumors on-treatment (I; n=4 for aPD-L1, n=6 for aPD-L1/aCTLA4) or tdLNs and PBMCs on-treatment, as well as PBMCs and tumors on-treatment (J; n=3 for aPD-L1, n=6 for aPD-L1/aCTLA4) in expanders (patients covering more than 90% of expanding TCRs; see legend of **Figure 4.2** for abbreviations).

Chapter 5

General discussion and conclusion

ICB therapies represent a promising avenue in cancer treatment; however, the current challenge arises from a gap in our understanding of the mechanisms underlying treatment responses. Bridging this gap is essential for improving patient stratification and adjusting therapies for patients who do not respond to current treatments. This dissertation focuses on advancing our understanding of neoadjuvant ICB in HNSCC patients. Leveraging single-cell and spatial multi-omics technologies, we posit that complimentary mechanisms are underlying responses to neoadjuvant aPD-L1 monotherapy and aPD-L1/aCTLA4 combination therapy. In the subsequent sections, we elaborate on our findings, elucidating their significance and how they contribute to the field. Furthermore, we critically examine the limitations inherent in our study, providing a transparent assessment that sets the stage for future research endeavors.

5.1 Synthesis of findings

Throughout this doctoral study, we characterized the TME of locally advanced HNSCC prior to and after one dose of ICB, while focusing on differences between neoadjuvant aPD-L1 *versus* aPD-L1/aCTLA4.

First, we could demonstrate that intratumoral T-cell expansion correlates with radiological tumor shrinkage after one cycle of ICB, suggesting that

T-cell expansion may be considered a surrogate of early response to ICB. Interestingly, the T-cell subclusters containing these expanded T-cells differed between aPD-L1 *versus* aPD-L1/aCTLA4. Whereas mainly *PDCD1+* CD8+ T-cells (CD8+ T_{EM}-, T_{RM}-, and T_{EX}-cells) expanded upon aPD-L1, we observed a substantial fraction of expanding T-cells to also represent CD4+ T-cells in the aPD-L1/aCTLA4 arm. Particularly, based on comparing relative proportions of expanding T-cells between pre- and on-treatment tumors, assessing TCR sharing between pre- and on-treatment tumors from each individual patient, and exploring T-cell densities along their trajectories, we reasoned that CD4+ $T_{N/CM}$-cells pre-treatment expand upon aPD-L1/aCTLA4 to become activated T_{H1}-cells on-treatment. Finally, spatial transcriptomics and proteomics analyses revealed increased co-localization of expanding CD4+ and CD8+ T-cells in tumor sections collected upon aPD-L1/aCTLA4, compared to aPD-L1. Whereas CD4+ T-cells seemed to shift towards a more activated T_{H1}-cell phenotype upon aPD-L1/aCTLA4, CD8+ T-cells also expanded upon both treatments, but no differences were observed between treatments.

Although expanding T-cell subclusters differed between treatment arms, a similar on-treatment TME was associated with T-cell expansion after aPD-L1 and aPD-L1/aCTLA4. Similar genes expressed in various immune cell populations also correlated with T-cell expansion, including cytotoxic effector genes (*e.g., GZMB, NKG7, PRF1, IFNG*) and immune cell attractants (*e.g., CXCL13*) in expanding T-cells, as well as increased expression of T-cell attractants (*CXCL9/10*) and genes associated with MHC class I antigen presentation (HLA genes, *CD40, etc.*) in DCs. B-cells on the other hand were characterized by a higher expression of immunoglobulin genes involved in humoral responses. Overall, these findings suggest common mechanisms and shared gene expression programs by which immune cells sustain a type 1 immune response which drives anti-tumor immunity during aPD-L1 and aPD-L1/aCTLA4 treatment. Interestingly, B-cells also expanded towards antibody-producing IgG plasma cells (predominantly IgG1), and the degree of this expansion correlated significantly with T-cell expansion, suggesting the former to also mediate treatment response. Notably, antibody-producing IgG plasma cells produce tumor-specific cytotoxic antibodies [111], [112], and IgG plasma cells are associated with improved ICB responses in the context of HNSCC [110], [113]. For instance, PD-1 blockade results in the activation of IgM^+ B-cells and IgG^+ plasma cells in a squamous cell carcinoma mouse model, and HNSCC patients responding to PD-1 blockade have high IgG and IgM serum levels [113]. We find dynamic changes of B-cells upon ICB using a single-cell multi-omics approach and expansion of IgG1 antibody-producing plasma cells. Our spatial analysis also highlights co-localization of expanding T-cells and CD79a+/CD138+ plasma cells with CD40+/PD-L1+ DCs in the vicinity of TLS. The latter are associated with favorable survival in HNSCC [114], [115]. Hence, given the expression of PD-1

on both T- and B-cells, aPD-L1 may function by blocking the PD-1/PD-L1 coinhibitory interaction between T- and/or B-cells and PD-L1-expressing DCs and/or macrophages. The latter can rescue the function of effector T-cells by abolishing immunosuppressive effects of B-cells [116].

In contrast, when analyzing which pre-treatment TME characteristics correlate with T-cell expansion, we observed mainly differences between treatment arms. While pre-treatment biopsies undergoing T-cell expansion upon aPD-L1 showed increased expression of genes involved in anti-tumor immunity, either in T-cells, DCs, or other TME-associated subclusters, this pre-existing immune reactivity was not critical for T-cell expansion on combined aPD-L1/aCTLA4 therapy. This is similar to NSCLC, where a pre-treatment TME characterized by type 1 immunity associates with aPD-L1-mediated T cell expansion [117], but also raises the question which factors in the TME determine response to a combination of aPD-L1/aCTLA4. Interestingly, in this regard, we could assess tdLNs collected on-treatment and show that upon aPD-L1/aCTLA4 CD4+ T-cells residing in the tdLNs traffic via the blood to the tumor, where they contribute to the expansion of CD4+ T-cells. First, we could show that *CTLA4* was expressed both in tdLNs and on-treatment tumor biopsies. However, since mainly $T_{N/CM}$- and T_{EM}-cells reside in tdLNs, which typically do not express *PDCD1* (PD-1), almost no *PDCD1* was detected in tdLNs. Myeloid cells were also much fewer detected in tdLNs than tumors, and as these represent the major source of PD-L1 in tumors, *CD274* (PD-L1) expression was lower in tdLNs. This led to the hypothesis that the direct effect of aCTLA4 would be more noticeable in tdLNs compared to aPD-L1, while in corresponding tumors the combined effect of aPD-L1 and aCTLA4 would be observed. Corroborating this hypothesis, our findings based on metrics of T-cell repertoire diversity showed that aCTLA4 triggers activation of $T_{N/CM}$-cell populations in tdLNs upon aPD-L1/aCTLA4, while no such effects were observed with aPD-L1 alone. When analyzing TCR sharing between compartments (on-treatment tumor, blood (PBMCs), and tdLNs), we found a significantly higher proportion of shared TCRs between CD4+ $T_{N/CM}$-cells in tdLNs and PBMCs, and CD4+ T_{EM}- and T_{H1}-cells in tumors comparing aPD-L1/aCTLA4 *versus* aPD-L1. Moreover, a higher proportion of these cells with shared TCRs were expanded on combination therapy. This suggests that CD4+ T-cells in the tdLNs differentiate into more activated CD4+ T-cells when trafficking via the blood to the tumor. The latter may also explain why a pre-existing adaptive immune response in the tumor was not required for T-cell expansion on combined aPD-L1/aCTLA4. These findings could have an important clinical impact, as they imply that aPD-L1/aCTLA4 treatment combinations may lead to more durable anti-tumor responses when tdLNs are still present (and for instance, have not been removed during prior surgery). Our observations are also consistent with previous findings in mice, which highlight that aCTLA4 affects CD4+ T-cells, allowing their expansion [77], [118]. This

is in line with Proshnevska *et al.* proposing two stages of tumor-specific T cell activation: initial activation in tdLNs and subsequent effector program acquisition within the tumor after additional co-stimulation [119]. We failed, however, to observe an effect of aCTLA4 on T_{REG}-cell depletion, as previously observed in murine models [18], [81] or in HNSCC by van der Leun *et al.* [83].

5.2 Critical remarks and future prospects

Despite these intriguing insights, several questions remain. In this chapter, I would like to highlight some limitations of this research project, as well as future steps to address these aspects.

5.2.1 Reflections on study design & methodology

In examining the limitations of our study design and methodology, a nuanced consideration of our findings becomes essential.

First and foremost, we investigated the effects of aPD-L1 *versus* aPD-L1/aCTLA4 on tumors and tdLNs after a single dose of ICB since tumors were resected after two weeks. Given this short time frame, we could not observe a significant difference in tumor shrinkage upon aPD-L1 *versus* aPD-L1/aCTLA4. Typically, clinical responses to immunotherapy are assessed by RECIST at least 4-6 weeks after start of treatment [120]. To measure the response in our short timeframe, we used T-cell expansion as a surrogate marker, similar to an earlier study on breast cancer using neoadjuvant aPD-1 [65]. T-cell expansion has been correlated at 2-4 weeks after start of treatment with best overall clinical response during the entire course of treatment in melanoma [97], [99], [121], and a similar correlation was observed in NSCLC [23]. However, to determine clinical response in the neo-adjuvant phase (prior to surgery) by RECIST, multiple doses should be delivered, and a true neo-adjuvant study should be performed.

Second, in accordance with this, it is conceivable that multiple doses of ICB could trigger alternative mechanisms of response. For instance, aPD-L1 may also induce T-cell trafficking from tdLNs, as previously reported in mice [122], [123] and in a limited cohort of 4 patients treated with aPD-L1 [124].

Third, whereas our trajectory and TCR sharing analyses support differentiation of CD4+ T-cells and their trafficking from tdLNs to the tumor, the possibility that combination therapy causes expansion without inducing differentiation or trafficking cannot formally be excluded based on our data. Tracing and

deep-sequencing experiments in tumors and tdLNs collected at multiple time points during treatment would have to be performed to more reliably conclude this. Moreover, aCTLA4 could possibly also stimulate the activation of CD8+ $T_{N/CM}$-cells. Albeit we did not observe clear effects on this population of cells, this may have been masked because CD8+ $T_{N/CM}$-cells represented only a very rare T-cell subcluster in tdLNs and tumors. This aligns with a limitation of 10x Genomic's scRNA-seq technology, where the detection of low-abundance transcripts or rare cell types is often impeded by noise and sensitivity issues.

Fourth, to distinguish whether the effects observed on combined treatment were depending on the synergy between aPD-L1 and aCTLA4, or solely induced by aCTLA4, a treatment arm consisting only of aCTLA4 would be required.

Finally, as already briefly touched upon, although we integrated transcriptomic data with proteomic and spatial information to enable a more nuanced interpretation of immunologic responses to different treatments, it is crucial to acknowledge the need for functional validation. While hypotheses can be derived from single-cell analyses obtained from a limited cohort, reverse translation strategies, also called bedside-to-benchtop studies, are essential to uncover the mechanistic basis for these observations and determine true causality. For instance, regarding T- and B-cell expansion as measured via scTCR-seq and scBCR-seq, it remains uncertain whether this response is tumor-specific and underlies ICB response. To determine the specificity of the observed clonal expansion identified via scRNA-seq, a versatile approach is recommended, including experiments such as antigen identification and functional assays. These complementary analyses aim to validate the observed immune response and ascertain its specificity toward tumor antigens.

Despite these limitations, we believe that we have made a meaningful contribution to the field by not only sharing our findings but also making our raw data publicly available. This includes offering a comprehensive catalogue of the dynamic changes in the TME of HNSCC patients undergoing ICB therapy. This resource can be used by the community to answer their research questions and further unravel the complexities of this domain.

5.2.2 Future directions and translational perspectives

The insights gained from this research set the stage for future steps that could advance cancer immunotherapy. Here I will focus on further exploring the T-cell receptor antigen-specificity, as well as the need to deepen our understanding of ICB non-response. Additionally, I will address the translational potential of single-cell findings in predictive biomarker development.

An unresolved question is whether the T-cells expanding in the TME upon ICB are tumor-specific. Many tumor-infiltrating T-cells may act as bystanders, lacking the ability to recognize tumor-specific antigens and effectively attack tumor cells. To study the **antigen specificity of expanding T-cells**, future endeavors could focus on the TCR sequences from T-cells that were most likely driving clinical responses to ICB, based on their expansion and expression of genes associated with tumor reactivity. Subsequently, a high-throughput screening platform could enable lentiviral directed cloning of the identified TCR sequences and rapid screening of HLA-matched APC lines transfected with cDNA from the corresponding tumor. This would allow for the characterization of the tumor antigens corresponding to these identified TCR sequences by detecting TCR signaling based on GFP reporters. By identifying TCRs with strong antitumor activity or specific tumor antigens driving antitumor immune responses, this knowledge holds promise for the future development of TCR-based cellular therapies or personalized anti-tumor vaccination strategies.

While our research has predominantly focused on understanding the TME associated with positive responses to ICB, an equally important yet less explored aspect lies in characterizing the **TME associated with non-response**. This exploration is pivotal for developing effective therapeutic strategies tailored to patients who do not benefit from current treatments. However, addressing this question is challenging due to the diverse nature of TMEs that may not respond to ICB monotherapy or combination therapy. Unlike the relatively uniform nature of responsive TMEs across patients, non-responsiveness can arise from various factors. Consider the cancer immunity cycle, which relies on a multitude of regulated events. Non-response may be attributed to several causes, including but not limited to, the presence and signaling of immunosuppressive immune cell (sub)types, the absence of neoantigens suitable for presentation on MHC molecules, or hindered infiltration of anti-tumorigenic immune cells.

Translating the insights gained from single-cell analysis regarding both ICB response and non-response into **predictive biomarkers** and strategic combination therapies represents a promising frontier for enhancing the precision and broadening the applicability of ICB. This is especially crucial for patients encountering resistance to ICB monotherapy. So far, many biomarkers have been proposed, but only a few have received clinical approval. Given the dynamic complexity of the TME and the multifaceted nature of ICB response, it is suggested that combinatorial biomarkers may offer better predictive power compared to single biomarkers. In our study, we explored the effects of aPD-L1 *versus* aPD-L1/aCTLA4 on tumors and tdLNs in a cohort of 20 patients, yielding hypotheses. While these insights are valuable for guiding the identification or development of rationale-based predictive biomarkers, the establishment of a robust biomarker set requires a larger cohort study. Independent evaluation of

signals obtained from various cell types through unbiased exploration in single-cell and spatial analyses is imperative. The performance of each individual biomarker can be compared and subsequently combined into a multimarker panel using algorithms to assess sensitivity and specificity, thereby evaluating the reliability of predictive models. Retrospective cohorts treated with ICB serve as valuable sources for biomarker research, whereas archived tumor tissues are amenable to immunohistochemistry and bulk gene expression analyses. These technologies are more practical for implementation in routine clinical settings, both in terms of cost and time efficiency, compared to single-cell technologies. Ultimately, the selected biomarkers should be evaluated in a randomized prospective cohort study to confirm their clinical utility.
Moreover, there is growing interest in **liquid or blood-based biomarkers**, primarily due to their non-invasive nature, allowing sample collection at multiple time points. This accessibility facilitates the assessment of relative changes over time and enables longitudinal profiling. Therefore, investigating whether the findings in the TME are reflected in the peripheral blood becomes particularly intriguing. However, challenges arise, as exemplified by the poor overlap in TCR repertoire between the tumor and PBMCs, but also the lack of spatial information of the TME, highlighting the difficulty in monitoring expanding T-cells solely in the blood. Achieving this may necessitate a combined tumor-PBMC analysis.

In conclusion, this multi-step process offers potential for deepening our understanding of T-cell responses, as well as ICB non-response, while also identifying and validating predictive biomarkers. These efforts hold promise for improving the care and outcomes of cancer patients undergoing ICB therapy, ultimately advancing the field of cancer immunotherapy.

Scientific acknowledgements & personal contributions

Chapter 1

The introduction was written by Amelie Franken.

Chapter 2

The objectives were written by Amelie Franken.

Chapter 3-4

Diether Lambrechts designed and supervised the single-cell experiments and wrote the Immunity manuscript together with Amelie Franken.

Paul Clement and Michel Bila designed the DUTRELASCO clinical study and supervised sample collection and clinical annotation, with important help from Jeroen Van Dessel and Sigrid Hatse. Pathological evaluation of H&E-stained tissue sections was carried out by Cedric van Aerde under the supervision of Esther Hauben. Radiologic imaging data were obtained and interpreted by Vincent Vandecaveye.

Thomas Van Brussel and Rogier Schepers performed all wet lab experiments, *i.e.*, sample dissociation, scRNA-seq, scTCR-seq, sc-BCR-seq, CITE-seq, and spatial proteomics (PhenoCycler) experiments, with the following exception: Sam Kint, Sebastiaan Vanuytven, Sarah Geurs, and Katy Vandereycke performed

the spatial transcriptomics (Visium) experiments under supervision of Thierry Voet.

Amelie Franken performed all bioinformatics data analyses, *i.e.*, scRNA-seq (sub)clustering, abundance testing, and gene expression analysis, scTCR-seq, scBCR-seq, CITE-seq, spatial transcriptomics, spatial proteomics, and statistical analyses, with the following exceptions:
- Bram Boeckx, Elodie Modave, and Gino Philips performed analyses with the CellRanger pipeline (*i.e.*, single-cell data demultiplexing, reference mapping, and generating cell-count matrices).
- Gino Philips performed pseudotime trajectory analyses.
- Aurelie Mechels performed TCR sharing analyses.
- Ayse Bassez' script was used to calculate T-cell expansion.
- Sam Kint, Sebastiaan Vanuytven, Sarah Geurs, and Katy Vandereyken performed sample quality control for spatial transcriptomics data.

Amelie Franken interpreted and visualized the data.

Chapter 5

The discussion was written by Amelie Franken.

Funding & conflict of interest

The DUTRELASCO study was supported by an AstraZeneca grant. This project was part of a VIB Grand Challenges project, which received support from the Flemish Government under the Management Agreement 2017-2021, the European Union's Horizon 2020 Research, the Innovation Programme (RESCUER), EU IMI2 IMMUCAN, and KU Leuven internal fund. The computational resources and services used in this work were provided by the VSC (Flemish Supercomputer Center), funded by the Research Foundation - Flanders (FWO) and the Flemish Government – department EWI. Diether Lambrechts is supported by an ERC fund and Stichting Tegen Kanker and Amelie Franken by Kom op tegen Kanker (2020). The spatial transcriptomics platform was supported by KU Leuven (Opening The Future, SymBioSys).

There are no conflicts of interest regarding the research presented in this manuscript.

Bibliography

[1] *Global cancer burden growing, amidst mounting need for services*, https://www.who.int/news/item/01-02-2024-global-cancer-burden-growing--amidst-mounting-need-for-services.

[2] D. Hanahan and R. A. Weinberg, "The Hallmarks of Cancer", en, *Cell*, vol. 100, no. 1, pp. 57–70, Jan. 2000, ISSN: 00928674. DOI: 10.1016/S0092-8674(00)81683-9. [Online]. Available: https://linkinghub.elsevier.com/retrieve/pii/S0092867400816839 (visited on 06/16/2023).

[3] D. Hanahan and R. A. Weinberg, "Hallmarks of Cancer: The Next Generation", en, *Cell*, vol. 144, no. 5, pp. 646–674, Mar. 2011, ISSN: 00928674. DOI: 10.1016/j.cell.2011.02.013. [Online]. Available: https://linkinghub.elsevier.com/retrieve/pii/S0092867411001279 (visited on 06/16/2023).

[4] A. D. Waldman, J. M. Fritz, and M. J. Lenardo, "A guide to cancer immunotherapy: From T cell basic science to clinical practice", en, *Nature Reviews Immunology*, vol. 20, no. 11, pp. 651–668, Nov. 2020, ISSN: 1474-1733, 1474-1741. DOI: 10.1038/s41577-020-0306-5. [Online]. Available: https://www.nature.com/articles/s41577-020-0306-5 (visited on 02/06/2024).

[5] D. S. Chen and I. Mellman, "Oncology Meets Immunology: The Cancer-Immunity Cycle", en, *Immunity*, vol. 39, no. 1, pp. 1–10, Jul. 2013, ISSN: 10747613. DOI: 10.1016/j.immuni.2013.07.012. [Online]. Available: https://linkinghub.elsevier.com/retrieve/pii/S1074761313002963 (visited on 06/16/2023).

[6] J. M. Den Haan, R. Arens, and M. C. Van Zelm, "The activation of the adaptive immune system: Cross-talk between antigen-presenting cells, T cells and B cells", en, *Immunology Letters*, vol. 162, no. 2, pp. 103–112, Dec. 2014, ISSN: 01652478. DOI: 10.1016/j.imlet.2014.10.011. [Online]. Available: https://linkinghub.elsevier.com/retrieve/pii/S016524781400220X (visited on 01/25/2024).

[7] O. Demaria, S. Cornen, M. Daëron, Y. Morel, R. Medzhitov, and E. Vivier, "Harnessing innate immunity in cancer therapy", en, *Nature*, vol. 574, no. 7776, pp. 45–56, Oct. 2019, ISSN: 0028-0836, 1476-4687. DOI: 10.1038/s41586-019-1593-5. [Online]. Available: https://www.nature.com/articles/s41586-019-1593-5 (visited on 06/20/2023).

[8] D. T. Debela, S. G. Muzazu, K. D. Heraro, M. T. Ndalama, B. W. Mesele, D. C. Haile, S. K. Kitui, and T. Manyazewal, "New approaches and procedures for cancer treatment: Current perspectives", en, *SAGE Open Medicine*,

[9] K. Thol, P. Pawlik, and N. McGranahan, "Therapy sculpts the complex interplay between cancer and the immune system during tumour evolution", en, *Genome Medicine*, vol. 14, no. 1, p. 137, Dec. 2022, ISSN: 1756-994X. DOI: 10.1186/s13073-022-01138-3. [Online]. Available: https://genomemedicine.biomedcentral.com/articles/10.1186/s13073-022-01138-3 (visited on 01/23/2024).

[10] E. F. McCarthy, "THE TOXINS OF WILLIAM B. COLEY AND THE TREATMENT OF BONE AND SOFT-TISSUE SARCOMAS", en,

[11] P.-W. Huang and J. W.-C. Chang, "Immune checkpoint inhibitors win the 2018 Nobel Prize", en, *Biomedical Journal*, vol. 42, no. 5, pp. 299–306, Oct. 2019, ISSN: 23194170. DOI: 10.1016/j.bj.2019.09.002. [Online]. Available: https://linkinghub.elsevier.com/retrieve/pii/S2319417019304998 (visited on 01/23/2024).

[12] C. Liu, M. Yang, D. Zhang, M. Chen, and D. Zhu, "Clinical cancer immunotherapy: Current progress and prospects", en, *Frontiers in Immunology*, vol. 13, p. 961 805, Oct. 2022, ISSN: 1664-3224. DOI: 10.3389/fimmu.2022.961805. [Online]. Available: https://www.frontiersin.org/articles/10.3389/fimmu.2022.961805/full (visited on 01/23/2024).

[13] P. Sharma, S. Goswami, D. Raychaudhuri, *et al.*, "Immune checkpoint therapy—current perspectives and future directions", en, *Cell*, vol. 186, no. 8, pp. 1652–1669, Apr. 2023, ISSN: 00928674. DOI: 10.1016/j.cell.2023.03.006. [Online]. Available: https://linkinghub.elsevier.com/retrieve/pii/S0092867423002246 (visited on 01/23/2024).

[14] J. B. Lee, H. R. Kim, and S.-J. Ha, "Immune Checkpoint Inhibitors in 10 Years: Contribution of Basic Research and Clinical Application in Cancer Immunotherapy", en, *Immune Network*, vol. 22, no. 1, e2, 2022, ISSN: 1598-2629, 2092-6685. DOI: 10.4110/in.2022.22.e2. [Online]. Available: https://immunenetwork.org/DOIx.php?id=10.4110/in.2022.22.e2 (visited on 01/12/2024).

[15] K. E. Yost, H. Y. Chang, and A. T. Satpathy, "Recruiting T cells in cancer immunotherapy", en, *Science*, vol. 372, no. 6538, pp. 130–131, Apr. 2021, ISSN: 0036-8075, 1095-9203. DOI: 10.1126/science.abd1329. [Online]. Available: https://www.science.org/doi/10.1126/science.abd1329 (visited on 12/22/2021).

[16] A. M. van der Leun, D. S. Thommen, and T. N. Schumacher, "CD8+ T cell states in human cancer: Insights from single-cell analysis", en, *Nature Reviews Cancer*, vol. 20, no. 4, pp. 218–232, Apr. 2020, ISSN: 1474-175X, 1474-1768. DOI: 10.1038/s41568-019-0235-4. [Online]. Available: http://www.nature.com/articles/s41568-019-0235-4 (visited on 04/01/2022).

[17] T. Yokosuka, M. Takamatsu, W. Kobayashi-Imanishi, A. Hashimoto-Tane, M. Azuma, and T. Saito, "Programmed cell death 1 forms negative costimulatory microclusters that directly inhibit T cell receptor signaling by recruiting phosphatase SHP2", en, *Journal of Experimental Medicine*, vol. 209, no. 6, pp. 1201–1217, Jun. 2012, ISSN: 1540-9538, 0022-1007. DOI: 10.1084/jem.20112741. [Online]. Available: https://rupress.org/jem/article/209/6/1201/41299/Programmed-cell-death-1-forms-negative (visited on 01/05/2024).

[18] S. C. Wei, C. R. Duffy, and J. P. Allison, "Fundamental Mechanisms of Immune Checkpoint Blockade Therapy", en, *Cancer Discovery*, vol. 8, no. 9, pp. 1069–1086, Sep. 2018, ISSN: 2159-8274, 2159-8290. DOI: 10.1158/2159-8290.CD-18-0367. [Online]. Available: http://cancerdiscovery.aacrjournals.org/lookup/doi/10.1158/2159-8290.CD-18-0367 (visited on 01/12/2022).

[19] D. M. Sansom, "CD28, CTLA-4 and their ligands: Who does what and to whom?", en, *Immunology*, vol. 101, no. 2, pp. 169–177, Oct. 2000, ISSN: 0019-2805, 1365-2567. DOI: 10.1046/j.1365-2567.2000.00121.x. [Online]. Available: https://onlinelibrary.wiley.com/doi/10.1046/j.1365-2567.2000.00121.x (visited on 01/23/2024).

[20] R. H. Schwartz, "The Role of 0D28, CTLA-4, and B7/BB1 in Interleukin-2 Production and Immunotherapy", en,

[21] P. S. Linsley, J. L. Greene, W. Brady, J. Bajorath, J. A. Ledbetter, and R. Peach, "Human B7-1 (CD80) and B7-2 (CD86) bind with similar avidities but distinct kinetics to CD28 and CTLA-4 receptors", en, *Immunity*, vol. 1, no. 9, pp. 793–801, Dec. 1994, ISSN: 10747613. DOI: 10.1016/S1074-7613(94)80021-9. [Online]. Available: https://linkinghub.elsevier.com/retrieve/pii/S1074761394800219 (visited on 01/05/2024).

[22] D. R. Leach, M. F. Krummel, and J. P. Allison, "Enhancement of Antitumor Immunity by CTLA-4 Blockade", en, *Science*, vol. 271, no. 5256, pp. 1734–1736, Mar. 1996, ISSN: 0036-8075, 1095-9203. DOI: 10.1126/science.271.5256.1734. [Online]. Available: https://www.science.org/doi/10.1126/science.271.5256.1734 (visited on 01/05/2024).

[23] P. M. Forde, J. E. Chaft, K. N. Smith, *et al.*, "Neoadjuvant PD-1 Blockade in Resectable Lung Cancer", en, *New England Journal of Medicine*, vol. 378, no. 21, pp. 1976–1986, May 2018, ISSN: 0028-4793, 1533-4406. DOI: 10.1056/NEJMoa1716078. [Online]. Available: http://www.nejm.org/doi/10.1056/NEJMoa1716078 (visited on 11/13/2023).

[24] A. C. Huang, R. J. Orlowski, X. Xu, *et al.*, "A single dose of neoadjuvant PD-1 blockade predicts clinical outcomes in resectable melanoma", en, *Nature Medicine*, vol. 25, no. 3, pp. 454–461, Mar. 2019, ISSN: 1078-8956, 1546-170X. DOI: 10.1038/s41591-019-0357-y. [Online]. Available: http://www.nature.com/articles/s41591-019-0357-y (visited on 12/22/2021).

[25] M. Chalabi, L. F. Fanchi, K. K. Dijkstra, *et al.*, "Neoadjuvant immunotherapy leads to pathological responses in MMR-proficient and MMR-deficient early-stage colon cancers", en, *Nature Medicine*, vol. 26, no. 4, pp. 566–576, Apr. 2020, ISSN: 1078-8956, 1546-170X. DOI: 10.1038/s41591-020-0805-8. [Online]. Available: https://www.nature.com/articles/s41591-020-0805-8 (visited on 01/05/2024).

[26] T. U. Marron, M. I. Fiel, P. Hamon, *et al.*, "Neoadjuvant cemiplimab for resectable hepatocellular carcinoma: A single-arm, open-label, phase 2 trial", en, *The Lancet Gastroenterology & Hepatology*, vol. 7, no. 3, pp. 219–229, Mar. 2022, ISSN: 24681253. DOI: 10.1016/S2468-1253(21)00385-X. [Online]. Available: https://linkinghub.elsevier.com/retrieve/pii/S246812532100385X (visited on 01/05/2024).

[27] S. P. Patel, M. Othus, Y. Chen, *et al.*, "Neoadjuvant–Adjuvant or Adjuvant-Only Pembrolizumab in Advanced Melanoma", en, *New England Journal of Medicine*, vol. 388, no. 9, pp. 813–823, Mar. 2023, ISSN: 0028-4793, 1533-4406. DOI: 10.1056/NEJMoa2211437. [Online]. Available: http://www.nejm.org/doi/10.1056/NEJMoa2211437 (visited on 01/05/2024).

[28] S. A. Patel and A. J. Minn, "Combination Cancer Therapy with Immune Checkpoint Blockade: Mechanisms and Strategies", en, *Immunity*, vol. 48, no. 3, pp. 417–433, Mar. 2018, ISSN: 10747613. DOI: 10.1016/j.immuni.2018.03.007. [Online]. Available: https://linkinghub.elsevier.com/retrieve/pii/S1074761318300839 (visited on 09/17/2019).

[29] U. Nindra, J. Hurwitz, D. Forstner, V. Chin, R. Gallagher, and J. Liu, "A systematic review of neoadjuvant and definitive immunotherapy in locally advanced head and neck squamous cell carcinoma", en, *Cancer Medicine*, vol. 12, no. 10, pp. 11 234–11 247, May 2023, ISSN: 2045-7634, 2045-7634. DOI: 10.1002/cam4.5815. [Online]. Available: https://onlinelibrary.wiley.com/doi/10.1002/cam4.5815 (visited on 01/23/2024).

[30] M. Gormley, G. Creaney, A. Schache, K. Ingarfield, and D. I. Conway, "Reviewing the epidemiology of head and neck cancer: Definitions, trends and risk factors", en, *British Dental Journal*, vol. 233, no. 9, pp. 780–786, Nov. 2022, ISSN: 0007-0610, 1476-5373. DOI: 10.1038/s41415-022-5166-x. [Online]. Available: https://www.nature.com/articles/s41415-022-5166-x (visited on 03/21/2024).

[31] *Global Cancer Observatory. International Agency for Research on Cancer. world Health Organization. Accessed January 2023.* https://gco.iarc.fr/en.

[32] N. Vigneswaran and M. D. Williams, "Epidemiologic Trends in Head and Neck Cancer and Aids in Diagnosis", en, *Oral and Maxillofacial Surgery Clinics of North America*, vol. 26, no. 2, pp. 123–141, May 2014, ISSN: 10423699. DOI: 10.1016/j.coms.2014.01.001. [Online]. Available: https://linkinghub.elsevier.com/retrieve/pii/S1042369914000028 (visited on 01/23/2024).

[33] L. Q. M. Chow, "Head and Neck Cancer", en, *n engl j med*, p. 13, 2020.

[34] D. E. Johnson, B. Burtness, C. R. Leemans, V. W. Y. Lui, J. E. Bauman, and J. R. Grandis, "Head and neck squamous cell carcinoma", en, *Nature Reviews Disease Primers*, vol. 6, no. 1, p. 92, Nov. 2020, ISSN: 2056-676X. DOI: 10.1038/s41572-020-00224-3. [Online]. Available: https://www.nature.com/articles/s41572-020-00224-3 (visited on 01/23/2024).

[35] R. L. Ferris, G. Blumenschein, J. Fayette, *et al.*, "Nivolumab for Recurrent Squamous-Cell Carcinoma of the Head and Neck", en, *New England Journal of Medicine*, vol. 375, no. 19, pp. 1856–1867, Nov. 2016, ISSN: 0028-4793, 1533-4406. DOI: 10.1056/NEJMoa1602252. [Online]. Available: http://www.nejm.org/doi/10.1056/NEJMoa1602252 (visited on 09/16/2019).

[36] J. Bauml, T. Y. Seiwert, D. G. Pfister, *et al.*, "Pembrolizumab for Platinum- and Cetuximab-Refractory Head and Neck Cancer: Results From a Single-Arm, Phase II Study", en, *Journal of Clinical Oncology*, vol. 35, no. 14, pp. 1542–1549, May 2017, ISSN: 0732-183X, 1527-7755. DOI: 10.1200/JCO.2016.70.1524. [Online]. Available: https://ascopubs.org/doi/10.1200/JCO.2016.70.1524 (visited on 01/05/2024).

[37] R. Mehra, T. Y. Seiwert, S. Gupta, *et al.*, "Efficacy and safety of pembrolizumab in recurrent/metastatic head and neck squamous cell carcinoma: Pooled analyses after long-term follow-up in KEYNOTE-012", en, *British Journal of Cancer*, vol. 119, no. 2, pp. 153–159, Jul. 2018, ISSN: 0007-0920, 1532-1827. DOI: 10.1038/s41416-018-0131-9. [Online]. Available: http://www.nature.com/articles/s41416-018-0131-9 (visited on 02/14/2020).

[38] E. E. W. Cohen, D. Soulières, C. Le Tourneau, *et al.*, "Pembrolizumab versus methotrexate, docetaxel, or cetuximab for recurrent or metastatic head-and-neck squamous cell carcinoma (KEYNOTE-040): A randomised, open-label, phase 3 study", en, *The Lancet*, vol. 393, no. 10167, pp. 156–167, Jan. 2019, ISSN: 01406736. DOI: 10.1016/S0140-6736(18)31999-8. [Online]. Available: https://linkinghub.elsevier.com/retrieve/pii/S0140673618319998 (visited on 04/25/2022).

[39] B. Burtness, K. J. Harrington, R. Greil, *et al.*, "Pembrolizumab alone or with chemotherapy versus cetuximab with chemotherapy for recurrent or metastatic squamous cell carcinoma of the head and neck (KEYNOTE-048): A randomised, open-label, phase 3 study", en, *The Lancet*, vol. 394, no. 10212, pp. 1915–1928, Nov. 2019, ISSN: 01406736. DOI: 10.1016/S0140-6736(19)32591-7. [Online]. Available: https://linkinghub.elsevier.com/retrieve/pii/S0140673619325917 (visited on 01/17/2022).

[40] R. Ferris, R. Haddad, C. Even, *et al.*, "Durvalumab with or without tremelimumab in patients with recurrent or metastatic head and neck squamous cell carcinoma: EAGLE, a randomized, open-label phase III study", en, *Annals of Oncology*, vol. 31, no. 7, pp. 942–950, Jul. 2020, ISSN: 09237534. DOI: 10.1016/j.annonc.2020.04.001. [Online]. Available: https://linkinghub.elsevier.com/retrieve/pii/S0923753420364346 (visited on 04/25/2022).

[41] L. L. Siu, C. Even, R. Mesía, *et al.*, "Safety and Efficacy of Durvalumab With or Without Tremelimumab in Patients With PD-L1–Low/Negative Recurrent or Metastatic HNSCC: The Phase 2 CONDOR Randomized Clinical Trial", en, *JAMA Oncology*, vol. 5, no. 2, p. 195, Feb. 2019, ISSN: 2374-2437. DOI: 10.1001/jamaoncol.2018.4628. [Online]. Available: http://oncology.jamanetwork.com/article.aspx?doi=10.1001/jamaoncol.2018.4628 (visited on 05/18/2022).

[42] AstraZeneca, *Update on KESTREL Phase III trial of Imfinzi with or without tremelimumab in the 1st-line treatment of recurrent or metastatic head and neck cancer*, https://www.astrazeneca.com/media-centre/press-releases/2021/update-on-kestrel-phase-iii-trial-for-imfinzi.html, Feb. 2021.

[43] J. D. Schoenfeld, G. J. Hanna, V. Y. Jo, *et al.*, "Neoadjuvant Nivolumab or Nivolumab Plus Ipilimumab in Untreated Oral Cavity Squamous Cell Carcinoma: A Phase 2 Open-Label Randomized Clinical Trial", en, *JAMA Oncology*, vol. 6, no. 10, p. 1563, Oct. 2020, ISSN: 2374-2437. DOI: 10.1001/jamaoncol.2020.2955. [Online]. Available: https://jamanetwork.com/journals/jamaoncology/fullarticle/2769892 (visited on 12/22/2021).

[44] J. L. Vos, J. B. W. Elbers, O. Krijgsman, *et al.*, "Neoadjuvant immunotherapy with nivolumab and ipilimumab induces major pathological responses in patients with head and neck squamous cell carcinoma", en, *Nature Communications*, vol. 12, no. 1, p. 7348, Dec. 2021, ISSN: 2041-1723. DOI: 10.1038/s41467-021-26472-9. [Online]. Available: https://www.nature.com/articles/s41467-021-26472-9 (visited on 08/16/2022).

[45] N. A. Giraldo, R. Sanchez-Salas, J. D. Peske, *et al.*, "The clinical role of the TME in solid cancer", en, *British Journal of Cancer*, vol. 120, no. 1, pp. 45–53, Jan. 2019, ISSN: 0007-0920, 1532-1827. DOI: 10.1038/s41416-018-0327-z. [Online]. Available: https://www.nature.com/articles/s41416-018-0327-z (visited on 03/19/2024).

[46] V. Addala, F. Newell, J. V. Pearson, A. Redwood, B. W. Robinson, J. Creaney, and N. Waddell, "Computational immunogenomic approaches to predict response to cancer immunotherapies", en, *Nature Reviews Clinical Oncology*, vol. 21, no. 1, pp. 28–46, Jan. 2024, ISSN: 1759-4774, 1759-4782. DOI: 10.1038/s41571-023-00830-6. [Online]. Available: https://www.nature.com/articles/s41571-023-00830-6 (visited on 01/23/2024).

[47] M. R. Stratton, P. J. Campbell, and P. A. Futreal, "The cancer genome", en, *Nature*, vol. 458, no. 7239, pp. 719–724, Apr. 2009, ISSN: 0028-0836, 1476-4687. DOI: 10.1038/nature07943. [Online]. Available: https://www.nature.com/articles/nature07943 (visited on 01/23/2024).

[48] Z. Wang, M. Gerstein, and M. Snyder, "RNA-Seq: A revolutionary tool for transcriptomics", en, *Nature Reviews Genetics*, vol. 10, no. 1, pp. 57–63, Jan. 2009, ISSN: 1471-0056, 1471-0064. DOI: 10.1038/nrg2484. [Online]. Available: https://www.nature.com/articles/nrg2484 (visited on 01/23/2024).

[49] Y. W. Kwon, H.-S. Jo, S. Bae, Y. Seo, P. Song, M. Song, and J. H. Yoon, "Application of Proteomics in Cancer: Recent Trends and Approaches for Biomarkers Discovery", en, *Frontiers in Medicine*, vol. 8, p. 747 333, Sep. 2021, ISSN: 2296-858X. DOI: 10.3389/fmed.2021.747333. [Online]. Available: https://www.frontiersin.org/articles/10.3389/fmed.2021.747333/full (visited on 01/23/2024).

[50] S. H. Gohil, J. B. Iorgulescu, D. A. Braun, D. B. Keskin, and K. J. Livak, "Applying high-dimensional single-cell technologies to the analysis of cancer immunotherapy", en, *Nature Reviews Clinical Oncology*, vol. 18, no. 4, pp. 244–256, Apr. 2021, ISSN: 1759-4774, 1759-4782. DOI: 10.1038/s41571-020-00449-x. [Online]. Available: https://www.nature.com/articles/s41571-020-00449-x (visited on 01/23/2024).

[51] L. Heumos, A. C. Schaar, C. Lance, *et al.*, "Best practices for single-cell analysis across modalities", en, *Nature Reviews Genetics*, Mar. 2023, ISSN: 1471-0056, 1471-0064. DOI: 10.1038/s41576-023-00586-w. [Online]. Available: https://www.nature.com/articles/s41576-023-00586-w (visited on 06/14/2023).

[52] S. Clark, *Single cell RNA-seq: An introductory overview and tools for getting started*, https://www.10xgenomics.com/blog/single-cell-rna-seq-an-introductory-overview-and-tools-for-getting-started, Sep. 2022.

[53] R. Salomon, D. Kaczorowski, F. Valdes-Mora, R. E. Nordon, A. Neild, N. Farbehi, N. Bartonicek, and D. Gallego-Ortega, "Droplet-based single cell RNAseq tools: A practical guide", en, *Lab on a Chip*, vol. 19, no. 10, pp. 1706–1727, 2019, ISSN: 1473-0197, 1473-0189. DOI: 10.1039/C8LC01239C. [Online]. Available: http://xlink.rsc.org/?DOI=C8LC01239C (visited on 01/23/2024).

[54] *Single cell immune profiling using Chromium 5' solution.* https://www.10xgenomics.com/resources/document-library?query=&page=1, 2023.

[55] E. Market and F. N. Papavasiliou, "V(D)J Recombination and the Evolution of the Adaptive Immune System", en, *PLoS Biology*, vol. 1, no. 1, e16, Oct. 2003, ISSN: 1545-7885. DOI: 10.1371/journal.pbio.0000016. [Online]. Available: https://dx.plos.org/10.1371/journal.pbio.0000016 (visited on 01/23/2024).

[56] J. Chiffelle, R. Genolet, M. A. Perez, G. Coukos, V. Zoete, and A. Harari, "T-cell repertoire analysis and metrics of diversity and clonality", en, *Current Opinion in Biotechnology*, vol. 65, pp. 284–295, Oct. 2020, ISSN: 09581669. DOI: 10.1016/j.copbio.2020.07.010. [Online]. Available: https://linkinghub.elsevier.com/retrieve/pii/S0958166920301051 (visited on 03/02/2023).

[57] P. Amaral, S. Carbonell-Sala, F. M. De La Vega, *et al.*, "The status of the human gene catalogue", en, *Nature*, vol. 622, no. 7981, pp. 41–47, Oct. 2023, ISSN: 0028-0836, 1476-4687. DOI: 10.1038/s41586-023-06490-x. [Online]. Available: https://www.nature.com/articles/s41586-023-06490-x (visited on 03/07/2024).

[58] C. Seydel, "Diving deeper into the proteome", en, *Nature Methods*, vol. 19, no. 9, pp. 1036–1040, Sep. 2022, ISSN: 1548-7091, 1548-7105. DOI: 10.1038/s41592-022-01599-9. [Online]. Available: https://www.nature.com/articles/s41592-022-01599-9 (visited on 03/07/2024).

[59] *Visium Spatial. Whole transcriptome discovery in the tissue context*, https://10xgenomics.com/platforms/visium.

[60] M. Elosua, P. Nieto, E. Mereu, I. Gut, and H. Heyn, "SPOTlight: Seeded NMF regression to Deconvolute Spatial Transcriptomics Spots with Single-Cell Transcriptomes", en, Bioinformatics, preprint, Jun. 2020. DOI: 10.1101/2020.06.03.131334. [Online]. Available: http://biorxiv.org/lookup/doi/10.1101/2020.06.03.131334 (visited on 12/22/2021).

[61] *Spatial Gene Expression for Fresh Frozen*, https://www.10xgenomics.com/support/spatial-gene-expression-fresh-frozen.

[62] *Akoya Biosciences. PhenoCycler*, https://www.akoyabio.com/phenocycler/.

[63] Y. Liu, J. Altreuter, S. Bodapati, S. Cristea, C. J. Wong, C. J. Wu, and F. Michor, "Predicting patient outcomes after treatment with immune checkpoint blockade: A review of biomarkers derived from diverse data modalities", en, *Cell Genomics*, vol. 4, no. 1, p. 100 444, Jan. 2024, ISSN: 2666979X. DOI: 10.1016/j.xgen.2023.100444. [Online]. Available: https://linkinghub.elsevier.com/retrieve/pii/S2666979X23002793 (visited on 01/23/2024).

[64] D. S. Thommen, V. H. Koelzer, P. Herzig, *et al.*, "A transcriptionally and functionally distinct PD-1+ CD8+ T cell pool with predictive potential in non-small-cell lung cancer treated with PD-1 blockade", en, *Nature Medicine*, vol. 24, no. 7, pp. 994–1004, Jul. 2018, ISSN: 1078-8956, 1546-170X. DOI: 10.1038/s41591-018-0057-z. [Online]. Available: http://www.nature.com/articles/s41591-018-0057-z (visited on 12/22/2021).

[65] A. Bassez, H. Vos, L. Van Dyck, *et al.*, "A single-cell map of intratumoral changes during anti-PD1 treatment of patients with breast cancer", en, *Nature Medicine*, vol. 27, no. 5, pp. 820–832, May 2021, ISSN: 1078-8956, 1546-170X. DOI: 10.1038/s41591-021-01323-8. [Online]. Available: http://www.nature.com/articles/s41591-021-01323-8 (visited on 12/22/2021).

[66] Y. Zhang, H. Chen, H. Mo, *et al.*, "Single-cell analyses reveal key immune cell subsets associated with response to PD-L1 blockade in triple-negative breast cancer", en, *Cancer Cell*, vol. 39, no. 12, 1578–1593.e8, Dec. 2021, ISSN: 15356108. DOI: 10.1016/j.ccell.2021.09.010. [Online].

Available: https://linkinghub.elsevier.com/retrieve/pii/S1535610821004992 (visited on 12/22/2021).

[67] A. Magen, P. Hamon, N. Fiaschi, *et al.*, "Intratumoral dendritic cell–CD4+ T helper cell niches enable CD8+ T cell differentiation following PD-1 blockade in hepatocellular carcinoma", en, *Nature Medicine*, vol. 29, no. 6, pp. 1389–1399, Jun. 2023, ISSN: 1078-8956, 1546-170X. DOI: 10.1038/s41591-023-02345-0. [Online]. Available: https://www.nature.com/articles/s41591-023-02345-0 (visited on 01/05/2024).

[68] R. Cabrita, M. Lauss, A. Sanna, *et al.*, "Tertiary lymphoid structures improve immunotherapy and survival in melanoma", en, *Nature*, vol. 577, no. 7791, pp. 561–565, Jan. 2020, ISSN: 0028-0836, 1476-4687. DOI: 10.1038/s41586-019-1914-8. [Online]. Available: http://www.nature.com/articles/s41586-019-1914-8 (visited on 01/27/2020).

[69] B. A. Helmink, S. M. Reddy, J. Gao, *et al.*, "B cells and tertiary lymphoid structures promote immunotherapy response", en, *Nature*, Jan. 2020, ISSN: 0028-0836, 1476-4687. DOI: 10.1038/s41586-019-1922-8. [Online]. Available: http://www.nature.com/articles/s41586-019-1922-8 (visited on 01/21/2020).

[70] N. S. Patil, B. Y. Nabet, S. Müller, *et al.*, "Intratumoral plasma cells predict outcomes to PD-L1 blockade in non-small cell lung cancer", en, *Cancer Cell*, vol. 40, no. 3, 289–300.e4, Mar. 2022, ISSN: 15356108. DOI: 10.1016/j.ccell.2022.02.002. [Online]. Available: https://linkinghub.elsevier.com/retrieve/pii/S1535610822000356 (visited on 05/18/2022).

[71] H. A. Qureshi, X. Zhu, G. H. Yang, M. Steadele, R. H. Pierce, N. D. Futran, S. M. Lee, E. Méndez, and A. M. Houghton, "Impact of HPV status on immune responses in head and neck squamous cell carcinoma", en, *Oral Oncology*, vol. 127, p. 105 774, Apr. 2022, ISSN: 13688375. DOI: 10.1016/j.oraloncology.2022.105774. [Online]. Available: https://linkinghub.elsevier.com/retrieve/pii/S136883752200063X (visited on 05/18/2022).

[72] M. H. Spitzer, Y. Carmi, N. E. Reticker-Flynn, *et al.*, "Systemic Immunity Is Required for Effective Cancer Immunotherapy", en, *Cell*, vol. 168, no. 3, 487–502.e15, Jan. 2017, ISSN: 00928674. DOI: 10.1016/j.cell.2016.12.022. [Online]. Available: https://linkinghub.elsevier.com/retrieve/pii/S009286741631738X (visited on 01/24/2024).

[73] F. Franco, A. Jaccard, P. Romero, Y.-R. Yu, and P.-C. Ho, "Metabolic and epigenetic regulation of T-cell exhaustion", en, *Nature Metabolism*, vol. 2, no. 10, pp. 1001–1012, Sep. 2020, ISSN: 2522-5812. DOI: 10.1038

/s42255-020-00280-9. [Online]. Available: https://www.nature.com/articles/s42255-020-00280-9 (visited on 01/10/2024).

[74] D. B. Doroshow, S. Bhalla, M. B. Beasley, L. M. Sholl, K. M. Kerr, S. Gnjatic, I. I. Wistuba, D. L. Rimm, M. S. Tsao, and F. R. Hirsch, "PD-L1 as a biomarker of response to immune-checkpoint inhibitors", en, *Nature Reviews Clinical Oncology*, vol. 18, no. 6, pp. 345–362, Jun. 2021, ISSN: 1759-4774, 1759-4782. DOI: 10.1038/s41571-021-00473-5. [Online]. Available: https://www.nature.com/articles/s41571-021-00473-5 (visited on 11/24/2023).

[75] D. Lau, S. Khare, M. M. Stein, P. Jain, Y. Gao, A. BenTaieb, T. A. Rand, A. A. Salahudeen, and A. A. Khan, "Integration of tumor extrinsic and intrinsic features associates with immunotherapy response in non-small cell lung cancer", en, *Nature Communications*, vol. 13, no. 1, p. 4053, Jul. 2022, ISSN: 2041-1723. DOI: 10.1038/s41467-022-31769-4. [Online]. Available: https://www.nature.com/articles/s41467-022-31769-4 (visited on 02/07/2023).

[76] T. Hakozaki, "Quantitative spatial profiling of PD-1/PD-L1 interaction in patients with cancer", en, *Translational Lung Cancer Research*, vol. 12, no. 6, pp. 1346–1349, Jun. 2023, ISSN: 22186751, 22264477. DOI: 10.21037/tlcr-23-56. [Online]. Available: https://tlcr.amegroups.com/article/view/73380/html (visited on 02/08/2024).

[77] S. C. Wei, J. H. Levine, A. P. Cogdill, *et al.*, "Distinct Cellular Mechanisms Underlie Anti-CTLA-4 and Anti-PD-1 Checkpoint Blockade", en, *Cell*, vol. 170, no. 6, 1120–1133.e17, Sep. 2017, ISSN: 00928674. DOI: 10.1016/j.cell.2017.07.024. [Online]. Available: https://linkinghub.elsevier.com/retrieve/pii/S0092867417308310 (visited on 04/08/2021).

[78] D. M. Pardoll, "The blockade of immune checkpoints in cancer immunotherapy", en, *Nature Reviews Cancer*, vol. 12, no. 4, pp. 252–264, Apr. 2012, ISSN: 1474-175X, 1474-1768. DOI: 10.1038/nrc3239. [Online]. Available: http://www.nature.com/articles/nrc3239 (visited on 12/22/2021).

[79] J. A. Seidel, A. Otsuka, and K. Kabashima, "Anti-PD-1 and Anti-CTLA-4 Therapies in Cancer: Mechanisms of Action, Efficacy, and Limitations", en, *Frontiers in Oncology*, vol. 8, p. 86, Mar. 2018, ISSN: 2234-943X. DOI: 10.3389/fonc.2018.00086. [Online]. Available: http://journal.frontiersin.org/article/10.3389/fonc.2018.00086/full (visited on 12/22/2021).

[80] L. S. K. Walker and D. M. Sansom, "The emerging role of CTLA4 as a cell-extrinsic regulator of T cell responses", en, *Nature Reviews Immunology*, vol. 11, no. 12, pp. 852–863, Dec. 2011, ISSN: 1474-1733, 1474-1741. DOI: 10.1038/nri3108. [Online]. Available: http://www.nature.com/articles/nri3108 (visited on 03/01/2022).

[81] A. Sharma, S. K. Subudhi, J. Blando, J. Scutti, L. Vence, J. Wargo, J. P. Allison, A. Ribas, and P. Sharma, "Anti-CTLA-4 Immunotherapy Does Not Deplete FOXP3 $^{+}$ Regulatory T Cells (Tregs) in Human Cancers", en, *Clinical Cancer Research*, vol. 25, no. 4, pp. 1233–1238, Feb. 2019, ISSN: 1078-0432, 1557-3265. DOI: 10.1158/1078-0432.CCR-18-0762. [Online]. Available: http://clincancerres.aacrjournals.org/lookup/doi/10.1158/1078-0432.CCR-18-0762 (visited on 04/04/2022).

[82] A. M. Luoma, S. Suo, Y. Wang, *et al.*, "Tissue-resident memory and circulating T cells are early responders to pre-surgical cancer immunotherapy", en, *Cell*, S0092867422007231, Jul. 2022, ISSN: 00928674. DOI: 10.1016/j.cell.2022.06.018. [Online]. Available: https://linkinghub.elsevier.com/retrieve/pii/S0092867422007231 (visited on 07/13/2022).

[83] A. M. van der Leun, J. J. H. Traets, J. L. Vos, *et al.*, "Dual immune checkpoint blockade induces analogous alterations in the dysfunctional CD8+ T cell and activated Treg compartment", eng, *Cancer Discovery*, pp. CD–22–0851, Aug. 2023, ISSN: 2159-8290. DOI: 10.1158/2159-8290.CD-22-0851.

[84] S. L. Topalian, P. M. Forde, L. A. Emens, M. Yarchoan, K. N. Smith, and D. M. Pardoll, "Neoadjuvant immune checkpoint blockade: A window of opportunity to advance cancer immunotherapy", en, *Cancer Cell*, vol. 41, no. 9, pp. 1551–1566, Sep. 2023, ISSN: 15356108. DOI: 10.1016/j.ccell.2023.07.011. [Online]. Available: https://linkinghub.elsevier.com/retrieve/pii/S1535610823002519 (visited on 01/25/2024).

[85] Y. Hao, S. Hao, E. Andersen-Nissen, *et al.*, "Integrated analysis of multimodal single-cell data", en, *Cell*, vol. 184, no. 13, 3573–3587.e29, Jun. 2021, ISSN: 00928674. DOI: 10.1016/j.cell.2021.04.048. [Online]. Available: https://linkinghub.elsevier.com/retrieve/pii/S0092867421005833 (visited on 08/22/2022).

[86] Q. Zhang, R. Huang, H. Hu, L. Yu, Q. Tang, Y. Tao, Z. Liu, J. Li, and G. Wang, "Integrative Analysis of Hypoxia-Associated Signature in Pan-Cancer", en, *iScience*, vol. 23, no. 9, p. 101 460, Sep. 2020, ISSN: 25890042. DOI: 10.1016/j.isci.2020.101460. [Online]. Available: https://linkinghub.elsevier.com/retrieve/pii/S2589004220306520 (visited on 05/02/2022).

[87] E. Dann, N. C. Henderson, S. A. Teichmann, M. D. Morgan, and J. C. Marioni, "Differential abundance testing on single-cell data using k-nearest neighbor graphs", en, *Nature Biotechnology*, vol. 40, no. 2, pp. 245–253, Feb. 2022, ISSN: 1087-0156, 1546-1696. DOI: 10.1038/s41587-021-01033-z. [Online]. Available: https://www.nature.com/articles/s41587-021-01033-z (visited on 11/25/2022).

[88] F. O. Martinez, S. Gordon, M. Locati, and A. Mantovani, "Transcriptional Profiling of the Human Monocyte-to-Macrophage Differentiation and Polarization: New Molecules and Patterns of Gene Expression", en, *The Journal of Immunology*, vol. 177, no. 10, pp. 7303–7311, Nov. 2006, ISSN: 0022-1767, 1550-6606. DOI: 10.4049/jimmunol.177.10.7303. [Online]. Available: http://www.jimmunol.org/lookup/doi/10.4049/jimmunol.177.10.7303 (visited on 12/22/2021).

[89] L. Zhang, X. Yu, L. Zheng, *et al.*, "Lineage tracking reveals dynamic relationships of T cells in colorectal cancer", en, *Nature*, vol. 564, no. 7735, pp. 268–272, Dec. 2018, ISSN: 0028-0836, 1476-4687. DOI: 10.1038/s41586-018-0694-x. [Online]. Available: http://www.nature.com/articles/s41586-018-0694-x (visited on 12/22/2021).

[90] K. Street, D. Risso, R. B. Fletcher, D. Das, J. Ngai, N. Yosef, E. Purdom, and S. Dudoit, "Slingshot: Cell lineage and pseudotime inference for single-cell transcriptomics", en, *BMC Genomics*, vol. 19, no. 1, p. 477, Dec. 2018, ISSN: 1471-2164. DOI: 10.1186/s12864-018-4772-0. [Online]. Available: https://bmcgenomics.biomedcentral.com/articles/10.1186/s12864-018-4772-0 (visited on 12/22/2021).

[91] G. S. Gulati, S. S. Sikandar, D. J. Wesche, *et al.*, "Single-cell transcriptional diversity is a hallmark of developmental potential", en, *Science*, vol. 367, no. 6476, pp. 405–411, Jan. 2020, ISSN: 0036-8075, 1095-9203. DOI: 10.1126/science.aax0249. [Online]. Available: https://www.science.org/doi/10.1126/science.aax0249 (visited on 06/09/2023).

[92] M. Lange, V. Bergen, M. Klein, *et al.*, "CellRank for directed single-cell fate mapping", en, *Nature Methods*, vol. 19, no. 2, pp. 159–170, Feb. 2022, ISSN: 1548-7091, 1548-7105. DOI: 10.1038/s41592-021-01346-6. [Online]. Available: https://www.nature.com/articles/s41592-021-01346-6 (visited on 08/16/2022).

[93] R. Wei, S. He, S. Bai, E. Sei, M. Hu, A. Thompson, K. Chen, S. Krishnamurthy, and N. E. Navin, "Spatial charting of single-cell transcriptomes in tissues", en, *Nature Biotechnology*, vol. 40, no. 8, pp. 1190–1199, Aug. 2022, ISSN: 1087-0156, 1546-1696. DOI: 10.1038/s41587-022-01233-1. [Online]. Available: https://www.nature.com/articles/s41587-022-01233-1 (visited on 09/06/2022).

[94] M. Weigert, U. Schmidt, R. Haase, K. Sugawara, and G. Myers, "Star-convex Polyhedra for 3D Object Detection and Segmentation in Microscopy", en, in *2020 IEEE Winter Conference on Applications of Computer Vision (WACV)*, Snowmass Village, CO, USA: IEEE, Mar. 2020, pp. 3655–3662, ISBN: 978-1-72816-553-0. DOI: 10.1109/WACV45572.2020.9093435. [Online]. Available: https://ieeexplore.ieee.org/document/9093435/ (visited on 02/16/2023).

[95] P. Bankhead, M. B. Loughrey, J. A. Fernández, *et al.*, "QuPath: Open source software for digital pathology image analysis", en, *Scientific Reports*, vol. 7, no. 1, p. 16 878, Dec. 2017, ISSN: 2045-2322. DOI: 10.1038/s41598-017-17204-5. [Online]. Available: https://www.nature.com/articles/s41598-017-17204-5 (visited on 02/16/2023).

[96] R. Wei, S. He, S. Bai, E. Sei, M. Hu, A. Thompson, K. Chen, S. Krishnamurthy, and N. E. Navin, "Spatial charting of single-cell transcriptomes in tissues", en, *Nature Biotechnology*, vol. 40, no. 8, pp. 1190–1199, Aug. 2022, ISSN: 1087-0156, 1546-1696. DOI: 10.1038/s41587-022-01233-1. [Online]. Available: https://www.nature.com/articles/s41587-022-01233-1 (visited on 09/06/2022).

[97] P. C. Tumeh, C. L. Harview, J. H. Yearley, *et al.*, "PD-1 blockade induces responses by inhibiting adaptive immune resistance", en, *Nature*, vol. 515, no. 7528, pp. 568–571, Nov. 2014, ISSN: 0028-0836, 1476-4687. DOI: 10.1038/nature13954. [Online]. Available: https://www.nature.com/articles/nature13954 (visited on 07/12/2023).

[98] N. Riaz, J. J. Havel, V. Makarov, *et al.*, "Tumor and Microenvironment Evolution during Immunotherapy with Nivolumab", en, *Cell*, vol. 171, no. 4, 934–949.e16, Nov. 2017, ISSN: 00928674. DOI: 10.1016/j.cell.2017.09.028. [Online]. Available: https://linkinghub.elsevier.com/retrieve/pii/S0092867417311224 (visited on 01/11/2022).

[99] V. Anagnostou, D. C. Bruhm, N. Niknafs, *et al.*, "Integrative Tumor and Immune Cell Multi-omic Analyses Predict Response to Immune Checkpoint Blockade in Melanoma", en, *Cell Reports Medicine*, vol. 1, no. 8, p. 100 139, Nov. 2020, ISSN: 26663791. DOI: 10.1016/j.xcrm.2020.100139. [Online]. Available: https://linkinghub.elsevier.com/retrieve/pii/S266637912030183X (visited on 01/11/2022).

[100] H. A. Abbas, D. Hao, K. Tomczak, *et al.*, "Single cell T cell landscape and T cell receptor repertoire profiling of AML in context of PD-1 blockade therapy", en, *Nature Communications*, vol. 12, no. 1, p. 6071, Dec. 2021, ISSN: 2041-1723. DOI: 10.1038/s41467-021-26282-z. [Online]. Available: https://www.nature.com/articles/s41467-021-26282-z (visited on 01/11/2022).

[101] A. K. Schneider, M. F. Chevalier, and L. Derré, "The multifaceted immune regulation of bladder cancer", en, *Nature Reviews Urology*, vol. 16, no. 10, pp. 613–630, Oct. 2019, ISSN: 1759-4812, 1759-4820. DOI: 10.1038/s41585-019-0226-y. [Online]. Available: http://www.nature.com/articles/s41585-019-0226-y (visited on 12/23/2022).

[102] L. Jardine, D. Barge, A. Ames-Draycott, S. Pagan, S. Cookson, G. Spickett, M. Haniffa, M. Collin, and V. Bigley, "Rapid Detection of Dendritic Cell and Monocyte Disorders Using CD4 as a Lineage Marker of the Human Peripheral Blood Antigen-Presenting Cell Compartment", en, *Frontiers in Immunology*, vol. 4, 2013, ISSN: 1664-3224. DOI: 10.3389/fimmu.2013.00495. [Online]. Available: http://journal.frontiersin.org/article/10.3389/fimmu.2013.00495/abstract (visited on 09/06/2023).

[103] B. Maier, A. M. Leader, S. T. Chen, *et al.*, "A conserved dendritic-cell regulatory program limits antitumour immunity", en, *Nature*, vol. 580, no. 7802, pp. 257–262, Apr. 2020, ISSN: 0028-0836, 1476-4687. DOI: 10.1038/s41586-020-2134-y. [Online]. Available: http://www.nature.com/articles/s41586-020-2134-y (visited on 12/22/2021).

[104] W. H. Fridman, M. Meylan, F. Petitprez, C.-M. Sun, A. Italiano, and C. Sautès-Fridman, "B cells and tertiary lymphoid structures as determinants of tumour immune contexture and clinical outcome", en, *Nature Reviews Clinical Oncology*, Apr. 2022, ISSN: 1759-4774, 1759-4782. DOI: 10.1038/s41571-022-00619-z. [Online]. Available: https://www.nature.com/articles/s41571-022-00619-z (visited on 04/27/2022).

[105] G. V. Sharonov, E. O. Serebrovskaya, D. V. Yuzhakova, O. V. Britanova, and D. M. Chudakov, "B cells, plasma cells and antibody repertoires in the tumour microenvironment", en, *Nature Reviews Immunology*, vol. 20, no. 5, pp. 294–307, May 2020, ISSN: 1474-1733, 1474-1741. DOI: 10.1038/s41577-019-0257-x. [Online]. Available: http://www.nature.com/articles/s41577-019-0257-x (visited on 04/08/2021).

[106] M. Najafi, N. Hashemi Goradel, B. Farhood, *et al.*, "Macrophage polarity in cancer: A review", en, *Journal of Cellular Biochemistry*, vol. 120, no. 3, pp. 2756–2765, Mar. 2019, ISSN: 0730-2312, 1097-4644. DOI: 10.1002/jcb.27646. [Online]. Available: https://onlinelibrary.wiley.com/doi/10.1002/jcb.27646 (visited on 12/22/2021).

[107] S. Hervas-Stubbs, J. L. Perez-Gracia, A. Rouzaut, M. F. Sanmamed, A. Le Bon, and I. Melero, "Direct Effects of Type I Interferons on Cells of the Immune System", en, *Clinical Cancer Research*, vol. 17, no. 9, pp. 2619–2627, May 2011, ISSN: 1078-0432, 1557-3265. DOI: 10.1158/1078-0432.CCR-10-1114. [Online]. Available: https://aacrjournals.o

rg/clincancerres/article/17/9/2619/12936/Direct-Effects-of-Type-I-Interferons-on-Cells-of (visited on 09/14/2023).

[108] F. Zhou, "Molecular Mechanisms of IFN- to Up-Regulate MHC Class I Antigen Processing and Presentation", en, *International Reviews of Immunology*, vol. 28, no. 3-4, pp. 239–260, Jan. 2009, ISSN: 0883-0185, 1563-5244. DOI: 10.1080/08830180902978120. [Online]. Available: http://www.tandfonline.com/doi/full/10.1080/08830180902978120 (visited on 09/14/2023).

[109] W. H. Fridman, M. Meylan, G. Pupier, A. Calvez, I. Hernandez, and C. Sautès-Fridman, "Tertiary lymphoid structures and B cells: An intratumoral immunity cycle", en, *Immunity*, S1074761323003655, Sep. 2023, ISSN: 10747613. DOI: 10.1016/j.immuni.2023.08.009. [Online]. Available: https://linkinghub.elsevier.com/retrieve/pii/S1074761323003655 (visited on 09/14/2023).

[110] M. Meylan, F. Petitprez, E. Becht, *et al.*, "Tertiary lymphoid structures generate and propagate anti-tumor antibody-producing plasma cells in renal cell cancer", en, *Immunity*, vol. 55, no. 3, 527–541.e5, Mar. 2022, ISSN: 10747613. DOI: 10.1016/j.immuni.2022.02.001. [Online]. Available: https://linkinghub.elsevier.com/retrieve/pii/S1074761322000814 (visited on 05/18/2022).

[111] C. Sautès-Fridman, F. Petitprez, J. Calderaro, and W. H. Fridman, "Tertiary lymphoid structures in the era of cancer immunotherapy", en, *Nature Reviews Cancer*, vol. 19, no. 6, pp. 307–325, Jun. 2019, ISSN: 1474-175X, 1474-1768. DOI: 10.1038/s41568-019-0144-6. [Online]. Available: http://www.nature.com/articles/s41568-019-0144-6 (visited on 10/31/2019).

[112] E. J. Colbeck, A. Ager, A. Gallimore, and G. W. Jones, "Tertiary Lymphoid Structures in Cancer: Drivers of Antitumor Immunity, Immunosuppression, or Bystander Sentinels in Disease?", en, *Frontiers in Immunology*, vol. 8, p. 1830, Dec. 2017, ISSN: 1664-3224. DOI: 10.3389/fimmu.2017.01830. [Online]. Available: http://journal.frontiersin.org/article/10.3389/fimmu.2017.01830/full (visited on 03/01/2022).

[113] S. S. Kim, S. Shen, S. Miyauchi, P. D. Sanders, I. Franiak-Pietryga, L. Mell, J. S. Gutkind, E. E. Cohen, J. A. Califano, and A. B. Sharabi, "B Cells Improve Overall Survival in HPV-Associated Squamous Cell Carcinomas and Are Activated by Radiation and PD-1 Blockade", en, *Clinical Cancer Research*, vol. 26, no. 13, pp. 3345–3359, Jul. 2020, ISSN: 1078-0432, 1557-3265. DOI: 10.1158/1078-0432.CCR-19-3211. [Online]. Available: http://clincancerres.aacrjournals.org/lookup/doi/10.1158/1078-0432.CCR-19-3211 (visited on 05/18/2022).

[114] A. T. Ruffin, A. R. Cillo, T. Tabib, *et al.*, "B cell signatures and tertiary lymphoid structures contribute to outcome in head and neck squamous cell carcinoma", en, *Nature Communications*, vol. 12, no. 1, p. 3349, Dec. 2021, ISSN: 2041-1723. DOI: 10.1038/s41467-021-23355-x. [Online]. Available: http://www.nature.com/articles/s41467-021-23355-x (visited on 12/22/2021).

[115] Q. Li, X. Liu, D. Wang, Y. Wang, H. Lu, S. Wen, J. Fang, B. Cheng, and Z. Wang, "Prognostic value of tertiary lymphoid structure and tumour infiltrating lymphocytes in oral squamous cell carcinoma", en, *International Journal of Oral Science*, vol. 12, no. 1, p. 24, Dec. 2020, ISSN: 1674-2818, 2049-3169. DOI: 10.1038/s41368-020-00092-3. [Online]. Available: https://www.nature.com/articles/s41368-020-00092-3 (visited on 12/22/2021).

[116] X. Xiao, X.-M. Lao, M.-M. Chen, *et al.*, "PD-1hi Identifies a Novel Regulatory B-cell Population in Human Hepatoma That Promotes Disease Progression", en, *Cancer Discovery*, vol. 6, no. 5, pp. 546–559, May 2016, ISSN: 2159-8274, 2159-8290. DOI: 10.1158/2159-8290.CD-15-1408. [Online]. Available: https://aacrjournals.org/cancerdiscovery/article/6/5/546/5542/PD-1hi-Identifies-a-Novel-Regulatory-B-cell (visited on 08/22/2023).

[117] P. Voabil, M. de Bruijn, L. M. Roelofsen, *et al.*, "An ex vivo tumor fragment platform to dissect response to PD-1 blockade in cancer", en, *Nature Medicine*, vol. 27, no. 7, pp. 1250–1261, Jul. 2021, ISSN: 1078-8956, 1546-170X. DOI: 10.1038/s41591-021-01398-3. [Online]. Available: http://www.nature.com/articles/s41591-021-01398-3 (visited on 12/22/2021).

[118] C. A. Chambers, M. S. Kuhns, J. G. Egen, and J. P. Allison, "CTLA-4-Mediated Inhibition in Regulation of T Cell Responses: Mechanisms and Manipulation in Tumor Immunotherapy", en, *Annual Review of Immunology*, vol. 19, no. 1, pp. 565–594, Apr. 2001, ISSN: 0732-0582, 1545-3278. DOI: 10.1146/annurev.immunol.19.1.565. [Online]. Available: https://www.annualreviews.org/doi/10.1146/annurev.immunol.19.1.565 (visited on 12/21/2022).

[119] N. Prokhnevska, M. A. Cardenas, R. M. Valanparambil, *et al.*, "CD8+ T cell activation in cancer comprises an initial activation phase in lymph nodes followed by effector differentiation within the tumor", en, *Immunity*, vol. 56, no. 1, 107–124.e5, Jan. 2023, ISSN: 10747613. DOI: 10.1016/j.immuni.2022.12.002. [Online]. Available: https://linkinghub.elsevier.com/retrieve/pii/S1074761322006069 (visited on 04/25/2023).

[120] B. Somarouthu, S. I. Lee, T. Urban, C. A. Sadow, G. J. Harris, and A. Kambadakone, "Immune-related tumour response assessment criteria: A comprehensive review", en, *The British Journal of Radiology*, vol. 91, no. 1084, p. 20 170 457, Apr. 2018, ISSN: 0007-1285, 1748-880X. DOI: 10.1259/bjr.20170457. [Online]. Available: https://academic.oup.com/bjr/article/7451882 (visited on 01/23/2024).

[121] R. N. Amaria, S. M. Reddy, H. A. Tawbi, *et al.*, "Neoadjuvant immune checkpoint blockade in high-risk resectable melanoma", en, *Nature Medicine*, vol. 24, no. 11, pp. 1649–1654, Nov. 2018, ISSN: 1078-8956, 1546-170X. DOI: 10.1038/s41591-018-0197-1. [Online]. Available: http://www.nature.com/articles/s41591-018-0197-1 (visited on 12/22/2021).

[122] S. A. Oh, D.-C. Wu, J. Cheung, *et al.*, "PD-L1 expression by dendritic cells is a key regulator of T-cell immunity in cancer", en, *Nature Cancer*, vol. 1, no. 7, pp. 681–691, Jul. 2020, ISSN: 2662-1347. DOI: 10.1038/s43018-020-0075-x. [Online]. Available: http://www.nature.com/articles/s43018-020-0075-x (visited on 12/22/2021).

[123] F. Dammeijer, M. van Gulijk, E. E. Mulder, *et al.*, "The PD-1/PD-L1-Checkpoint Restrains T cell Immunity in Tumor-Draining Lymph Nodes", en, *Cancer Cell*, vol. 38, no. 5, 685–700.e8, Nov. 2020, ISSN: 15356108. DOI: 10.1016/j.ccell.2020.09.001. [Online]. Available: https://linkinghub.elsevier.com/retrieve/pii/S1535610820304323 (visited on 05/18/2022).

[124] M. K. Rahim, T. L. H. Okholm, K. B. Jones, *et al.*, "Dynamic CD8+ T cell responses to cancer immunotherapy in human regional lymph nodes are disrupted in metastatic lymph nodes", en, *Cell*, vol. 186, no. 6, 1127–1143.e18, Mar. 2023, ISSN: 00928674. DOI: 10.1016/j.cell.2023.02.021. [Online]. Available: https://linkinghub.elsevier.com/retrieve/pii/S0092867423001642 (visited on 11/23/2023).

Acknowledgements

"The whole is greater than the sum of its parts."

– Aristotle

My doctoral journey has been a remarkable adventure marked by growth, discovery, and companionship, all thanks to the collective efforts of everyone mentioned here. It brings me great joy to acknowledge the contributions of each and every one of you.

Firstly, my gratitude goes to the esteemed members of my jury for their dedicated time and commitment in evaluating my work. Your guidance and feedback have been pivotal in refining my scientific thinking and elevating the quality of my research. Professor Alejandro Sifrim, thank you for approaching my work with fresh perspectives and encouraging exploration of alternative viewpoints. Professor Abhishek Garg, your insights in immunology have considerably expanded my understanding – thank you. Professor Damya Laoui and Doctor Henoch Hong, your contributions have been instrumental in shaping my thesis and I am genuinely grateful for your involvement. I also extend my gratitude to Professor Patrick Callaerts for accepting the responsibility of chairing my defense.

My journey owes its existence to my promoter, Diether. Your belief in my abilities and the engaging projects you provided have paved the way for this enriching experience. Thank you for showing me the ropes in academic writing. Additionally, your talent for bringing together a wonderful group of individuals cannot go unnoticed. I am grateful for the privilege of having met every single one of you, including Roos, Marlies, Laurien, Ayse, Ingrid, Sarah, Evy, Liselore, Juan, Dora, David, Bia, Aurelie, Rogier, Thomas, Elena, Francesca, Pierre, Kaat, Laura, Tina, Tom, Gino, Sam, Heesoo, Ling, Razgar, Orian, Jieyi, Dries, Pieter, Bram, Sylvia, Frederik, Toon, Charlotte, Siel, and Vincent.

To effectively conduct translational research, collaboration with medical experts is indispensable. Professor Clement, Paul, the moments we shared were profoundly enriching, and I feel fortunate to have had you as my co-promoter. Your encouragement during my final doctoral plan was invaluable. Additionally, Michel, your surgical expertise and diligent patient follow-up were crucial for the success of this research. You both reminded me of the importance and purpose behind our research endeavors. I sincerely hope to have made a modest contribution to patient care in the future, it is this aspect that truly brings satisfaction. I express my heartfelt gratitude to the patients and their families for their willingness to participate in these studies. Also thank you Jeroen, Sigrid, and Sara, your consistent kindness and support played a pivotal role in our fruitful partnership.

Reflecting on this journey fills me with immense gratitude. Not only did I enjoy a stunning office view, but more importantly, I also had the pleasure of having Rogge as my back-to-back neighbor. Whether discussing running shoes, bikes, or even the fine art of "stoot" or "lint voegen", you always brought fresh insights and a delightful piece of cake to sweeten the conversation. As Rogge always says, "voor niks gaat de zon op" – you don't get owt for nowt. But with you around, every moment felt like a gift that keeps on giving (also, dixit Rogge). Which brings me to the other half of this dream team, Thomas, your steady hand keeps this ship sailing smoothly. Your modesty and compassion for others are evident to all who know you, and I hope you are aware of just a fraction of the positive impact you have on those around you. And let's not forget your talent for dad jokes – always ready with a witty remark to lighten the mood.

As our cozy corner nears completion, it becomes evident that this triangle was destined to form. Lieke, your readiness to offer suggestions and feedback, regardless of the topic or time, is truly appreciated. Thanks for being the rock star you are - Sam Manson does not even come close. Speaking about rock-solid energy, Francesca, your unstoppable determination and positivity inspire us all. Grazie di cuore for all you bring to our team. Together with Elena, Rogge, Thomas, Lieke, Mohammad, Gabriele (and Razgar on Fridays), thanks for the much-needed kicker breaks from time to time that keep us 'sane'. These were often followed by a ping pong game to loosen up the shoulders. Thank you, Sam, for being my protective wall against fierce smashes, and Toon for unconsciously bringing the laughs. And believe me, you're not an 'idioot'.

Razgar, your exceptional mentoring skills have been a cornerstone of my academic journey. Your guidance, patience, and depth of knowledge have not only helped me perfecting serves but also mastering spin. At the same time, your dedication and sense of humor never fail to brighten our days beyond the table. It is always a delight talking with you and Sayma - Pierre and I count ourselves fortunate to have crossed paths with such an inspiring duo.

Although in a different field, Orian, thank you for peaking my immunological learning curve and for being my personal career coach every now and then. This certainly helped setting the stage for my next career endeavor(s). And Bia, thanks to your flood of job listings, I hardly had to search for positions on my own. Your unwavering support and listening ear only enriched this journey further.

In addition to this, our lunch breaks sometimes revealed pleasant insights into the personalities of some, like Jieyi's humble demeanor hiding a remarkable sense of humor. Heesoo, your contagious smile always warmed our gatherings. Evy, thank you for keeping us informed about all upcoming events and for maintaining impeccable organization. Gino, thanks for the nice conversations but also for always being keen to help, even when another trajectory analysis was looming on the horizon. Together with Laura and Kaat, you move mountains. The boundless energy you ladies possess is truly inspiring.

Also the brief encounters in the hallways deserve a special mention. These moments, where genuine smiles and chats are exchanged, brighten up the day. Thanks Halimah, Koen, Katy, Dries, and many others.

Shifting focus to those behind the scenes... A big shout out to my friends for infusing a breath of fresh air, offering perspective during our invigorating runs, bike rides, tennis games, and leisurely gatherings over drinks and board games. It is always a pleasure.

Mom, Dad, thank you for always being there for me, no matter what. From a young age, I was fortunate to learn from two role models who radiate creativity and ambition. I think my mindset and belief in creating opportunities can be traced back easily. Gertjan, from our childhood days when teaming up to persuade our parents, to the joy of creating a friendship beyond our family home, our bond has been unconditional. Sharing the journey of pursuing our PhDs together in Leuven, which started right here at Arenberg, provided a sense of security, knowing I could always rely on you. And soon, with Dilara by your side, it became even more evident that you are truly content and fulfilled. Dilara, your Christmas favor unexpectedly transformed into collective train workaholism and late-nighters. Thank you so much for all the efforts you put into editing this thesis in LaTeX. Without your unstoppable dedication, Gertjan might have deemed it a mere piece of Word incompetence...

Finally, I have arrived to my most significant finding in the lab. Pierre, from the very beginning, your genuine and caring nature stood out to me, as it did to many of us. What initially began as a scientific collaboration quickly blossomed into lengthy lunch breaks and personal cycling records (on less-than-ideal bikes). Thank you for allowing me to see beyond the surface and discover the passionate,

culturally enriched, humorous, groovy dancer that you are. Your willingness to join me in pursuing sometimes ambitious ideas and trusting our shared adventures means a lot to me. You have been a constant inspiration, and I have no doubt that you will continue to be so. I can't wait for more adventures with you by my side. And just when I thought I had discovered all, I met my family-in-law. Colette, Luc, Charlotte, and Willem, you are the warmest and most generous people I could have ever wished for. Thank you for always embracing me with open arms.

Cheers to the beautiful journey we have shared and the countless adventures that lie ahead! I genuinely hope our paths will cross again in the future.

Curiculum vitae

Education

2019 - present	Doctor of Biomedical sciences (PhD) VIB - KU Leuven Centre for Cancer Biology, Leuven, Belgium
2017 - 2019	Master of Biomedical sciences - *Magna cum laude* VIB - KU Leuven Centre for Cancer Biology, Leuven, Belgium Harvard Medical School - Massachusetts General Hospital, Boston, USA Honours Programme: Transdisciplinary Insights
2014 - 2017	Bachelor of Biomedical sciences – *Cum laude* KU Leuven, Leuven, Belgium Universitat de Barcelona, Barcelona, Spain
2008 - 2014	Secondary education: Science-Mathematics Sint-Augustinus, Bree, Belgium

Research experience

2019 - present	Full-time PhD Project Laboratory of Translational Genetics VIB-KU Leuven Centre for Cancer Biology, Leuven, Belgium
	IMMUcan Collaborator
2018 - 2019	Master's Thesis Research Project Laboratory for Molecular Cancer Biology VIB-KU Leuven Centre for Cancer Biology, Leuven, Belgium
	Master Internship Melanoma Center Harvard Medical School, Massachusetts General Hospital, Boston, USA
2018	Student Employee Laboratory of Clinical Bacteriology & Mycology UZ Leuven, Leuven, Belgium
2017 - 2018	Research Internship Laboratory of Immunobiology; Laboratory for Molecular Cancer Biology; Laboratory of Digestion & Absorption (TARGID) KU Leuven, Leuven, Belgium
2017	Volunteer Researcher Lipid Metabolism in Cancer Laboratory KU Leuven, Leuven, Belgium
2016	Bachelor Internship Universitat de Barcelona, Barcelona, Belgium BioNMR Research Group

Publications

A. Franken*, M. Bila*, A. Mechels, S. Kint, J. Van Dessel, V. Pomella, S. Vanuytven, G. Philips, O. Bricard, J. Xiong, B. Boeckx, S. Hatse, T. Van Brussel, R. Schepers, C. Van Aerde, S. Geurs, V. Vandecaveye, E. Hauben, V. Vander Poorten, S. Verbandt, K. Vandereyken, J. Qian, S. Tejpar, T. Voet, P. M. Clement, D. Lambrechts, "CD4+ T cell activation distinguishes response to anti-PD-L1+anti-CTLA4 combination therapy from aPD-L1 monotherapy", Immunity (2024), 57: 541-558. * These authors share equal contributions.

M. Bila, **A. Franken**, J. Van Dessel, M. Garip, S. Verbandt, V. Pomella, V. Vander Poorten, S. Tejpar, D. Lambrechts, S. Hatse, P. Clement, "DUTRELASCO: Insights from immune checkpoint inhibition response on peripheral blood immune cell subsets and soluble plasma biomarkers in oral squamous cell carcinoma", Manuscript in preparation, 2024.

M. Bila, **A. Franken**, J. Van Dessel, M. Garip, S. Verbandt, V. Pomella, S. Hatse, T. Van Brussel, R. Schepers, C. Van Aerde, J. Van Berne, K. Goffin, V. Vandecaveye, E. Hauben, T. Voet, S. Tejpar, V. Vander Poorten, D. Lambrechts, P. Clement, "Durvalumab With or Without Tremelimumab in Resectable Locally Advanced Squamous Cell Carcinoma of the Oral Cavity (DUTRELASCO)", Manuscript in preparation, 2024.

E. Van Loon, J. Callemeyn, B. Lamarthée, P. Koshy, D. Anglicheau, P. Cippa, **A. Franken**, W. Gwinner, W. Kuypers, D. Kuypers, P. Marquet, A. Rinaldi, T. Van Brussel, A. Van Craenenbroeck, T. Vaulet, D. Lambrechts, M. Naesens, "Active immunological participation and metabolic shutdown of kidney structural cells during kidney transplant rejection", American Journal of Transplantation, under review 2023.

M. Bila, **A. Franken**, J. Van Dessel, M. Garip, J. Meulemans, R. Willaert, A. Hoeben, V. Vander Poorten, P. Clement, "Exploring long-term responses to immune checkpoint inhibitors in recurrent and metastatic head and neck squamous cell carcinoma", Oral Oncology (2023), 149: 106664.

B. Lamarthée, J. Callemeyn, Y. Van Herck, A. Antoranz, D. Anglicheau, P. Boada, J.U. Becker, T. Debyser, F. De Smet, K. De Vusser, M. Eloudzeri, **A. Franken**, W. Gwinner, P. Koshy, D. Kuypers, D. Lambrechts, P. Marquet, V. Mathias, M. Rabant, M.M. Sarwal, A. Senev, T.K. Sigdel, B. Sprangers, O. Thaunat, C. Tinel, T. Van Brussel, A. Van Craenenbroeck, E. Van Loon, T. Vaulet, F. Bosisio, M. Naesens, "Transcriptional and spatial profiling of the kidney allograft unravels a central role for FcγRIII+ innate immune cells in rejection", Nature communications (2023): 14(1), 4359.

A. Franken*, P. Van Mol*, S. Vanmassenhoven, E. Donders, R. Schepers, T. Van Brussel, C. Dooms, J. Yserbyt, N. De Crem, D. Testelmans, W. De wever, K. Nackaerts, J. Vansteenkiste, R. Vos, S. Humblet-Baron, D. Lambrechts*, W. Wauters*, "Single-cell transcriptomics identifies pathogenic T-helper 17.1 cells and pro-inflammatory monocytes in immune checkpoint inhibitor-related pneumonitis", J Immunother Cancer 10.9 (2022): e005323. * These authors share equal contributions.

J. Qian, S. Olbrecht, B. Boeck, H. Vos, D. Laoui, E. Etlioglu, E. Wauters, V. Pomella, S. Verbandt, P. Busschaert, A. Bassez, **A. Franken**, M. Vanden Bempt, J. Xiong, B. Weynand, Y. van Herck, A. Antoranz, F. Maria Bosisio, B. Thienpont, F. Giuseppe, I. Vergote, A. Smeets, S. Tejpar, D. Lambrechts, "A pan-cancer blueprint of the heterogenous tumor microenvironment revealed by single-cell profiling", Cell research 30.9 (2020): 745-762.

F. Bocken*, E. Brennan*, N. Claessens*, D. Claeys*, S. Debeaussaert*, T. Dubois*, **A. Franken***, B. Vanwyngaerden*, J.R. Nova Blanco, K. Becher, P. Vandenbroeck, "Facing the Future: A Blueprint for a Resilient and Equitable Society", Transdisciplinary Insights 2.1 (2018): 1-37. * These authors share equal contributions.

Presentations

2023 Tumor Microenvironment Conference (Keystone Symposia, Vancouver, Canada)

2022 External Advisory Board (KU Leuven - Center for Human Genetics, Leuven, Belgium)
General Assembly (IMMUcan, Lausanne, Switzerland)
Pointillism Steering meeting (KU Leuven – CCB, Leuven, Belgium)

2021 Scientific Advisory Board (IMMUcan, Virtual)
VIB Seminar (VIB Virtual Conference)

2020 Emerging technologies in Single Cell Research (VIB Virtual Conference)

Grants

2021 - 2025 FWO Fundamental Research project grant

2020 Emmanuel van der Schueren starting grant (Kom op tegen Kanker)

FACULTY OF MEDICINE
DEPARTMENT OF HUMAN GENETICS
VIB
Herestraat 49
B-3000 Leuven
amelie.franken@kuleuven.be